

Chapter 9: Predicting Thermooxidative Degradation and Performance of High-Temperature Polymer Matrix Composites

G.A. Schoeppner¹, G.P. Tandon² and K.V. Pochiraju³

¹US Air Force Research Laboratory, Wright-Patterson Air Force Base, OH, USA

²University of Dayton Research Institute, Dayton, OH, USA

³Stevens Institute of Technology, Hoboken, NJ, USA

9.1 Introduction

Polymer matrix composites (PMCs) used in aerospace high-temperature applications, such as turbine engines and engine-exhaust-washed structures, are known to have limited life due to environmental degradation. Predicting the extended service life of composite structures subjected to mechanical, high temperature, moisture, and corrosive conditions is challenging due to the complex physical, chemical, and thermomechanical mechanisms involved. Additionally, the constituent phases of the material, in particular the matrix phase, continuously evolve with aging time. It is the aging-dependent evolution of the constituent properties that makes prediction of the long-term performance of PMCs in high-temperature environments so challenging. A comprehensive prediction methodology must deal with several complications presented by the highly coupled material aging, damage evolution, and thermooxidation processes.

While carbon fibers may be more resistant to oxidation and have longer relaxation times than the polymer matrix, the mechanical performance of the fiber–matrix interface at high temperatures may be critical to the evolution of damage and composite failure. The properties of the fiber–matrix interface

or interphase region¹ are a function of the interaction of the fiber and matrix during the manufacturing process, the chemical compatibility of the fiber, and the sizing (if applicable) on the fiber.

To deal with the aforementioned complex interactions, modeling is expected to incorporate mechanisms active at multiple scales (constituent, microstructural, lamina, and laminate scales) and multiple domains of response (chemical, thermal, and mechanical). The motivation is to develop robust, life-performance, prediction modeling capabilities for designers who currently use cost prohibitive experimentally based design allowables and use weight loss to evaluate the thermal-oxidative stability of material systems.

In the face of such complexity and lack of knowledge regarding material behavior, industry currently relies on the use of environmental “knockdown factors” for the design of composite aerospace structures which operate in aggressive environments. One of the current methodologies used for determining environmental knockdown factors for designing composite aerospace structures is to determine reduced material allowables for each of the lamina properties (laminate ultimate strengths, notched strengths, fatigue, flexure properties, bearing strengths, etc.) for each of the material forms used in the structure. The material forms may include unitape, woven cloth, fiber preforms with mold filling, etc.

The large variety of tests performed on a statistically sufficient number of replicates for the various environmental conditions adds tremendous cost to the materials qualification and design allowables process. In addition, the worst case environmental extreme conditions are typically used for determining reduced materials allowables to help circumvent risk associated with the variability and inaccurate prediction of service environments. In addition to the environmental knockdown factors, damage tolerance knockdown factors are also applied to the designs. The damage tolerance factors may be determined through damaging full-scale components and testing them for a predetermined number of life cycles in a hot/wet environment. Using this approach, the end-of-life properties are measured and used in the allowables determination process for designing components.

The aerospace engine community (where high-temperature polymer matrix composites (HTPMCs) are most prevalent) often designs to end-of-life properties, and it is accepted that at the end of life for certain lightly

¹ Although fiber–matrix interface and fiber–matrix interphase are often used interchangeably, we formally define the fiber–matrix interface as the two-dimensional surface defined by the common fiber and matrix surfaces. We define the fiber–matrix interphase as the three-dimensional matrix region directly around the fiber that may have properties distinct from the bulk matrix properties.

loaded structures, the composites may have cracks. On the other hand, for highly loaded or critical structures, the presence of cracks, even at the end of life, is not accepted. This traditional approach for determining material design allowables, taking into account extremes in-service environments, requires significant testing (cost and schedule). For cost savings and risk mitigation, designers often resort to previously qualified materials, thereby negating the potential benefits of new material advancements. By developing a life prediction/performance modeling capability, the cost and time associated with developing material design allowables can provide opportunities for the insertion of new advanced materials.

This chapter focuses on predicting the performance of PMCs in high-temperature environments where thermooxidative conditions are extreme and the material is used near its tolerance limits. For the current design methodology used by aerospace structure designers, composites are considered to be “chemically static,” ignoring the evolution of the chemical/environmental degradation and nonelastic mechanical response. However, the empirical design allowables are based on the expected end-of life properties by testing specimens that have been aged under representative service environments for the design life.

This chapter outlines the current state of the art, the shortcomings of existing capabilities, and future challenges for addressing modeling needs for PMCs in high-temperature oxidative environments. It is believed that the approach presented provides the methodology to accurately model both short- and long-term environmental effects on composite laminates for facilitating design allowables generation (including history-dependent failure prediction) and for predicting life expectancy (degradation state) for fielded composite structures.

A valuable resource for understanding the high-temperature behavior of PMCs is the tremendous volume of long-term high-temperature aging data generated in the NASA High-Speed Research (HSR) program. The HSR effort was a national effort to develop the next-generation supersonic passenger jet designed for a 60,000-h life with temperatures approaching 177°C. To meet the vehicle requirements, PMCs with high glass transition temperatures T_g and, thus, high-temperature use capabilities were thermo-mechanically loaded for very long-aging times.

The long-term testing conducted in this program demonstrates the challenge of using PMCs in high-temperature environments. An important contribution to understanding the high-temperature performance of the polymer composites evaluated in the program is the use of viscoelastic formulations to model long-term behavior [21, 42, 49, 68, 115, 116]. The assumption inherent in the use of these viscoelastic formulations is that the material is chemically static or the original chemical structure is thermally

recoverable [98]. Although these formulations are an important aspect of the overall methodology to model the performance of HTPMCs, a comprehensive review of such is beyond the scope of the current discussion. The discussion here is limited to modeling the thermooxidative aging of HTPMCs and the role of the various constituents. Although hygrothermal degradation, which is a significant concern for HTPMCs, is not specifically addressed here, the methodology described herein can be applied to modeling hygrothermal degradation behavior. As with oxidation, hygrothermal degradation involves transport and chemical reactions of the polymer with the diffused media. The primary challenge for modeling the coupling of oxidative and hygrothermal degradation of HTPMCs is an understanding of the numerous degradation mechanisms.

Several major aging mechanisms that lead to weight loss and damage growth and, hence, degradation of the performance of the polymer resin, fibers, and their composite can be identified. They are:

- *Physical aging.* The thermodynamically reversible volumetric response due to slow evolution toward thermodynamic equilibrium is identified as physical aging. The decreased molecular mobility and free-volume reduction lead to strain and damage development in the material.
- *Chemical aging.* The nonreversible volumetric response due to chain scission reactions and/or additional crosslinking, hydrolysis, depolymerization, and plasticization is classified as chemical aging. A dominant chemical aging process for HTPMCs is thermooxidative aging – which is the nonreversible surface diffusion response and chemical changes occurring during oxidation of a polymer (hence a modality of chemical aging). The oxidative aging may lead to either the reduction in molecular weight as a result of chemical bond breakage and loss in weight from outgassing of low molecular weight gaseous species, or chain scission and formation of dangling chains in polymer networks.
- *Mechanical stress-induced aging.* Mechanical and thermal fatigue loading cause micromechanical damage growth within the material. The damage evolution, in turn, exacerbates the physical aging and thermooxidative response of the material. This aging mechanism may be the least understood and least modeled by researchers.

The capability to predict the performance of HTPMCs for both primary and secondary structural applications is elusive. The highly coupled physical, chemical, and mechanical response of these materials to the extreme hygrothermal environments provides formidable challenges to the composite mechanics community. Polymers (in particular amorphous polymers) have been studied from the standpoint of physical aging [98], chemical aging [66], and strain-dependent aging [118]. Although models to predict

the aging response of polymers are available and the fiber response can be assumed to be elementary, the ability to model the thermooxidative aging of the fiber–matrix system (presence of fiber–matrix interface/interphase region complicates the issue with a coupling or sizing agent) is lacking.

While the time-dependent physical, chemical, and damage-induced degradation mechanisms have been studied for some resin systems, polymer composite thermal oxidation studies from a mechanistic perspective are nascent. Notable exceptions to this are the recent works of the groups of Colin and Verdu [27], Colin et al. [32], Skontorp et al. [97], Wang et al. [121], and Pochiraju and Tandon [73, 74], Tandon et al. [104], and past work by Wise et al. [125], Celina et al. [22], and McManus et al. [62]. Equally important are the experimental characterization efforts by such groups as Bowles et al. [14, 19], Tsuji et al. [113], Abdeljaoued [1], Johnson and Gates [49], and Schoeppner et al. [91]. However, most literature is confined to thermal oxidation of neat polymer systems and there are limited studies that correlate the thermochemical decomposition of high-temperature polymers to the resulting mechanical performance. Such works include Meador et al. [63–65] and Thorp [107] for PMR-15 high-temperature composites and Lincoln [56] for 5250-4 bismaleimide (BMI) composites.

Current emphasis is on the implementation and extension of multiscale models to represent the polymer behavior/properties as a function of the degradation state to include chemical degradation kinetics, micromechanical models with time-dependent polymer constitutive relationships, and ply-level and laminate level models to predict structural behavior. The behavior of the composite will, thus, be dependent on its current chemical, physical, and mechanical state as well as its service history. This multidisciplinary modeling approach will provide generalizable analytical and design tools for realistic prediction of performance, durability, and use life of HTPMCs.

The following requirements are identified for the formulation of the predictive thermooxidation models:

- *Appropriate mechanistic and kinetic modeling of polymer environmental degradation.* For the highly crosslinked polyimide composite of interest, the reactivity of the end cap is often a primary concern [63, 107]. Although the primary, and in some cases secondary, oxidation and hydrolytic degradation mechanisms can be identified, determination of mechanisms up to the final state of degradation is difficult if not impossible. Predicting thermal, physical, and mechanical performance based on the chemical state of the polymer is currently impractical for all but the very simplest of polymer systems. In the absence of this predictive capability, empirical correlation of the chemical state (if known) to mechanical properties is used to help define the constitutive models.

- *Polymer constitutive models that incorporate the chemical, thermal, and deformation state and history dependence.* Linear viscoelastic constitutive models have been successfully used to model the physical aging of the polymer phase of polymer composites used in high-temperature environments. Beyond physical aging, accounting for the effects of chemical aging (oxidative and nonoxidative) in a constitutive model requires path/history-dependent relationships. Constitutive models and/or empirically derived correlations that account for the dominant behavior of the material provide alternatives to models that can predict performance based on the chemical degradation state.
- *Integrated mechanistic models that explicitly represent fiber–matrix phases and interfaces to predict lamina properties.* The highly critical fiber–matrix interface/interphase region may govern the oxidative behavior of HTPMCs, but significant challenges exist in measuring properties of the interphase region. Prediction of strength/failure requires knowledge of the constituent properties, including strength and toughness, as a function of the degradation state or aging history. It is beyond current modeling capabilities to predict mechanical properties based on the chemical state of the polymer. For lack of a robust constitutive model, simplifying assumptions regarding the history-dependent properties can be made as a first-order approximation to predict the material behavior.
- *Structural laminate models with lamina property descriptions and discrete ply representations for laminate and composite failure modeling under history-dependent environmental service loads.* As for the micro-mechanical scale in which the fiber, matrix, and interphase regions are represented explicitly, the residual stresses on the ply-level and laminate level scales play a critical role in the thermal oxidation process. Accurate representation of the free-edge interlaminar stresses in multi-directional composites, taking into account stress-assisted diffusion, is essential for accurately modeling the oxidation-susceptible free surfaces.
- *Experimental validation of the simulation and transition into designer assistance tools and property databases.* To transfer the prediction methodology from scientists to designers, a new generation of tools that incorporate the simulation methods and experimental databases needs to be developed. To facilitate adoption of the tools by designers, any such development must be in collaboration with the practitioners from the airframe and propulsion segments of the aerospace industry. This methodology of tool development in collaboration with design practitioners was used in the DARPA Accelerated Insertion of Materials – Composite (AIM-C) program [82].

For those steps described above where prediction capability is lacking, experimental/empirical means must be used to represent the behavior of the material. It is these empirical relationships that preserve the capability to make predictions on how materials will behave when mechanistic models are not available. Experimental validation of predictive models for a given geometric scale provides a basis for building models at higher geometric scales. As an example, polymer constitutive models can be validated by testing neat resin polymers but validation of such models on the lamina or laminate scale is not viable. This is due to the fact that fibers mask the polymer degradation behavior particularly for the fiber-dominated composite properties. Additionally, fibers can exacerbate some degradation mechanisms of polymer due to the introduction of fiber–matrix residual stresses and the introduction of fiber–matrix interface/interphase.

The multiscale modeling levels and the vital links between the various model levels are illustrated in Fig. 9.1. This description of the hierarchical scheme is an idealized representation of the methodology needed to mechanistically model the behavior of PMCs in aggressive environments. In particular, a kinetic description of the polymer phase of the material is necessary when the materials are subjected to or susceptible to chemical changes or degradation.

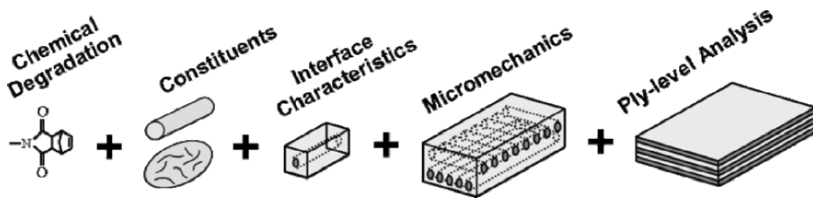


Fig. 9.1. Multiscale modeling levels

The primary focus of the discussion in this work is on predicting isothermal-oxidative aging of unitape laminates with particular focus on the composites using PMR-15 high-temperature polymer. Additionally, the reinforcement is limited to polyacrylonitrile (PAN)-based carbon fibers. PMR-15 is a widely used addition polyimide with a maximum service temperature of approximately 288°C. Among the class of high-temperature polymers are the bismaleimides, Avimid-N, thermosetting polyimides (AFR700B, LARC RP46), and phenylethynyl-terminated polyimides (PETI-5, AFR-PE-N) resin systems. Each of these material systems has unique degradation reactions, mechanisms, and kinetics particular to their chemical structure. Although experimental observations and predictions of the behavior of PMR-15 neat resin and composites are not necessarily representative of the behavior of these other high-temperature polymer

material systems, the modeling methodology and procedures for determining material parameters may be directly applicable to predicting their behavior. On the other hand, the observed behavior of other high-temperature material systems can deviate significantly from PMR-15 and such deviations will be noted when appropriate. Current polymer and polymer matrix composite modeling approaches for chemical and physical aging, as well as the modeling process for predicting thermooxidative degradation, are discussed in the following sections.

9.1.1 Physical Aging of Polymers and PMCs

At temperatures below a polymer's glass transition temperature (T_g), the material is in a nonequilibrium state and undergoes a time-dependent rearrangement toward thermodynamic equilibrium. During this rearrangement (relaxation) toward the equilibrium state, there are time-dependent changes in volume, enthalpy, and entropy, as well as mechanical properties and this is known as *physical aging*. Physical aging is characterized by changes in stiffness, yield stress, density, viscosity, diffusivity, and fracture energy (toughness) as well as embrittlement in some polymeric materials. The physical aging rate depends on the distance the aging temperature is from the material's T_g . Therefore, the closer the aging temperature to the T_g , the greater the polymer molecular mobility and the greater the relaxation rate, while the driving force defined as the entire path to the equilibrium state, decreases.

Practical considerations of physical aging only become important when aging temperatures are near the T_g . Physical aging is a reversible process known to be easily altered with stress and temperature. For high-temperature PMCs that are used at temperatures near the material's T_g , physical aging may dramatically affect the time-dependent mechanical properties (creep and stress relaxation) and rate-dependent failure processes [56]. For highly crosslinked polyimide systems, it is difficult to separate the physical aging from chemical aging effects when conducting tests near the T_g because the aging effects are coupled. Whereas in some simple polymer systems, physical aging can be reversed by heating the polymer above the T_g and quenching, heating highly crosslinked polymers above the T_g induces chemical aging, thereby, altering the thermodynamic equilibrium state.

Earlier studies on the effects of physical aging on polymer composite behavior were conducted by Sullivan [99], McKenna [59], and Waldron and McKenna [118]. The majority of the reported work on predicting the long-term performance of PMCs in high-temperature environments is limited to physical aging models and the use of linear viscoelastic and

time–temperature superposition models [21]. Inherent in the use of physical aging models is the assumption that the aging process is thermoreversible, therefore nonreversible chemical aging cannot be properly modeled using this approach. That is, the effects of irreversible processes, e.g., chemical decomposition, hydrolytic degradation, oxidation, etc., are neglected in these models or are assumed to be implicitly accounted for in determining the physical aging parameters. However, chemical aging can be the primary life-limiting degradation process for HTPMCs used at temperatures near their T_g . Neglecting the modeling of the chemical degradation for composites in an oxidative environment will likely result in inaccurate and nonconservative predictions of performance.

9.1.2 Chemical Aging of Polymers and PMCs

Chemical aging, unlike physical aging, is typically not thermoreversible. Hydrolysis (the chemical reaction of the polymer with water) and oxidation (the chemical reaction of the polymer with oxygen) are the primary forms of chemical degradation in HTPMCs. The chemical changes occurring during oxidation include chemical bond breaks that result in a reduction in molecular weight, mechanical response changes, and a local loss of mass associated with outgassing of oxidation byproducts. Although the rate of oxidative chemical reactions is, in part, governed by the availability of reactive polymer, the oxygen concentration, and the reaction temperature for high T_g glassy polymers, the rate of oxidation can be greater than the rate of diffusion of oxygen into the polymer. For such circumstances, the oxidative process is diffusion rate limited. Diffusion rate-limited oxidation of neat polymer specimens typically results in the development of an oxidative layer or graded oxidative properties near the free surfaces of the specimen. Within the oxidized region of the polymer, it is typical that the tensile strength, strain to failure, flexural strength, density, and toughness decrease while the modulus increases. The effect of oxidation on changes in the T_g is dependent on the specific polymer system. Some polymers initially have a decrease and then an increase in T_g , others may have only a decrease, and still others may only have an increase in T_g . This may be due to competing chemical and physical aging phenomenon [56] or differences in the oxidation reaction mechanisms. Since HTPMCs typically operate at temperatures near their initial design T_g , any changes in the local or global T_g can have detrimental effects on performance.

Determination of the primary, secondary, and tertiary chemical degradation mechanisms in high-temperature polyimide composites is an extremely challenging task [92] but can yield substantial benefits for designing new

polyimides that are less susceptible to degradation. The primary and secondary oxidation mechanisms for PMR-15 were determined by Meador et al. [63–65] in a series of tests on model compounds. It was determined that the nadic end group, in which the aliphatic carbons are consumed during oxidation, is the primary rapid mechanism for weight loss. The second, longer-term mechanism is the oxidation of the diamine bridging methylene to the carbonyl group. As part of a separate effort, Thorp [107] determined that the nadic end group is also responsible for the primary hydrolytic degradation mechanism. Similar types of studies have led to the development of polyimides with a more thermally stable phenylethynyl end group as a replacement for the degradation-susceptible nadic end group. These new material developments include the family of phenylethynyl-terminated polyimides such as NASA's PETI resins [47] and the Air Force-developed AFR-PE-N resins that are more thermally stable than PMR-15 [123].

9.1.3 Mechanical Stress-Induced Aging

Elevated temperatures can have a dominating effect on the strength and stiffness of HTPMCs [76], and the strength and stiffness at the operating temperature are primary considerations for selecting suitable materials for a given application. Primary consideration is also given to the long-term durability of the material in the elevated temperature environment. The effects of long-term mechanical loading on PMCs at elevated temperatures are manifested in the creep–relaxation response (viscoelastic–plastic behavior) and the load-induced damage developed under thermomechanical cyclic loading. Often a linear elastic representation of the fiber-dominated composite properties is sufficient, while various time-dependent linear and nonlinear viscoelastic–plastic models [85, 86] may be needed to represent the resin- or matrix-dominated properties for high-temperature applications. Additionally, there is a strong coupling between chemical aging and the damage development due to the changes in stiffness, strength, and toughness that occur during long-term aging.

For the purpose of the discussion here, mechanical stress-induced aging is associated with stress-assisted diffusion and aging as well as thermo-mechanical-induced damage or cracking. The development of damage in HTPMCs exacerbates the chemical and physical aging by introduction of stress concentrations that accelerate physical aging effects and exacerbates the chemical aging by introducing pathways for oxidants and other agents to advance deeper into the material. Damage typically takes the form of matrix cracks and fiber–matrix interface debonds, with the micromechanical

cracks and transverse ply cracks coalescing to form larger ply-level cracks. For this reason, the resin- or matrix-dominated properties are of primary interest for modeling the high-temperature aging response.

The mechanistic approach of modeling discrete damage, such as transverse ply cracks [58, 89], provides accurate assessments of the effective response for a given damage state but has limitations on the number of discrete cracks or amount of discrete damage that can be represented. Therefore, mechanistic damage modeling is often reserved for analyzing local details and small components, or it can be used as a local model in a global analysis. Ultimately, for modeling large structures, phenomenological approaches of continuum damage mechanics [4, 100] can be used to represent the evolution of effective local damaged properties through the constitutive relationships, whereby widespread dispersed damage can be more easily represented.

9.2 Experimental Characterization and Observation

The research presented here focuses on PMR-15 resin, carbon fibers, and PMR-15/carbon fiber composites. Although other HTPMC material systems are of interest, the open literature contains very little data for all but the PMR-15 material. Other materials may behave significantly different from the PMR-15 material system, however the modeling methodology given here should be applicable to modeling thermal oxidation in other polymer systems. Thermooxidative aging experiments, which include the effects of both physical and chemical aging, were conducted on the neat polymer and composite specimens. Model development and experiments focus on thermo-oxidative degradation while hydrolytic degradation will be addressed in subsequent research efforts. The spatial and temporal variability of the oxidized material and the ensuing mechanical properties were monitored to determine material parameters for the implemented models.

Determination of model parameters for the multiscale modeling effort entails experimental characterization of the composite constituents, namely the fiber and the matrix polymer. However, characterization of the fiber and matrix is not sufficient to predict the behavior of the composite due to the critical fiber–matrix interface/interphase that develops during the cure process. Although a direct measure of the properties in the interface/interphase region is challenging, indirect measures of the influence of the fiber–matrix interphase based on experimental observation of the composite behavior can be used to predict the model parameters for the interphase.

9.2.1 Fiber Oxidation Degradation

The effects of service temperatures and oxidation on the mechanical properties of high-temperature polymer composites are primarily manifested in the polymer-dominated properties, namely the transverse properties (perpendicular to the fiber direction) and the shear properties. However, the fiber-dominated properties may be affected by degradation of the fiber and deterioration of the fiber–matrix interface. This may be particularly true for composites with glass fibers [44] in which magnesium and sodium can leach out from the fiber and possibly contribute to polymer/interface degradation. It is reported that graphite fibers containing significant amounts of sodium and potassium as contaminants are less thermooxidatively stable than graphite fibers with very low alkali metal contents [39, 43]. Studies conducted by Bowles and Nowak [12] indicate that extreme oxidative erosion of the Celion 6000 graphite fiber occurs at elevated temperatures in the presence of the polyimide matrix.

Bowles [8] has investigated the effects of different fiber reinforcements on thermooxidative stability of various fiber-reinforced PMR-15 composites. The ceramic Nicalon and Nextel fibers were found to drastically accelerate thermal oxidation of the corresponding composites because of the active fiber–matrix interface. Compared to polyimide matrices, reinforcing carbon fibers [60] are usually far more stable at the elevated temperatures considered. Studies conducted by Wong et al. [126] indicate that IM6 carbon fibers are more stable than the G30-500 fibers within the first 600 h during thermal oxidation at 371°C. The oxidation rate of the IM6 fibers then increases substantially, leading to complete decomposition of the fibers during the final stage. The sudden increase in the oxidation rate in the IM6 fibers implies the possibility of change in degradation mechanisms.

The three PAN-based carbon fibers of interest to the present body of work are two low modulus carbon fibers T650-35 and G30-500 that are typically used in HTPMCs, and one intermediate modulus carbon fiber, IM7. Isothermal aging studies were recently conducted [105] on these three types of fibers to study their oxidation behavior. Both sized and unsized fibers were exposed to different elevated temperatures for varying time periods in an attempt to understand the influence of the fiber sizing/coupling agent on their thermooxidative stability. Note that aging of the bare fibers may not necessarily be representative of the behavior of the in situ fibers embedded in the matrix, because the exposed surface area of the fibers in the composite is only a very small percentage of the total surface area of the fibers. Thermal degradation was quantified by the amount of weight loss measured, while degradation of mechanical properties was

measured using single-filament tests on unaged and aged fibers. Finally, surface morphology changes were monitored in an attempt to relate physical and surface changes to the decreases in mechanical performance as a function of aging.

Weight loss studies

Figure 9.2 shows that the thermal degradation (as measured by weight loss) of unsized T650-35 carbon fibers is substantial for moderate temperatures above 316°C. It is seen that there is a large (~40%) weight reduction of T650-35 carbon fibers after 2,000 h of aging at 343°C. At the lower temperature of 232°C, the weight loss is not significant and the weight loss as a function of time follows approximately a linear relationship. However, as the aging temperature is increased to 343°C, the T650-35 fibers are observed to lose weight rapidly. There seems to be a change in slope in the weight loss curve at around 750 h of aging, possibly signifying a change of degradation mechanism. Typically, the weight loss data for neat polymer specimens are normalized with respect to the specimen surface area, since oxidative weight loss occurs from losses on exposed surfaces and edges of the specimen. Note that carbon fibers have an extremely large surface area due to their small diameter (typically 4–8 μm) and large aspect ratio (typically >1,000).

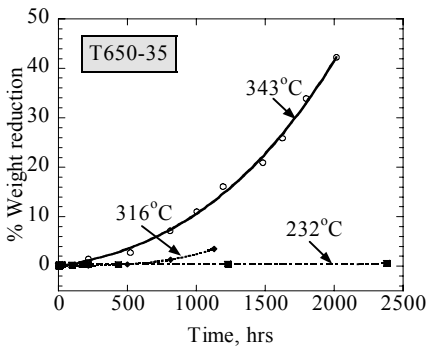


Fig. 9.2. Weight loss of T650-35 carbon fiber as a function of aging temperature

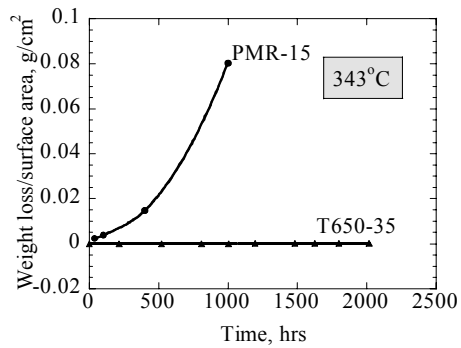


Fig. 9.3. Normalized weight loss of T650-35 fiber and PMR-15 resin

Figure 9.3 shows a comparison of the normalized weight loss of T650-35 carbon fiber and PMR-15 neat resin at 343°C. Note that the normalized fiber weight loss is almost negligible compared to that of neat resin over the entire 2,000 h of aging time. Thus, even though the carbon fiber loses a significant weight fraction with aging at elevated temperatures, the weight

loss normalized by the fiber surface area is negligible compared to that of the resin. Weight loss studies on sized fibers [105] indicate that the sizing/coupling agent is released within a short time period (~24 h) of aging beyond which the weight loss trend is similar to the corresponding unsized fibers.

Mechanical properties

Single fiber specimens were tested at room temperature in tension using the single-filament test. Figures 9.4 and 9.5 show the normalized failure strength and failure strain, respectively, of unsized T650-35 carbon fibers aged at 343°C. The strengths and failure strains are normalized with respect to their corresponding unaged values, such that the observed decreases are a reflection of the reduction resulting from isothermal aging. A minimum of ten fibers were tested for each condition considered, and the standard deviation is shown as the error bar across the measured mean values. There is some scatter in the strength and failure strain data which is typically encountered in single fiber testing as failure is sensitive to the presence of flaws over the fiber gage length. Fibers aged at the elevated temperature of 343°C show a large decrease in the strength after 1,000 h of aging. The significant decrease in mechanical strength signifies that the carbon fibers should not be treated as static entities when composites containing these fibers are aged at this temperature for extended periods. However, the reported data are a worst case scenario in which all surfaces of the fibers are exposed during aging. In situ fibers of the composite have only a small fraction of their total surface area exposed to the oxidizing environment and should, therefore, suffer less degradation. Further, test data from single-filament testing [105] indicate that application of fiber sizing may

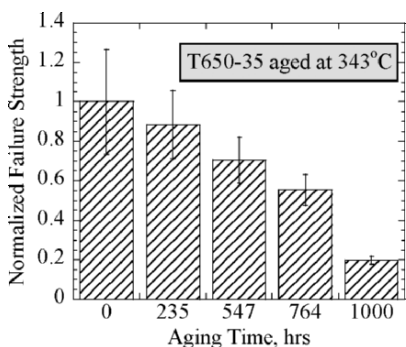


Fig. 9.4. Normalized strength of unsized T650-35 carbon fibers aged at 343°C

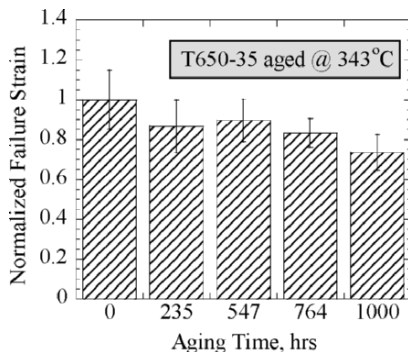


Fig. 9.5. Normalized failure strain of unsized T650-35 fibers aged 343°C

result in an improved performance of the carbon fiber in the unaged condition but could result in some loss of mechanical performance after aging at elevated temperatures. Failure is sensitive to the presence of flaws, and it is likely that the sizing/coupling agent on the fiber helps to decrease the influence of the fiber surface flaws resulting in a slightly better performance in the unaged condition.

Surface characterization

Scanning electron microscope (SEM) microstructural studies were conducted to determine the carbon fiber surface morphology changes during long-term isothermal aging. Figure 9.6a compares the SEMs of unsized T650-35 carbon fiber in the unaged condition with that of the fiber aged for 1,052 h at 343°C in Fig. 9.6b. No significant visible damage or surface morphology changes are observed, although some minimal amount of pitting is visible on the previously smooth fiber surfaces after 1,052 h of aging. Thus, the fiber surfaces provide little indication of the deterioration in the mechanical performance of the aged fiber.

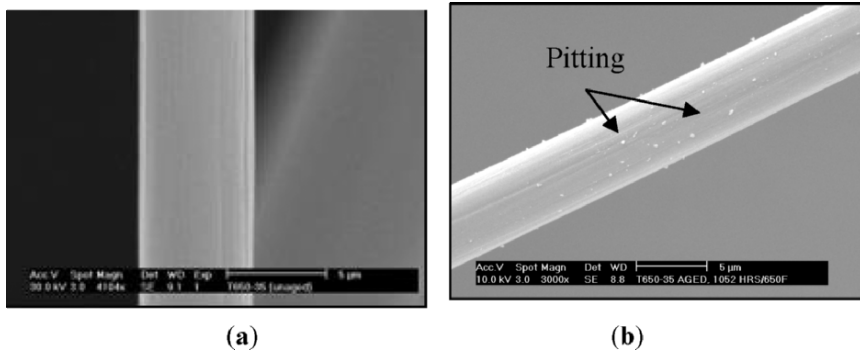


Fig. 9.6. SEMs showing surface morphology of unsized T650-35 carbon fibers in (a) the unaged condition and (b) aged for 1,052 h at 343°C

Anisotropic diffusivity

It has been established that the fibers account for only a minimal amount of the total weight loss for HTPMCs. However, the role of fibers in the composite oxidation process, in particular their role in transporting oxygen into the composite, is not fully understood. Extruded PAN carbon fibers exhibit a preferred orientation in which the graphitic layers may extend for thousands of angstroms and extend straight for hundreds of angstroms parallel to the fiber axis providing high-strength and high-stiffness along

the fiber axis direction. The mechanical (stiffness and strength) and thermal (coefficient of thermal expansion [52] and thermal conductivity [51]) properties of these oriented PAN-based fibers are highly anisotropic in nature. Typical density values of these fibers range between 1.75 and 1.86 g cm⁻³ and a porosity of approximately 15% with most of the porosity appearing in needle-shaped forms with axes of the needles parallel to the fiber axis [77]. Therefore, it follows that the diffusivity of the fibers will likely be anisotropic in nature. Unfortunately, experimental measures of carbon fiber diffusivity have not been obtained.

Numerous researchers have attributed the anisotropic diffusivity of unidirectional laminates to the preferential oxidation along the fiber–matrix interface or along the interphase region. However, the interphase region is a very small-volume percentage of the composite and a very small area fraction of the surface area. It is questionable that the diffusion of oxygen through and subsequent oxidation of the interphase region by itself can have such a significant effect on the composite oxidation process. More likely, the rapid oxidation rate along the fiber length indicates that, in addition to diffusion of oxygen from the specimen surface to the oxidation front, the interphase region has a supplemental oxygen path or source. Two possible mechanisms or scenarios for the supplemental oxygen source to the interphase are being investigated. Firstly, if oxidation in the interphase region leads to early fiber–matrix interface debonds, the debonds provide a pathway for oxygen to penetrate deeper into the composite. Knowing that there are residual curing stresses at the fiber–matrix interface, it is likely that such a scenario would entail the interface debond propagating along with the oxidation front. The second scenario is that the oxygen diffuses into the composite along the fiber and to the fiber–matrix interface at a rate much greater than through the neat resin or interphase. Based on the anisotropic oxidation behavior of unidirectional composites, the axial diffusivity of the fibers would have to be much greater than the diffusivity of the resin. Unfortunately, quantitative measures of the diffusivity of carbon fibers are lacking. Although one might anticipate that the bulk diffusivity of carbon is representative of that of the PAN fibers, this would only be the case if the morphology of the fibers and bulk carbon match, which in general is not the case.

For unit cell modeling of the diffusion behavior of unidirectional composites, the diffusivity of the resin, the interphase, and the fiber constituents must be defined. Only the diffusivity of the resin phase can be defined with any certainty due to lack of experimental data on the diffusivity of the

fiber and interphase. Therefore, the role and the relative contribution of the fiber and the interphase to the effective diffusivity cannot be rigorously determined.

9.2.2 Neat Resin Behavior

The attributes of the oxidation process of high-temperature polymers and polymer composites vary depending on the chemistry of the polymers being tested. The high-temperature aging behavior of several neat polymer resins and their composites has been studied [1, 10, 13, 14, 26, 37, 38, 53, 64, 65, 95, 113]. In PMR-15, the oxidized material near the specimen's free surfaces is observed to have a darker appearance than the unoxidized interior using bright-field light microscopy. Recent studies [19, 28, 63, 78, 90, 119] document the growth of the thermooxidative layer and the changes in elastic moduli and chemical composition resulting from isothermal aging. It has been observed for PMR-15 that the polymer degradation occurs mainly within a thin surface layer that develops and grows during thermal aging. Ripberger et al. [78] reported an oxidation layer thickness of approximately 55 μm after 50 h aging and a layer thickness of between 107 and 129 μm after 342 h of aging for PMR-15. Additionally, the interior core of the specimens (specimens greater than 2 mm thick) is generally protected from oxidative degradation during thermal aging and is relatively unchanged after aging.

In this work, for both the neat polymer and composite specimens that are used to monitor the propagation of oxidation, samples are dry-sectioned from aged larger specimens, as shown in Fig. 9.7, potted in 828-D230 epoxy resin, and cured at room temperature for 3 days. This sectioning procedure allows monitoring of four of the exposed free surfaces of the large specimen. The large specimens are subsequently placed back in the oven to continue the aging process. The diamond blade used to section these

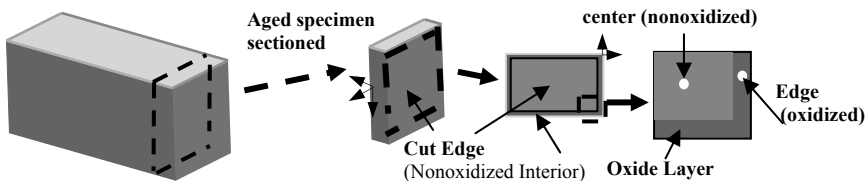


Fig. 9.7. Oxidation measurement procedures

samples is washed with acetone and wiped clean with paper towels prior to cutting to minimize the amount of contamination from the cutting wheel. The specimens are then wet-sanded with 600-grit sandpaper and distilled water and polished using a 0.3- μm alumina polishing media. Since the oxidized layer forms on all exposed free surfaces and propagates to the interior of the sample, the oxidized region is easily seen in the cross section. These potted specimens are used for both nanoindentation testing (MTS Nanoindenter XP) and optical and dark-field microscopy (Nikon Microphot-FXL, Model F84006) measurements. The MTS Nanoindenter has an X–Y positional stage with a resolution of 0.5 μm and a force resolution of 50.0 nN. The reported transitional resolution for the Nikon positioning stage is 1.0 μm . A Philips XL30 ESEM with energy dispersive spectroscopy (EDS) analysis capabilities is also used to examine the damage and the chemical state of the aged composite specimens.

Figure 9.8 shows a photomicrograph of a PMR-15 neat resin specimen isothermally aged in ambient air at 343°C for a period of 196 h. The figure clearly shows the oxidized region (much like a picture frame) on the two adjacent exposed free surfaces of the specimen. Between the outer oxidized layer and interior unoxidized region is a transition region, which is the active “reaction” or “process” zone. These observations allow easy measuring and characterization of the oxidized layer and the transition

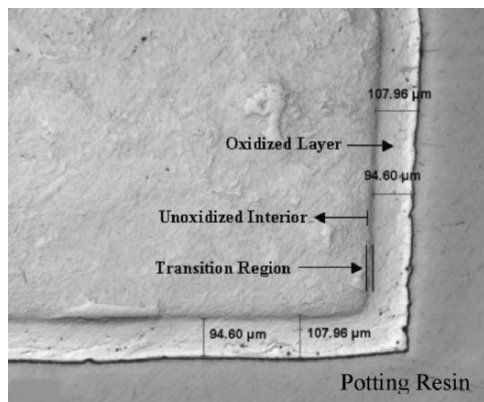


Fig. 9.8. Photomicrograph of PMR-15 resin after 196 h of aging at 343°C showing oxide layer formation, transition region, and unoxidized interior

regions as a function of aging temperature and time. Figure 9.9 shows the evolution of the oxidized layer and the active “reaction” zone thicknesses as a function of aging time. Within the first hour, an oxidized layer 11.0 μm thick forms on the exposed specimen surfaces. The thickness of the oxidized layer is seen to approach a plateau value as the oxidation growth rate reduces considerably for longer aging time periods, whereas the thickness of the active “reaction” zone remains nearly constant for the aging times considered.

PMR-15 samples aged in air were also evaluated using a nanoindenter by scanning across the oxidized layer, through the active “process” or “reaction” zone, and into the unoxidized central area of the specimen. The indentations were spaced so as to give a minimum of three data points within each region. These measurements were repeated at several locations around the perimeter of the oxidized sample.

Figure 9.10 shows the variation of elastic moduli from three individual scans as a function of distance from the specimen’s edge for a specimen aged in air for 196 h at 343°C. The data are normalized to the modulus of the unaged material as determined by nanoindentation. Scatter exists in the data as a result of sampling through different regions of the specimen. This figure illustrates the spatial variability and the heterogeneous nature of the oxidation formation. In general, the modulus of the material in the oxidized region is higher toward the outer exposed surface than it is near the inner reaction zone. The modulus increase in the oxidation zone is consistent with embrittlement of the oxidized region.

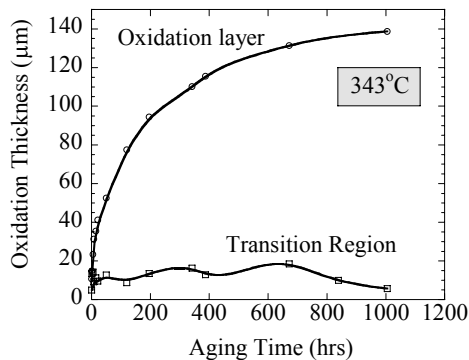


Fig. 9.9. Evolution of oxidation layer and transition region thickness with aging time

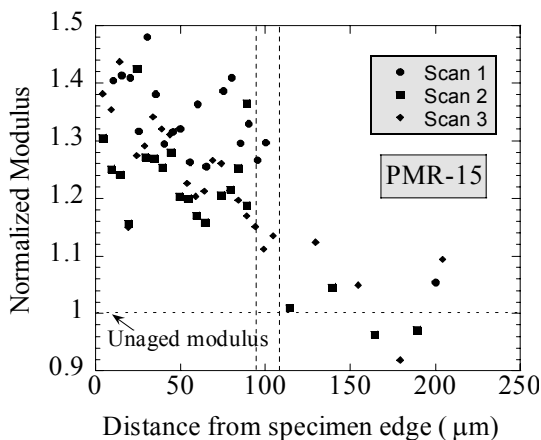


Fig. 9.10. Normalized modulus of PMR-15 resin after 196 h of aging at 343°C

Based on optical observations, the three distinct specimen regions are identified in Fig. 9.10 as the higher modulus oxidized surface layer, the lower modulus unoxidized interior, and the reaction zone or transition region in which the modulus reduces from the oxidized to unoxidized values. The average thickness measurements of oxidized zones and the transition zone, as obtained from optical measurements, are plotted as dotted vertical lines in Fig. 9.10. It is observed that the average thickness of the oxidation layer and active “reactive” zone measured by optical methods is in good agreement with the boundaries of three regions suggested by the nanoindentation data. Similar observations were made by Johnson et al. [50] using atomic force microscopy (AFM). They summarized that the outer “plateau” region is a homogeneous oxidized layer, which is a result of a zero-order reaction. The transition reaction zone is a diffusion-controlled oxidation zone, which is a result of a first-order reaction, and the third region in the specimen interior is the unoxidized PMR-15.

Figure 9.11 shows the average elastic moduli of the oxidized region and the unoxidized interior of PMR-15 specimens aged at 343°C as a function of aging time [78]. In addition, the average elastic moduli of a PMR-15 specimen thermally aged in a nonoxidizing environment is shown in the figure. The reported average values of all the moduli measurements made within their respective regions include data from multiple scans. There is only a marginal increase in the modulus of the oxidized layer with aging time, as seen in Fig. 9.11. Thus, once the material oxidizes, little change in material modulus occurs with aging time.

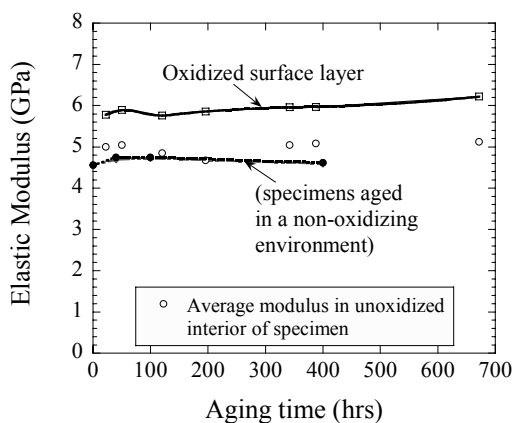


Fig. 9.11. Variation of elastic moduli with aging time

The open circle data points in Fig. 9.11 are the average modulus values in the interior, i.e., in the unoxidized region, for the specimens aged in air. These measurements are in good agreement with the elastic modulus of neat resin specimens aged in a nonoxidizing environment. Because the oxidation process is diffusion limited, the interior of the aged specimens is not oxidized and has properties similar to that of the specimens aged in a nonoxidizing or inert environment. These results, therefore, validate the assumptions of Tsuji et al. [113] that the properties of the specimens aged in a nonoxidizing environment can be taken to be similar to the properties of the unoxidized core material in the air-aged specimens.

Oxidation of the surface layer typically leads to a decrease in local density and a weight loss (due to outgassing of oxidation byproducts) both of which contribute to the shrinkage of the oxidized layer generating tensile stresses and possibly “spontaneous” cracks [14, 29, 38, 63, 78]. For PMR-15 neat resin specimens aged in air at 343°C, surface cracks in the outer oxidized layer begin to appear after 200 h of aging. These crack faces provide additional diffusion surfaces, create pathways for oxidants to penetrate deeper into the material, and accelerate the material degradation and growth of the oxidation layer [78].

Figure 9.12 shows the measured crack density as a function of aging time. The crack density is computed by dividing the total number of cracks formed on the sample edges at a given cross section by the specimen’s perimeter. As one would expect, crack density increases with aging time. Beyond 800 h of aging, the severe degradation makes the crack density too complex to quantify. Figure 9.13 shows that, after 342 h of aging, crack depths have already reached 263 μm into the surface of the polymer. The

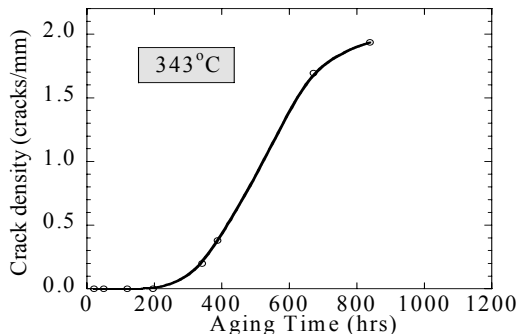


Fig. 9.12. Measurement of surface crack density for specimens aged in air

photomicrograph suggests that the cracks formed in several steps (primary, secondary, and tertiary cracks). As the cracks propagate into the surface and widen, new oxidative surfaces form around the crack front and subsequent cracking occurs. Thus, oxidants are able to penetrate further into the sample through extensive cracking.

Figure 9.14 illustrates severe oxidation damage observed in PMR-15 neat resin specimens after 670 h of aging in air at 343°C. Note the appearance of voids in the oxidized layer with a larger concentration near the surface. The voids form because inward diffusion of oxygen is slower than outward diffusion of degradation byproducts [63].

While optical microscopy techniques are successfully used to monitor oxidation in PMR-15 resin, the same is not true for other polyimide systems, such as the recently developed AFR-PE-4 resin, because the optical characteristics of the polyimide do not change when it is oxidized. Other techniques, such as dark-field imaging [95], polarized light microscopy,

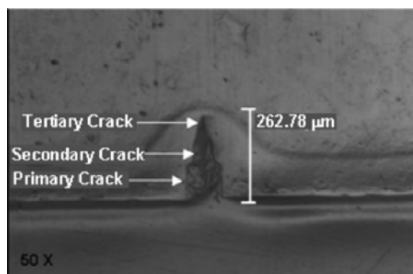


Fig. 9.13. Crack penetration depth after 342 h of aging in air at 343°C

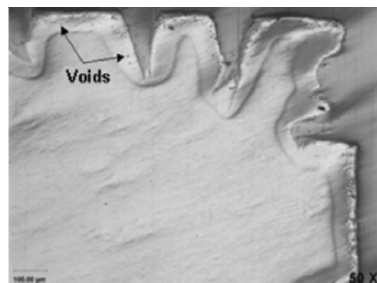


Fig. 9.14. Damaged PMR-15 from isothermal aging at 343°C for 670 h

and scanning electron microscopy in backscatter mode [63], were also used without successfully being able to optically view the oxidation layer [79]. This challenging problem motivated the use of surface analysis techniques, such as XPS and FTIR, in an attempt to detect changes in surface chemistry as a means to monitor oxidation development. Although these surface analysis techniques are able to detect increased concentrations of oxygen in the surface regions of aged specimens, the techniques are not sensitive enough to provide a quantitative measure of the extent of oxidation. Therefore, changes in the moduli, as measured by nanoindentation scans, are used to provide a quantitative measure of the degree of oxidation and monitor the propagation of the oxidation.

9.2.3 Composite Behavior

The anisotropic oxidative response of PMCs was first documented by Nelson [67] when he observed that the oxidation process is sensitive to the surface area for the different test specimen geometries that he investigated. He found that the dominant degradation mechanism for the graphite/polyimides is oxidation of the matrix at the laminate edges. Additionally, the materials degraded preferentially at the specimen surface perpendicular to the fiber (axial surface) and the rate of oxidation is hastened by microcracks opening on the axial surface increasing the surface area for oxidation. The anisotropic nature of oxidation in HTPMCs has also been observed by numerous other investigators including the works of Nam and Seferis [66] and Skontorp [95]. Although it is well documented that unidirectional composites preferentially oxidize in the fiber direction [11, 66, 67], details of the rate of oxidation propagation in the orthogonal directions of unidirectional composites are not well documented. There is also substantial evidence that, for woven composites, the oxidation preferentially advances in the in-plane direction along the fiber paths [20]. The oxidation in the transverse direction (normal to the specimen's top and bottom or tool surfaces) is typically constrained by the presence of the fibers.

When testing a T650-35/PMR-15, 8-harness, satin-weave graphite fiber material, Bowles [9] observed two types of surface degradations. Higher temperature aging (288–316°C) results in the formation of a light-colored surface layer that propagates into the material causing voids and microcracks to initiate and grow within the surface layer. At temperatures lower than 288°C, specimens show the same advancement of voids and microcracks into the surface but the oxidized light band of matrix material is not visible. That is, at lower temperatures, oxidation does not cause a visible change in the color of the polymer.

Composite oxidation is primarily a surface reaction phenomenon controlled by the diffusion and rate of reaction of oxygen with the material so that surfaces with different microstructural characteristics are expected to exhibit different oxidation behavior due to differences in diffusivity. Resin cure shrinkage and mismatches in the coefficient of thermal expansion of the fibers and matrix during the composite cure process give rise to localized micromechanical residual stresses in the fiber–matrix interphase region. The diffusion process in materials has been shown to increase with increasing stress levels even becoming nonlinear, as a function of stress, for materials with linear mechanical behavior [122]. Therefore, the highly stressed fiber–matrix interphase regions tend to oxidize at an accelerated rate compared to the lower stressed matrix phase of the composite.

Additionally, the local stoichiometry of the resin may be altered in the fiber–matrix interphase region by the presence of glass fiber-reinforced coupling agents or graphite fiber-reinforced sizing agents. Woven and braided preforms require the use of a fiber coupling or sizing agents to protect the fibers from damage during the weaving and braiding process. Owing to the significant use of woven fiber prepreg and preforms in HTPMC applications, the proper selection of fiber sizing is of paramount concern. The presence of the sizing can have a strong influence on the fiber–matrix interphase or interfacial properties [17, 70, 114] and can ultimately affect the local diffusivity and/or thermal-oxidative stability.

Using the notation of Bowles and Nowak [12], three different types of composite surfaces can be defined for unidirectional composite specimens as S_1 = area of nonmachined resin-rich surfaces (top and bottom or tool surfaces), S_2 = area of surfaces cut parallel to fibers, and S_3 = area of surfaces cut perpendicular to fibers. For woven composites, three different surface types can be similarly defined as Σ_1 = area of nonmachined resin-rich surfaces, Σ_2 = area of surfaces cut perpendicular to warp fibers, and Σ_3 = area of surfaces cut perpendicular to fill fibers. Figure 9.15 illustrates the surface area types for both the unidirectional and woven composites.

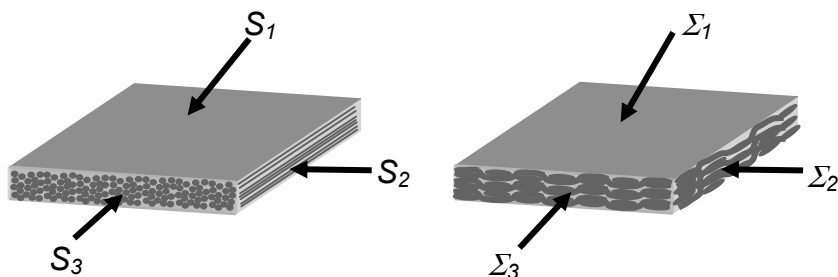
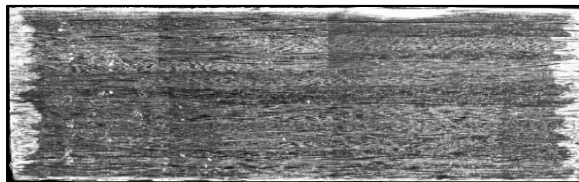


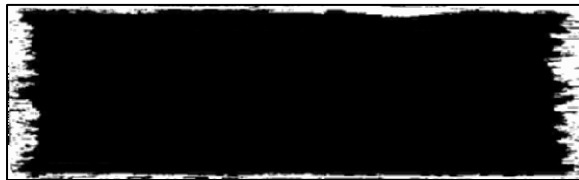
Fig. 9.15. Types of surface areas for unidirectional and woven composites

Dark-field microscopy [95] is used to monitor the oxidation propagation rates in both the axial direction (along the fiber) and the transverse direction (transverse to the fibers) of unidirectional G30-500/PMR-15 composites aged in air at 288°C. Test specimens are removed from the aging oven at specified times, and a small cross section of the specimen is cut off and mounted in an epoxy plug for polishing, as illustrated in Fig. 9.7. The original specimen is then placed back into the oven until the next specified aging time.

Figure 9.16 shows (a) the original stitched micrograph and (b) an enhanced micrograph that clearly distinguishes the white oxidized material from the black unoxidized material. The oxidation layer appears as a frame around the composite specimen just as seen in aged neat resin PMR-15 samples in Fig. 9.8. The specimen aged for 197 h is shown to have only minimal oxidation transverse to the fibers, but has moderate oxidation development in the axial direction. The method of enhancing the micrograph consists of constructing (using Adobe Photoshop® 7.0) a complete image of the entire composite by stitching together individual micrographs using standard light microscopy in the grayscale mode. Once the image is constructed, the apparent light-oxidized region is best fit in the lab mode to a pure white, specified as having a lightness value of 100, while the remaining unoxidized regions of the image are given a lightness value of zero. Thus, this image processing creates exactly two distinct grayscale colors: black and white.



(a)



(b)

Fig. 9.16. (a) Array of eight stitched photomicrographs of oxidized specimen cross section and (b) enhanced micrograph of the specimen cross section

Figure 9.17 shows enhanced micrographs of G30-500/PMR-15 unidirectional composites after 407, 1,200, and 2,092 h of aging at 288°C that clearly show that oxidation substantially increases in both the axial and transverse directions with aging time. Next, the overall level of oxidation is quantified by measuring the percentage of the specimen cross-sectional surface area that is oxidized. Using the constructed enhanced micrograph image, a histogram of the image is used to determine the ratio of white to black pixels and the ratio is used to quantify the amount of surface area of the composite cross section that is oxidized. Quantification of the oxidation area using this process is a two-dimensional computation and does not account for stochastic variations of the oxidized cross section through the thickness of the specimen.

Figure 9.18 shows the average of the extent of the axial oxidation along the fiber direction as a function of aging time at 288°C. The figure also includes the average of the extent of the transverse oxidation from the enhanced micrographs. Figure 9.18 shows the dominance of the axial oxidation degradation as compared to the transverse degradation in composites which is attributed to the higher effective diffusivity on the S_3 surfaces. Figure 9.19 compares the oxidation growth in the transverse direction (from S_1 surface) of the composite to the oxidation growth in neat resin PMR-15. It appears that the presence of fibers may initially retard growth of oxidation in the transverse directions. Figures 9.18 and 9.19 show the significant differences between the oxidative behavior of the constituents and the composite owing to the fiber–matrix microstructure that may cause increases in diffusion and reaction rates.

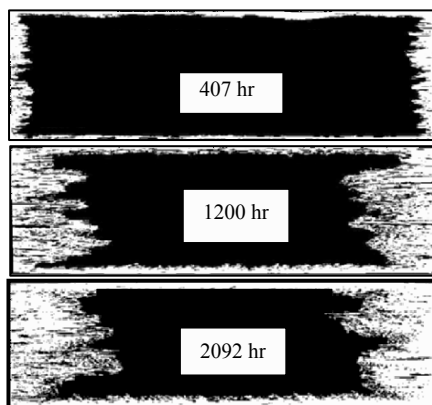


Fig. 9.17. Unidirectional G30-500/PMR-15 at 407, 1,200 and 2,092 h of oxidation at 288°C

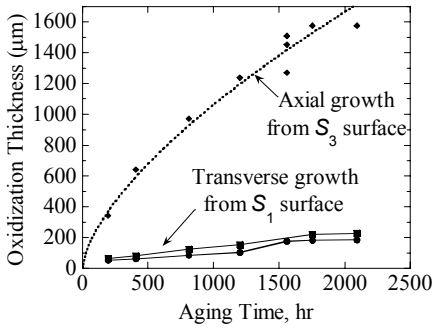


Fig. 9.18. Comparison of oxidation growth in S_1 and S_3 directions of composite

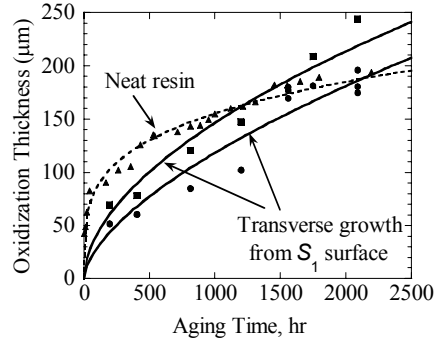


Fig. 9.19. Comparison of oxidation growth in S_1 direction of composite and in neat resin PMR-15

A Philips XL30 environmental scanning electron microscope (ESEM) is used to document and characterize the surfaces of the aged specimens. Figure 9.20 shows the photomicrographs of polished cross sections of axial surfaces S_3 for both nonoxidized and oxidized specimens of the PMR-15 unidirectional composites. It is commonly known that, when composite specimens are polished for imaging, the stiffer fibers wear at a slower rate than the parent matrix, leading to topographic differences between the fibers and the surrounding matrix. For the oxidized specimen (Fig. 9.20b), oxidative degradation of the fibers exacerbates the uneven polishing or rounding of the fibers as compared to the nonoxidized specimen shown in Fig. 9.20a. The PAN-based G30-500 fiber has a typical skin-core structure in which crystalline sheets are oriented radially in the skin but form a random granular-like structure in the core [71]. This construction of the fiber's cross section is not expected to polish evenly.

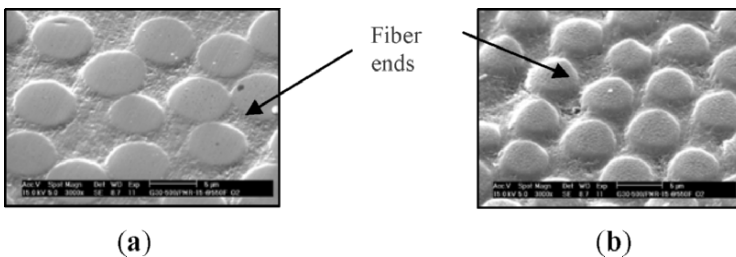


Fig. 9.20. SEM micrograph of the specimen cross section in (a) nonoxidized and (b) oxidized region of the composite

Development of damage at the fiber-matrix interface

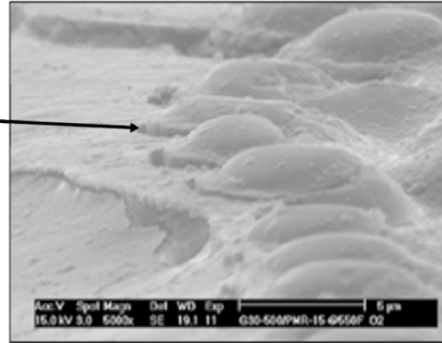


Fig. 9.21. Debonding at fiber-matrix interface at the oxidized fiber end

Higher magnification of an oxidized axial surface, as seen in Fig. 9.21, shows details of the rounding of the oxidized fibers and the opened interfacial fiber-matrix cracks [80].

In Fig. 9.22, a high magnification view of a transverse cross section S_2 for a specimen aged in air at 288°C for 2,092 h shows significant fiber-matrix debonding indicative of that shown in Fig. 9.21. Additionally during sectioning and polishing, the PMR-15 matrix resin fragmented in the highly oxidized regions. Figure 9.23 shows cracking on the axial S_3 surface that included both fiber-matrix debonding and matrix cracking that progressively open during the aging process. The fiber-matrix debonds that are evident on both the axial and transverse sections are a result of mass loss, shrinkage, and increased brittleness of the resin due to oxidation. The cracks provide added surfaces and pathways for oxidants to penetrate deeper into the composite during aging. Therefore, once cracking initiates on the axial surface at the fiber-matrix interface, an acceleration of the degradation occurs.

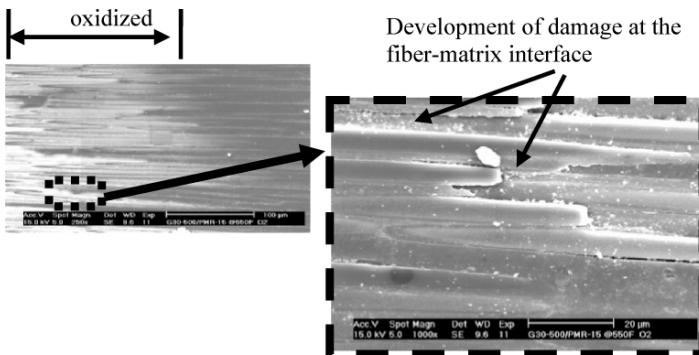


Fig. 9.22. Debonding/delamination at fiber-matrix interface in unidirectional composite

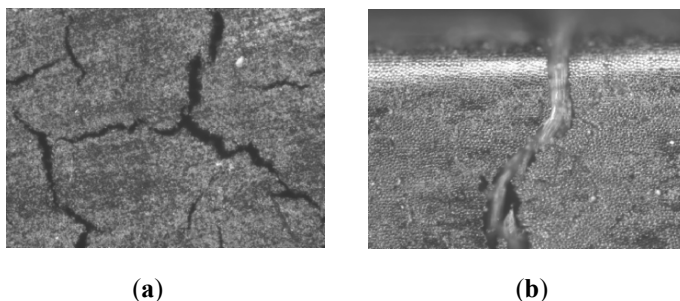


Fig. 9.23. Photomicrographs of axial surface S_3 of a unidirectional specimen aged for 1,864 h at 288°C showing (a) matrix cracking perpendicular to fiber ends and (b) close-up view of a matrix crack providing pathway for enhanced diffusion

9.3 Accelerated Aging/Oxidation

Accelerated aging methods are needed to evaluate materials which are to be used under long-term exposure to elevated temperature in oxidative environments. The need for accelerated test methods for HTPMCs is manifested in the requirement to characterize these materials for their expected service life which can be several thousands of hours. The cost of aging these materials for this extended period is often prohibitive. A good accelerated test method neither introduces extraneous damage/degradation mechanisms nor omits any actual mechanisms at its use temperature. Moreover, the method must be validated by comparing mechanical properties, damage modes, and physical aging parameters, such as weight loss, with those from specimens tested under real-time conditions. Since the use temperature of HTPMCs is often near the glass transition temperature of the material, the ability to accelerate aging by increasing the temperature is limited. The use of pressure to accelerate the oxidative aging process is used in the aircraft engine community based in part on the fact that engine parts experience elevated pressures during use. Other conditioning factors reported in the literature include aging in different gaseous environments, aging under load, exposure to ultraviolet radiation, and exposure to moisture. An extensive assessment of accelerated test methods conducted for the HSR program is found in the HSR Materials Durability Guide [2, 41].

The only way to know if an aging mechanism can be properly accelerated is to identify and understand the mechanism and how it will be affected by acceleration [41]. Although we do not fully understand the oxidation mechanism in HTPMCs, we can determine some of the functional relationships that govern aging. For example, elevated pressure aging should not change the oxidative chemical mechanism but should accelerate it.

The acceleration of aging would be a result of increased transport of the oxygen to the interior of the specimen. Since the oxidation process is not reaction rate limited but diffusion rate limited, the elevated pressure would effectively increase diffusion rate, thereby accelerating the oxidation process. Specimens subjected to accelerated aging conditions will not necessarily have the same degradation state as specimens aged in standard conditions. This is evidenced by the fact that the elevated pressure aging specimens have a significantly greater oxidation layer thickness [103] than the ambient pressure-aged specimens. The accelerated aging test must be accompanied by analysis methods to relate the nonaccelerated aging data to the accelerated aging data. These analysis methods and tools will provide capabilities to predict the performance of the material in more general service environments.

9.3.1 Elevated Temperature Aging

Thermally activated rate processes are typically accelerated by increasing temperature. Acceleration by temperature occurs by reducing the activation energy of chemical bond rupture in the polymer macromolecule. Unfortunately, elevated temperature may promote degradation processes that do not occur at application temperatures. Temperature can also affect the rate of degradation by increasing the thermal stress in polymer composites caused by differences in the thermal expansion coefficient of the constituents.

A series of tests was conducted on two carbon/epoxy systems by Tsotsis [108, 109] and Tsotsis and Lee [110] to assess key factors in the characterization of the thermooxidative stability of composite materials. Mechanical properties were determined from specimens aged in air at 177°C up to several thousand hours. After 1,000 h at different temperatures, differential scanning calorimetry (DSC) as well as glass transition temperature T_g measurements suggest that higher aging temperatures lead to more highly crosslinked microstructures which may not be representative of actual aging at use temperatures. Aging below, but near the T_g , gives degradation rates that are nonlinear with respect to temperatures, thereby making estimates of useful lifetimes difficult at best.

Recent work by Ripberger et al. [78] and Tandon et al. [103] also examines the use of elevated temperature to accelerate the rate of thermooxidative degradation in PMR-15 resin. While the oxidized layer thickness is similar for all of the aging temperatures up to approximately 1,000 h, as shown in Fig. 9.24, the effect of elevated temperature on the weight loss

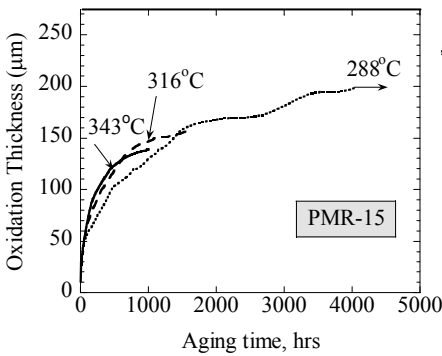


Fig. 9.24. Influence of aging temperature on the oxidation layer growth

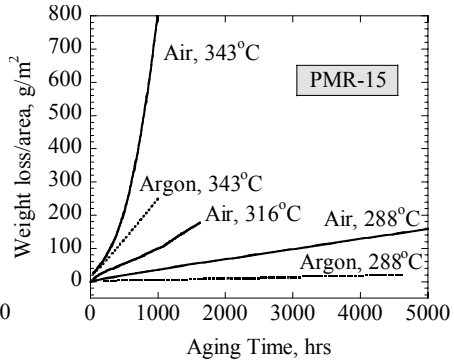


Fig. 9.25. Oxidation weight loss for air- and argon-aged neat resin PMR-15

is not similar. For the specimens aged at 288°C, which is near the use temperature, the majority of the weight loss is due to oxidation since the weight loss in an inert argon environment at 288°C is small. However, for specimens aged at 343°C, a substantial weight loss percentage is attributed to the nonoxidizing thermal aging (aging in an inert argon environment), as shown in Fig. 9.25. The aggressive 343°C aging temperature is near the glass transition temperature of the material. Thermal aging in an inert environment is believed to involve chemical changes associated with chain scission reactions, additional crosslinking, or reduction of crosslink density, etc., that can result in changes to the molecular weight of the polymer, altering the physical and mechanical properties. Thus, there is likely a change in the thermal aging mechanism between the specimens aged at 288 and 343°C. Therefore, one needs to be extremely careful in accelerated aging by elevating the temperature above the use temperature since the materials already operate near the T_g and one must be certain that the aging mechanisms do not change at the elevated temperature or be able to account for any changing mechanisms.

9.3.2 Elevated Pressure Aging

The rate of oxidation is sensitive to the partial pressure of oxygen at the composite surface and acceleration can be achieved by increasing the partial pressure of oxygen within the aging chamber. Increasing the partial pressure of oxygen can be achieved in one or two ways. First, the partial pressure of oxygen can be increased by increasing the mole fraction of oxygen in the

aging chamber. For example, pure oxygen (O_2) can be used instead of ambient air. However, the use of pure oxygen in a high-temperature aging chamber may be a safety concern. Second, the partial pressure of oxygen in air can be increased by increasing the total pressure since the partial pressure of oxygen is directly proportional to the total air pressure. By studying the dependence of the flexural strength of glass-reinforced epoxy resin on temperature and oxygen pressure, Ciutacu et al. [25] demonstrated the importance of oxygen pressure as an accelerating factor in thermo-oxidative degradation. The results showed that the same thermo-oxidative degradation mechanisms for glass-reinforced epoxy resin occurred both in air and oxygen, at the pressure and temperatures used.

Subsequent studies conducted by Tsotsis et al. [111, 112] demonstrated that higher pressures of air or oxygen tend to increase the rate of degradation of polymeric composites. The methodology proposes augmenting elevated temperature aging with elevated pressure to accelerate the rate of thermo-oxidative degradation. The test results showed a distinct accelerating effect with the use of elevated pressures especially for the tensile shear AS4/3501-6 coupons. The results also suggested that elevated pressure may be a good tool for significantly reducing screening times for materials that will be subjected to long exposure in oxygen-containing environments at elevated temperatures.

Recent work by Tandon et al. [103] examined the use of elevated pressure in conjunction with a realistic use temperature to accelerate the rate of thermo-oxidative degradation in PMR-15 resin. Neat resin specimens were isothermally aged over a range of time periods in a pressure chamber (see Fig. 9.26), with a continuous supply of pressurized air, and placed inside an air-circulating oven at an elevated temperature. Unlike a sealed closed chamber in which the oxygen supply is depleted for long-aging

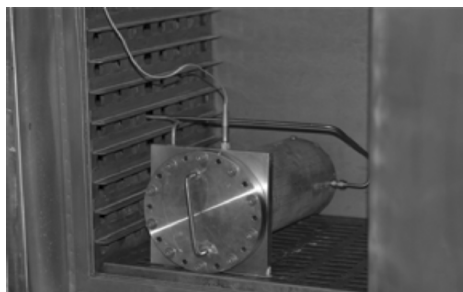


Fig. 9.26. Elevated pressure aging chamber placed inside the oven

times, the chamber maintains a target pressure while replenishing the air. Steel tubing attached to regulated house air (with two in-line desiccators) delivers a continuous supply of dry air and maintains a constant pressure of 0.414 MPa (60 psi). The second desiccator contains a purifier that removes any contaminants and impurities with an effective molecular diameter of more than 5 Å from the dry air before it enters the pressure chamber.

It is observed that the elevated pressure aging of the PMR-15 neat resin presumably has a significant effect on the rate of diffusion of oxygen into the specimen, accelerating the oxidation process and allowing the oxygen to diffuse deeper into the interior of the specimens. This results in greater oxidation layer thicknesses than are achievable in ambient air pressure environments as shown in Fig. 9.27. The effect of aging in 0.414 MPa (60 psi) pressured air further results in nearly a twofold increase in the rate of volume change and increases the weight loss rate of neat resin specimens by approximately a factor of 2 (see Fig. 9.28). Further, mechanical testing reveals that the specimens aged in the pressurized air environment have by far the lowest failure strain and that the strength reduction rate is large for short-aging times, as shown in Fig. 9.29. Since the oxidation process in PMR-15 resin is diffusion limited vs. reaction rate limited, the oxidation process is accelerated by the pressure leading to significant increases in mechanical property degradation.

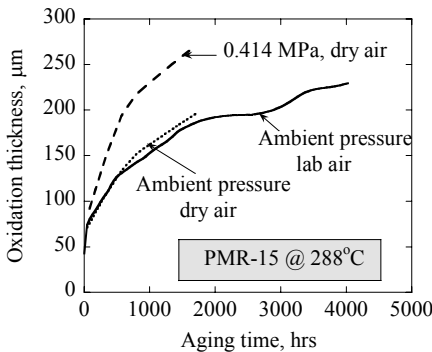


Fig. 9.27. Oxidation layer thickness for ambient and elevated pressure aging

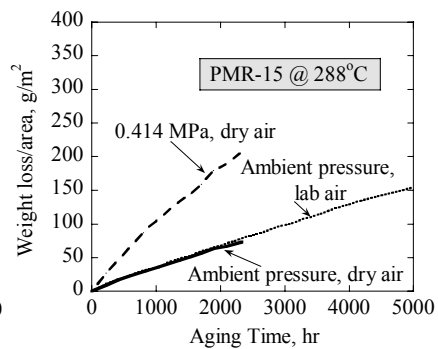


Fig. 9.28. Weight loss of ambient and elevated pressure-aged PMR-15 resin

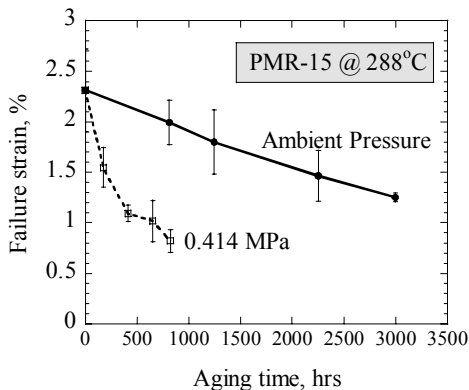


Fig. 9.29. Failure strain for specimens aged at ambient and elevated pressures

9.3.3 Stress-Assisted Aging

In a study by Bowles et al. [15], both unidirectional and crossply (± 45) PMR-15 laminates were isothermally aged at 288°C for up to 1,000 h. They found that the weight loss of the crossply laminates is much greater than that of the unidirectional laminates. The primary reason given for the greater weight loss in the crossply laminates is that free-edge cracks, resulting from interlaminar residual stresses, in the crossply laminates are much more prominent and result in more extensive advancement of oxidation into the interior of the composite. Therefore residual stresses, both at the fiber–matrix micromechanical level as previously discussed and at the ply level, play an important role in the degradation process. Residual curing stresses and mechanical load-induced stresses contribute to aging in several ways that include influencing chemical reactions and enhancing diffusion [81]. Stresses can accelerate chemical reactions that cause bond rupture, accelerate chain scission reactions, and alter activation energy for chemical reactions. Popov et al. [75] showed that residual stress and externally applied stress have exactly the same effect on oxidation rate. They further observed that oxidation may induce stresses locally and that these stresses may subsequently influence reactions.

The effect of mechanical stress on long-term thermal aging was investigated in NASA's HSR program [2]. It was observed that the addition of mechanical stress has an accelerating effect on changes in the glass transition temperature in IM7/K3B composites. However, after 10,000 h of aging at 177°C under a constant axial load (loaded to 3,000 $\mu\text{m}/\text{m}$ strain level), the axial stress applied during aging had little or no effect on aged,

unnotched tensile properties of quasi-isotropic layups for both IM7/K3B and IM7/PETI-5 composites. However, these findings cannot be generalized to other properties of the composites. Thermal aging primarily influences the matrix-dominated properties of composites, and the unnotched tensile strength of quasi-isotropic laminates is greatly influenced by the properties of the fibers aligned in the load direction.

To investigate the coupling effects of aging time, temperature, and stress, a low-cost pretensing fixture (inspired by the preload fixture design under the HSR program) was recently developed that allows thermal aging of neat resin specimens under applied load at elevated temperatures. A photograph of the test fixture is shown in Fig. 9.30. The specimen is securely tightened in between the two crossheads with the lower end kept fixed while the upper end is spring loaded to the desired stress level. The fixture assembly is then placed in the oven which is heated to the specified aging temperature, and the specimen is allowed to age for the specified time.



Fig. 9.30. Preload aging fixture for neat resin specimens

Figure 9.31 compares the total thickness of the oxidized region measured in toughened bismaleimide (5250-4) neat resin at 177°C for accelerated aging environments measured using the optical methods, as discussed earlier. Similar to the case of PMR-15 resin, aging under pressure (0.414 MPa (60 psi)) results in far greater oxidation zone thicknesses than are achievable in ambient air pressure environments. Additionally, using the tension aging test fixture shown in Fig. 9.30 (loaded to a stress level of 13.79 MPa (2 ksi)), results in a small increase in oxidation zone thickness at longer aging times compared to an unloaded specimen in an ambient lab air environment. The stress level of 13.79 MPa is chosen based on uniaxially tension-loaded specimens tested at 177°C to ensure that the mechanical response of the neat resin is limited to elastic behavior at the elevated temperature. The tensile strength of the resin reduces considerably under accelerated pressure aging, while only minor decreases are observed under stress-assisted aging when comparing the performance to ambient air pressure-aged specimens.

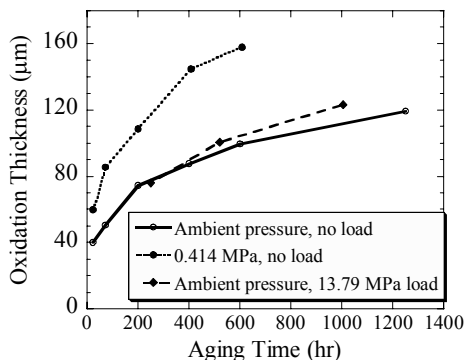


Fig. 9.31. Oxidation layer thickness for 5250-4 for accelerated aging conditions

9.4 Hierarchical Modeling

For effective design of aerospace components with HTPMCs, long-term stiffness and strength prediction and failure mechanism modeling is critical. A framework for hierarchical modeling of composite behavior from its constituent scale to its laminate scale, comprised of predictive models for the fiber(s), matrix, and interface/interphase long-term performance under aging conditions, is shown in Fig. 9.32. Although unit cell models have been used for the prediction of stiffness and strength of the composites, comprehensive unit cell scale constitutive behavior modeling of the HTPMCs under thermooxidation- and stress-induced damage evolutions is lacking.

As discussed previously, three major mechanisms drive age-related degradation of the polymeric matrix composite materials. They are (1) physical aging: creep and relaxation predominantly of the matrix and interphase, (2) chemical aging dominated by the thermooxidative degradation of the resin and the fiber–matrix interphase, and (3) micromechanical damage evolution and its effects on the constitutive and failure behavior of the material. While these effects have been studied for the neat resin in reasonable detail, the studies on composite behavior are nascent. Prediction of the mechanical behavior of HTPMCs under long-term thermomechanical fatigue and harsh environmental conditions requires rigorous simulation of physical aging and its effect on the viscoelastic behavior, the thermo-oxidative aging processes, and the damage evolution in the material constitutive behavior descriptions [53, 95, 120]. Several researchers, e.g., McManus and Cunningham [61], Wang and Chen [119], McManus et al.

[62], Schieffer et al. [87], Schoeppner and Curliss [88], and Colin and Verdu [27], have developed or are developing model-based design capabilities to predict the service life of the HTPMCs. Although mechanism-based models are preferred for predictive capability, when the primitive mechanisms are not understood, phenomenological models can be used. In this context, the relationship between the thermooxidative state of the polymers of interest and their mechanical properties is beyond current mechanistic modeling capabilities. Therefore, researchers rely on empirical correlations to describe the relationship between mechanical properties and aging history for HTPMCs.

The mechanism-based modeling approach, in which individual roles of constitutive materials and the fiber–matrix interface/interphase are recognized, is required to accurately represent the anisotropy of the physical aging, the diffusion and reaction kinetics, the stress-aging coupling, etc., to the level of fidelity required for predicting the performance and failure of HTPMC structures. Mechanism-based models whose aim is to model the relevant physics of the oxidation processes and degradation may be better suited than phenomenological models to predict the local spatial variation of the degradation state in structural components. In the same spirit as the hierarchical process shown in Fig. 9.32, McManus

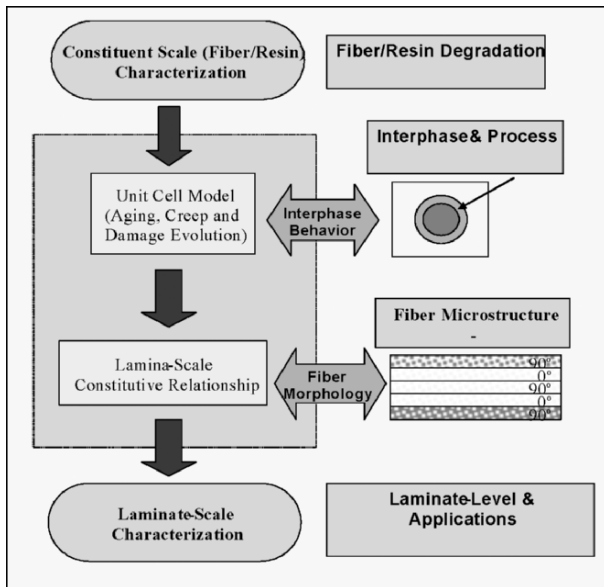


Fig. 9.32. Hierarchical modeling for long-term composite performance

et al. [62] and Schieffer et al. [87] presented approaches that model the various transport and degradation mechanisms at the appropriate geometric level. Using a micromechanical analysis, Schieffer et al. [87] predicted both the oxygen concentration profiles and the oxygen consumption through the thickness of unidirectional specimen by coupling diffusion kinetics and oxygen chemical reactions in the polymer. The model describes an oxygen concentration gradient in the oxidized layer that decreases from its maximum at the free surfaces of the composite laminate toward the interior of the specimen.

Additionally, simulations show that the volume variation of resin shrinkage in the oxidized layer is sufficient to initiate fiber–matrix interface debonding after only a few hours of aging. Micromechanical models, such as described by Schieffer et al. [87], can be coupled to three-dimensional ply-level analyses, e.g., [48], that are capable of modeling the spatial variability of degradation and accounting for the ply-level residual stresses that influence the oxidative degradation.

As shown in Fig. 9.33, a model that depicts the three essential aging mechanisms characterized by scalar state variables can be conceived. The physical aging, including its effect on creep/relaxation behavior, has been characterized by appropriate time–temperature–age shifting and is denoted by the ζ -axis. The thermooxidative development is defined by the state variable ϕ which typically denotes the oxidized material fraction at any

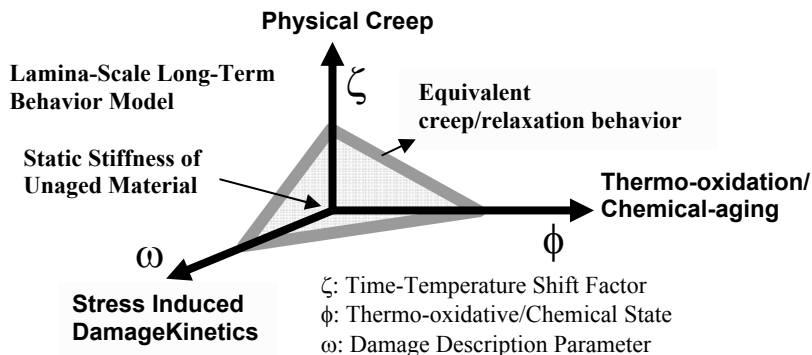


Fig. 9.33. The long-term lamina scale behavior model with various aging mechanisms. The shaded area illustrates the aging conditions with equivalent creep and relaxation behavior

material point in the structure. Although, the oxidation growth is being studied using a diffusion–reaction model and experimental characterization, the effect of oxidation on the mechanical behavior remains to be discussed. HTPMC structures subjected to extreme thermal loading are expected to undergo micromechanical damage evolution during their lifetime. The damage state in the composite is represented using a state variable ω . The damage growth dramatically influences the thermooxidative processes as well as the creep/relaxation behavior. Damage evolution and its influence on the oxidative and creep behavior must be characterized and simulated in the constitutive behavior model. The other coupled effects that include the effect of the oxidative layer on the creep behavior and the effect of the creep/relaxation behavior on the damage growth can contribute significantly to stiffness and strength degradation. Formulation of a failure or damage evolution law based on the stress/strain or fatigue state as well as the aging state of the material (for example, using parameters representing the three aging mechanisms) is a crucial step in designing structures with HTPMCs.

In this work, constituent level modeling of the fiber and the matrix is utilized in the unit cell analysis. The diffusion–reaction model for the polymer is developed using material parameters based on the evaluation of neat resin properties, and the models are compared to the oxidation development in the neat resin material. As discussed previously, the analysis is primarily focused on the PMR-15/carbon composite material system. Therefore, the polymer oxidation modeling utilizes PMR-15 neat resin material data from the literature and from experiments conducted for this modeling effort. Although it is recognized that the PAN-based carbon fibers of interest will degrade at temperatures above approximately 300°C (570°F), it is assumed that the fibers have static properties for the purpose of modeling the unit cell oxidation behavior.

9.4.1 Polymer Oxidation Modeling

The focus of the polymer modeling is twofold (1) to understand changes in the polymer properties with service environment exposure and (2) to accurately model these changes in the appropriate constitutive model that will be integrated in the micromechanics representation. The chemical mechanisms responsible for the initiation of thermal and/or oxidative degradation in high-temperature polyimide resins have been the subject of several extensive studies [63–65]. However, understanding and tracking these chemical processes beyond their initial stages is daunting and currently impractical for the class of high-performance polyimides used for aerospace applications.

If the primary, secondary, and tertiary chemical degradation mechanisms become known, their use in a multiscale modeling methodology to predict service performance will depend on the ability to predict mechanical properties based on the chemical state, using techniques such as molecular dynamics. To date, such capability does not exist for highly crosslinked polyimide materials. However, the effect of thermooxidative degradation can be approximated and modeled at a continuum level by representing the effective behavior of the material using suitable semiempirical or parametric models.

Figure 9.34 shows the various mechanisms of the thermooxidative degradation of the polymer. Note that the illustration shows the mechanisms as individual events. However, in reality the mechanisms are coupled, some may be dominant, and the sequence of their occurrence can be a function of the material and the aging environment, i.e., temperature, pressure, etc.

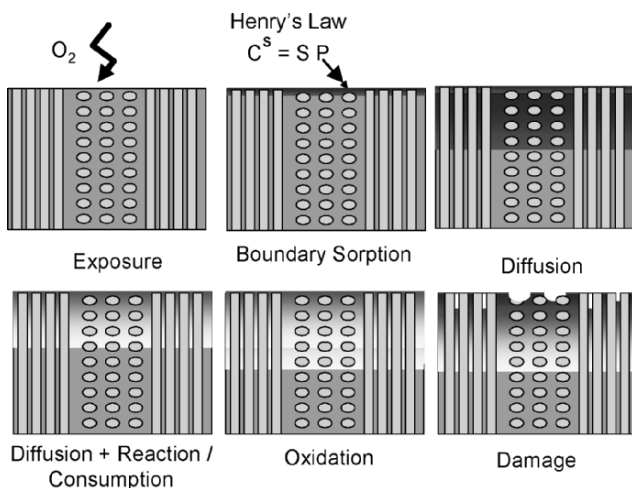


Fig. 9.34. Six phases of thermooxidative damage evolution which include exposure to oxygen environment, sorption at the boundary, diffusion/reaction, oxidative layer growth, and material damage

The oxidative behavior of a resin system is primarily controlled by the diffusivity of oxygen into the material and the kinetics of reaction of oxygen with the composite. The kinetics of reaction entails descriptions of both the oxygen consumption rate (or generally termed as the oxidation reaction rate) and the polymer (substrate) conversion rate (often overlooked in analyses). The substrate conversion rate is generally related to

the oxygen consumption rate. While the oxygen availability is controlled by the diffusivity, the polymer availability is controlled by the chemistry and molecular composition of the polymer. As oxygen diffusivity is a non-terminal process, the reaction cessation is typically governed by the polymer availability. Materials differ in the nature of the oxidation behavior observed during experimentation depending on the relative dominance of the diffusive behavior and polymer availability or the reaction kinetics.

Experimental observations suggest that the behavior of PMR-15 is diffusion controlled, and the reaction rate is high enough to consume the available polymer in observable time periods (tens of hours). Therefore, growth of oxidation into the polymer is observed with a clear oxidized, active reaction, and unoxidized regions and the growth of the oxidized region with time. Other materials may behave significantly different from the PMR-15 material, however the modeling methodology given here should be applicable. Materials such as AFR-PE-4 and BMI do not show this clear demarcation indicating either slow reaction rates or conversely large polymer availability for reaction.

As an idealized representation of oxidized neat polymer PMR-15, three distinct material regions, representing different levels of oxidation, as illustrated in Fig. 9.35 can be used. Using this representation, the material phases are the oxidized polymer phase (typically near the surface, Region I), the active reaction zone (where a mix of oxidized and unoxidized polymers exists, Region II), and an unoxidized polymer (typically in the interior of the specimen, Region III). The region composed of the oxidized (I) and active oxidation zones (II) will be referred to as the *oxidative surface layer*. Although this three-phase description is analogous to the two-phase models (or skin/core models) described by Nam and Seferis [66] and Salin and Seferis [83], the description of three phases enables extension to situations with high conversion ratios in which the constancy of the substrate

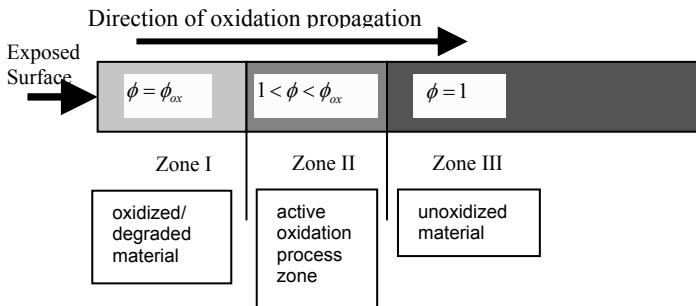


Fig. 9.35. The three zones in thermooxidation. The oxidized region is followed by active zone separating the oxidized and unoxidized regions

concentration is no longer valid and the substrate depletion leads to an autoretardation of the oxidation kinetics. A practical consequence is a decrease of the oxidation rate in the superficial (Region I) layers of the specimen, where the high conversion ratios are reached first, which leads to a moving of the oxidation front toward the specimen core. Such an extension was proposed by Colin and Verdu [27] and Colin et al. [33] and successfully applied to the thermal oxidation of amine-crosslinked epoxy and bismaleimide resins.

Sorption and diffusion modeling

For an aging process involving the diffusion and consumption of small molecules like O_2 by reaction with the polymer, there are critical conditions of reaction rate and/or thickness above which the process becomes kinetically controlled by the diffusion of the small molecules into the polymer [5]. Suitable lifetime prediction models must involve the thickness distribution of the oxidation reaction products. The latter can be predicted from diffusion laws, such as Fick's second law modified by a term relating the rate of consumption of the diffusing oxygen to the chemical reaction. In this analysis, $C(x, y, z, t)$ is defined as the concentration field of oxygen at any time within a domain with a diffusivity of D_{ij}^* and consumptive reaction with a rate, $R^*(C)$. The oxygen concentration is tracked through the Fickian diffusion equation with a reaction term and orthotropic diffusivity, as given by (9.1)

$$\frac{\partial C}{\partial t} = \left(D_{11}^* \frac{\partial^2 C}{\partial x^2} + D_{22}^* \frac{\partial^2 C}{\partial y^2} + D_{33}^* \frac{\partial^2 C}{\partial z^2} \right) - R^*(C) \quad (9.1)$$

subject to the boundary conditions:

$$C = C^S \text{ on the exposed boundaries,}$$

$$dC / dt = 0 \text{ on symmetry boundaries.}$$

The sorption on the exposed boundaries is given by Henry's equation

$$C^S = SP^0, \quad (9.2)$$

where S is the solubility (which is the maximum quantity of solute that can dissolve in a certain quantity of solution at a specified temperature) and P^O is the partial pressure of the oxygen in the environment. The solubility S is assumed to be temperature independent in this analysis. Therefore, increasing the pressure of the gas in the system (or increasing the molar volume V/n in $PV = nRT$) increases the boundary concentration C^S . In (9.1), the superscript * is used to denote additional dependencies of these parameters on the substrate temperature and oxidation state. These dependencies are further detailed in the ensuing subsections.

When the polymer reacts with oxygen at a given point, the sites on the polymer available for oxidation become depleted and available oxygen molecules will continue to diffuse into the interior of the polymer to react. Therefore, a polymer availability state variable ϕ is defined that quantifies the availability of active polymer sites for reaction. For the sake of simplicity, a reactive site depletion parameter ϕ_{ox} is defined at which the oxygen will predominantly diffuse rather than react with the polymer. In reality, the material will continue to oxidize. However, the rate of conversion of the polymer to oxides in this region may be much slower. The state variable ϕ is parameterized to have the range $\phi_{ox} < \phi < 1$, where ϕ_{ox} denotes completely oxidized polymer (idealized assumption) and $\phi = 1$ denotes unoxidized polymer. The introduction of the polymer oxidation state parameter ϕ , therefore, enables quantitative tracking of the reaction within the polymer. The reaction rate function $R^*(C)$ is influenced by the temperature T and available oxygen concentration C and is also a function of the polymer substrate oxidation state variable ϕ as shown in (9.3)

$$R^*(C) = g(\phi)R(C, T), \quad (9.3)$$

where $g(\phi)$ describes the reaction rate dependence on the oxidation state variable and $R(C, T)$ defines the reaction rate dependence on the concentration and temperature. The function $R(C, T)$ is defined as the reaction rate when there is an abundance of polymer reaction sites.

In isothermally aged PMR-15 specimens in an ambient air environment, modulus measurements using nanoindentation reveal that the oxidized region (I) has an approximately uniform modulus over the entire region, whereas the modulus of the active oxidation zone (II) decreased monotonically from Zone I stiffness levels to Zone III stiffness levels. As an idealization for PMR-15, it is therefore assumed that all of the reactions take place in the active reaction zone (II). In some other polymer systems, the diffusion–reaction relationship is such that the active reaction zone (II) encompasses the entire oxidative surface layer.

Figure 9.36 is an illustration of elastic modulus measurements made across the thickness of neat resin specimens of the polyimide AFR-PE-4 using nanoindentation. The data have been normalized with respect to the modulus of the unaged resin and show that there is no definitive region (I) in which the polymer is considered to be completely oxidized. Rather, the modulus decreases monotonically from the surface of the specimen to the unoxidized interior region (III). While the active zone (II) modeling describes the reaction rate and its dependence on oxygen availability (concentration fields), the diffusion–reaction system will be stationary (will not propagate into the polymer) if enough polymer in the reaction zone (II) is available for reaction. However, for longer aging times of tens to hundreds of hours, the active reaction zone (II) will propagate into the interior of the polymer.

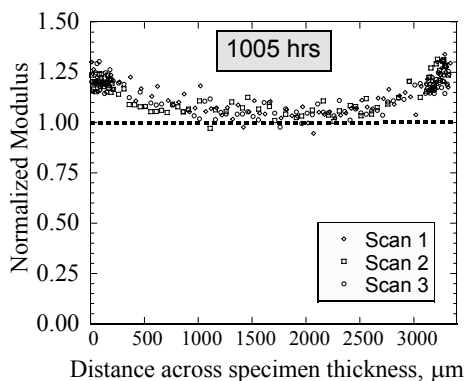


Fig. 9.36. Normalized oxidation modulus profile through entire thickness of AFR-PE-4 neat resin specimen

Oxidative aging leads to a reduction in molecular weight as a result of chemical bond breakage and loss in weight from outgassing of low molecular weight gaseous species. The most common assumption relating the reaction rate and weight loss is to assume that the rate of change in weight (dW/dt) is proportional to the reaction rate $R(C, T)$, i.e.,

$$dW / dt \propto -R(C, T), \quad (9.4)$$

where the negative sign is introduced in (9.4) since the rate of change in weight is negative and the oxygen consumption rate is positive. The oxidation state parameter at any point in the material is determined as the current weight of the material over its original (unoxidized) weight, i.e.,

$$d\phi / dt \propto dW / dt. \quad (9.5)$$

Combining (9.4) and (9.5), we obtain

$$d\phi(t)/dt = -\alpha R(C, T), \quad (9.6)$$

where α is a proportionality parameter that, in general, is time and temperature dependent. The initial state of the polymer is taken to be $\phi = 1$ and the final state (where the reaction terminates after complete conversion of the polymer) is taken to be $\phi = \phi_{\text{ox}}$. The solution to the system of (9.1)–(9.6) provides the transient evolution of oxygen concentration profiles and the oxidation state in the polymer domain. The system of differential equations constituting the kinetic model, in which is added an equation describing the substrate depletion, is solved numerically without any simplifying assumptions (concerning the long kinetic chains, the stationary state, or the existence of a relationship between the termination rate constants). This model accurately predicts the continual increase of the thickness of oxidized layer in the domain of high conversion ratios.

Temperature, pressure, and oxidation state dependence

The diffusivity of oxygen in the polymer depends on the temperature and the substrate oxidation state ϕ of the polymer material. It is assumed that the polymer is stress free. The temperature dependence of the diffusivities is expressed in its usual Arrhenius form as

$$D_{ij} = D_{ij}^0 \exp(-E_{ij}^a / RT), \quad (9.7)$$

where the gas constant R should not be confused with the concentration-dependent consumption reaction rate $R(C, T)$. If it is assumed that the neat resin is isotropic, (9.7) can be simply expressed as $D_{ij} = D^0 \exp(-E^a / RT)$. Using permeability tests at lower temperatures, Abdeljaoued [1] determined the preexponent (D^0) and the activation energy parameters (E^a) of PMR-15 neat resin in its virgin state, i.e., unoxidized condition, assuming isotropic diffusivity of the neat polymer. Direct experimental determination of the diffusivity parameters is usually nontrivial due to thin specimens required for observing gas permeability in reasonable timescales. Anisotropic diffusivity measurements are considerably more complicated due to the number of parameters that are needed. A diffusivity value of $53.6 \times 10^{-6} \text{ mm}^2 \text{ min}^{-1}$ is calculated for PMR-15 resin at 288°C using (9.7) in conjunction with the unoxidized preexponent D^0 and the activation energy parameters E^a listed in Table 9.1.

In general, the diffusivities for each of the material regions will be different, while the diffusivity of the oxidized polymer layer (Region I) is the controlling parameter since the diffusion of oxygen through the oxidized layer is the source of oxygen supply to the active reaction zone (Region II). For lack of experimental measurements of the diffusivities of

Table 9.1. PMR-15 polyimide resin diffusivity parameters

	Unoxidized, $\phi = 1$ (Abdeljaoued [1])	Oxidized, $\phi = \phi_{\text{ox}}$ (estimated using model [74])
D°	$6.10 \times 10^{-11} \text{ m}^2 \text{ s}^{-1}$	$8.90 \times 10^{-11} \text{ m}^2 \text{ s}^{-1}$
E^{a}	19,700 J mol ⁻¹	
R	8.31447 J (mol K) ⁻¹	

the oxidized (I) and active reaction (II) regions for the PMR-15 material, it is initially assumed that the diffusivities for the three regions are equivalent and equal to the unoxidized region (III) diffusivity. Later, simulations are presented where the distribution of the diffusivity D_{ij} in the active reaction zone (Region II) is assumed to be a linear interpolation of the diffusivities of the oxidized (Region I) and unoxidized (Region III) materials, denoted by D_{ij}^{ox} and D_{ij}^{un} , respectively. The oxidation state variable ϕ dependence on the diffusivity is introduced using a rule of mixtures, namely

$$D_{ij}^* = D_{ij}(T, \phi) = \langle D_{ij}^{\circ} \rangle_{\text{un}} \exp(-\langle E_{ij}^{\text{a}} \rangle_{\text{un}} / RT) \frac{\phi - \phi_{\text{ox}}}{1 - \phi_{\text{ox}}} + \langle D_{ij}^{\circ} \rangle_{\text{ox}} \exp(-\langle E_{ij}^{\text{a}} \rangle_{\text{ox}} / RT) \frac{1 - \phi}{1 - \phi_{\text{ox}}}. \quad (9.8)$$

The $\langle \rangle_{\text{un}}$ notation is used to denote the quantities for the unoxidized ($\phi = 1$) substrate state and the $\langle \rangle_{\text{ox}}$ is used to denote those of oxidized state ($\phi = \phi_{\text{ox}}$). Therefore, the temperature-dependent diffusivity needs to be characterized for oxidized and unoxidized states, and for polymer states $\phi_{\text{ox}} < \phi < 1$ such that the diffusivity is given by linear interpolation using (9.8). For the remainder of this manuscript, superscripts and subscripts “ox” and “un” will be used with model parameters whenever needed for clarity. For clarification, unoxidized material does not imply unaged material.

The reaction rate term $R(C, T)$ in (9.3) models the reaction of the oxygen with the polymer for the case that there is an excess of polymer reaction sites. The reaction modeling presented here assumes that the reaction

products (water and other volatiles) leave the polymer instantaneously, and modeling of the outgassing is not considered. The basic autooxidation scheme (BAS) that describes a simple kinetics oxidation scheme for polymers [45] is used. It is further assumed that the expression for the oxygen consumption rate determined in the stationary state remains valid in the domain of high conversion ratios.

Typically, the reaction rate is modeled with the Arrhenius-type kinetics model with a saturated reaction rate R_O as given by $R_O(T) = R'_O \cdot \exp(-R^a / RT)$ for capturing the temperature dependence of the reaction rates [37, 62] or using mechanistic reaction models [1, 31, 33, 87, 117] for capturing the oxygen concentration dependence. The rate constant R'_O and the activation parameter R^a determine the temperature dependence of the reaction rate. The reaction rate function is reduced when the oxygen availability is reduced or when the substrate is fully converted, as given by (9.9)

$$R^*(C) = g(\phi)R(C, T) = \left[\frac{\phi - \phi_{ox}}{1 - \phi_{ox}} \right] R_O(T) f(C). \quad (9.9)$$

The models by Colin et al. [31, 33] and Abdeljaoued [1] differ on how the concentration dependence is expressed. To determine the saturation reaction rate R_O , an active reaction zone (II) analogy is employed. Considering the diffusion–reaction equation (9.1), the proportion of the diffusivity vs. reaction rate determines the zone over which the oxygen diffuses in and oxygen gets consumed by the reaction. This zone is indicative of the saturation reaction rate R_O in (9.9). The lower the reaction rate, the larger the active reaction zone (II) for a constant diffusivity. The function $f(C)$ in (9.9) models the situation in which the amount of oxygen available for reaction is lower than that required for the maximum reaction rate under saturation conditions. The reduction in reaction rate can be modeled following Abdeljaoued [1] using (9.10) or Colin et al. [31, 33] using (9.11):

$$f(C) = \frac{\beta C}{1 + \beta C}, \quad (9.10)$$

$$f(C) = \frac{2\beta C}{1 + \beta C} \left[1 - \frac{\beta C}{2(1 + \beta C)} \right]. \quad (9.11)$$

The former model (9.10) has been used for epoxy and bismaleimide matrices, and the latter model (9.11) has been used for the PMR-15 polyimide resin systems. Figure 9.37 shows the dependence of the reaction rate on the concentration as modeled by (9.10) and (9.11). The abscissa has a normalized concentration parameter βC in which the parameter β non-dimensionalizes the concentration field. According to (9.10), the saturation reaction rate is reached more slowly and at considerably higher concentration βC values than for (9.11). The expression given by (9.11) allows the saturation reaction rate to be reached quicker and at a finite βC value. For βC values of greater than approximately 3 (corresponding to $R(C,T)/R_0 \sim 90\%$), the reaction rate remains relatively uniform. For this analysis, the concentration dependence, as modeled in (9.11), was chosen for the simulations. The oxygen concentration at which the reaction behavior changes from an accelerated rate to approximately a uniform reaction rate can be easily controlled by varying the value of β (with a constant βC equal to 3).

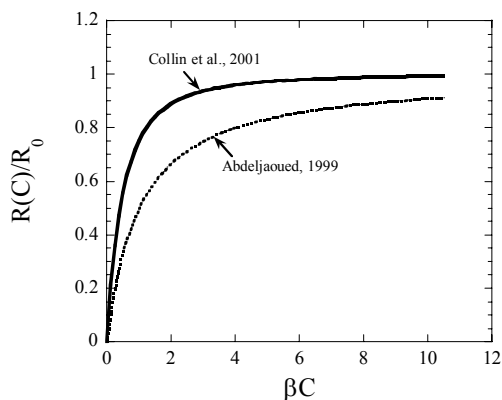


Fig. 9.37. Typical model of reaction rate dependence on concentration

The value of β can be determined from weight loss data obtained from specimens aged at two different oxygen partial pressures, typically in pure O_2 and in air. This formulation leads to the reaction rate approaching the saturation reaction rate $R(C,T) \rightarrow R_0(T)$ when the concentration approaches infinity $C \rightarrow \infty$. That is, when the reaction is not oxygen deprived the reaction rate reaches a maximum saturation rate, $R_0(T)$. To determine this value, weight loss measurements at two concentrations which translate to the reaction rates at those two concentration values are needed. Since the weight loss is taken to be proportional to the oxygen consumption rate, the ratio of the weight loss determined at

two concentrations is the same as $R_1(C_1, 288^\circ\text{C})/R_2(C_2, 288^\circ\text{C})$. For example, from Abdeljaoued [1], the ratio of the weight loss between pure O_2 ($C_2 = 3.74 \text{ mol m}^{-3}$) and air ($C_1 = 0.79 \text{ mol m}^{-3}$) is about 0.7 at a temperature of 288°C . Therefore,

$$\frac{2\beta C_1}{1 + \beta C_1} \left[1 - \frac{\beta C_1}{2(1 + \beta C_1)} \right] = 0.7 \frac{2\beta C_2}{1 + \beta C_2} \left[1 - \frac{\beta C_2}{2(1 + \beta C_2)} \right]. \quad (9.12)$$

Solving (9.12) produces three roots $[-3.5593, -0.42657, 0.91947]$ with only one physically feasible value for PMR-15 resin to be $\beta = 0.919$.

The oxygen consumption expression contains two key parameters of the oxidation kinetics (1) the maximal oxidation rate of the polymer when excess oxygen is available $R_O = k_3^2[\text{PH}]^2/k_6$ for a given temperature T and (2) the reciprocal of the critical oxygen concentration beyond which oxygen excess is reached $\beta = k_2 k_6 / (2k_5 k_3 [\text{PH}])$. The reaction rate parameters k_2 , k_3 , k_5 , and k_6 for the BAS are not determined explicitly to calculate the model parameters but describe mechanistically how R_O and β are related to the kinetics of oxidation [32]. It is clear that both R_O and β are dependent on the substrate concentration or the availability of polymer reaction sites $[\text{PH}]$. However, it is assumed that only R_O is especially affected by the substrate depletion and that the macroscopic weight loss measurements can be used to determine the reaction and polymer consumption parameters.

Correlation with weight loss observations

Experimental weight loss data are used to determine the value of ϕ_{ox} for PMR-15 neat resin. To determine this value, a relation between the oxidation layer size and the weight loss must first be established. In an inert gaseous environment, polymers undergo physical and nonoxidative chemical aging only, whereas in an oxidizing environment, specimens will undergo physical, nonoxidative chemical aging, and oxidative aging. The differences in the aging behavior of the specimens aged in an inert gaseous environment and those aged in an oxidizing gaseous environment can then be attributed to oxidative aging. Thermal aging experiments were conducted in both an inert atmosphere (argon) and an oxidative atmosphere (air), and the weight loss was recorded at various time intervals to determine the effect of oxidation on weight loss.

Let the initial dimensions of a specimen be given by length L , width W , and thickness T . For a particular aging time, if the weight loss fraction

(weight loss/original weight) in the inert atmosphere is given as γ and weight loss fraction after the same time period in air is given by ε , then the weight loss fraction due to oxidation alone is $(\varepsilon - \gamma)$. Let the observed thickness of the completely oxidized region (I) and the active oxidation layer (II) be denoted by t_o and t_a , respectively, as shown in Fig. 9.38. The initial volume of the specimen V , the volume of the fully oxidized region V_o , and the volume of the active oxidation zone V_a are, therefore, given by:

$$V = LWT, \tag{9.13}$$

$$V_o = \{LWT - (L - 2t_o)(W - 2t_o)(T - 2t_o)\}, \tag{9.14}$$

$$V_a = \{LWT - V_o - (L - 2(t_a + t_o))(W - 2(t_a + t_o))(T - 2(t_a + t_o))\}. \tag{9.15}$$

Assuming that ϕ varies linearly in the active oxidation zone (II) from ϕ_{ox} to 1, the total weight loss is the sum of the weight loss in the oxidized zone (I) and the active zone (II) and is equal to the weight loss in the specimen, i.e.,

$$\left[(1 - \phi_{ox})V_o + \left(\frac{1 - \phi_{ox}}{2} \right) V_a \right] \rho = (LWT)[\varepsilon - \gamma]\rho. \tag{9.16}$$

Solving for ϕ_{ox} ,

$$\phi_{ox} = 1 - \frac{V(\varepsilon - \gamma)}{V_o + \frac{1}{2}V_a}. \tag{9.17}$$

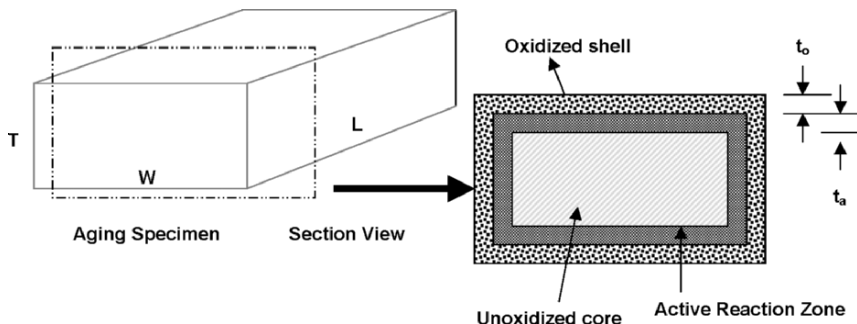


Fig. 9.38. Geometry of the specimen used for aging with all boundaries exposed to oxygen. The oxidized layer, active reaction zone, and the unoxidized regions are illustrated in the sectional view

Equations (9.13)–(9.17) are used to determine the value of ϕ_{ox} from oxidation layer size observations and weight loss data from aging specimens in inert (γ) and oxidative (ε) environments. The values of ϕ_{ox} as determined from the experimental data from PMR-15 aging tests are observed to decrease with aging time. This observation indicates that the oxidized region (I) material continues to degrade and lose weight with increasing aging time. Material loss from the specimen free surfaces and volumetric shrinkage are both observed during oxidative aging experiments and these effects are predominant for PMR-15 neat resin specimens beyond 100 h of aging, especially at 343°C. Therefore, for PMR-15 resin, the ϕ_{ox} value is determined by averaging the predictions during the initial time period of 100 h at 288°C. The average ϕ_{ox} value as determined by (9.17) using experimental weight loss data is 0.187, which implies that the completely oxidized polymer weighs about 18.7% of the unoxidized polymer. Recognizing that the model represents an idealization of the oxidation process, in reality the nonzero ϕ_{ox} value may simply represent a state of the polymer at which the reaction rate is very slow compared to oxidation of unaged polymer. Unless otherwise mentioned, all of the simulations presented herein are performed using the average ϕ_{ox} value of 0.187. Determination of the oxidation parameter ϕ_{ox} by (9.17) is applicable up to the temperature-dependent aging time that surface cracks appear in the oxidized zone (I) of the specimen. Once surface cracks appear, the relationship is no longer valid.

Oxidation-dependent modulus change

Aging of the polymer at elevated temperatures results in changes of the mechanical properties of the material. Changes in the stiffness of the neat resin can occur for aging in both oxidizing and nonoxidizing environments. For oxidized regions (I) of PMR-15 neat resin specimens, the stiffness is greater than that of the unoxidized regions (III) and greater than that of unaged resin. Based on nanoindentation data, a profile of the modulus change across the oxidized (I), active (II), and unoxidized zones (III) of PMR-15 neat resin specimens is shown in Figs. 9.39 and 9.40 for specimens aged at 288 and 343°C, respectively. Based on data from Figs. 9.39 and 9.40, as well as other PMR-15 specimens, it is observed that the oxidized regions of the specimens can be represented as having a nearly constant modulus. The modulus change as a function of the state variable ϕ can then be expressed as

$$E(\phi, t) = E_{\text{non}} \exp \left(k_{\text{ox}} \frac{1 - \phi}{1 - \phi_{\text{ox}}} + k_{\text{un}} \frac{\phi - \phi_{\text{ox}}}{1 - \phi_{\text{ox}}} \right), \quad (9.18)$$

where E_{non} is the nonaged (as opposed to unoxidized) modulus of the resin, parameter k_{ox} models oxidation-dependent modulus changes, and parameter k_{un} models the unoxidized time-dependent modulus changes due to physical/chemical aging [125]. Solid plots of the modulus profiles using (9.18), as they compare to the nanoindentation data, are shown in Figs. 9.39 and 9.40.

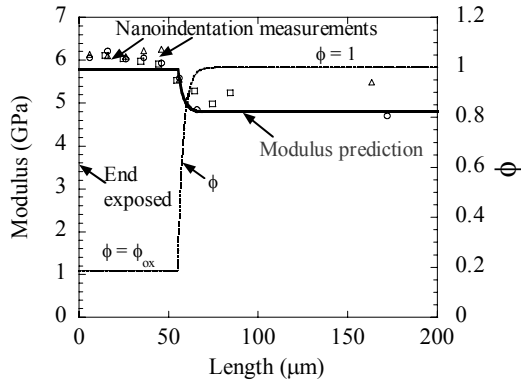


Fig. 9.39. Profile of oxidation layer modulus for PMR-15 aged at 288°C for 50 h

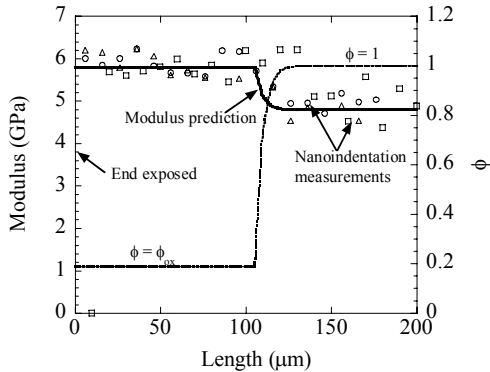


Fig. 9.40. Profile of oxidation layer modulus for PMR-15 aged at 343°C for 541 h

Oxidation simulations for neat polymer

The capability to obtain direct measurements of all of the properties of the PMR-15 for each of the three material regions that are needed to populate the parameters for the model is lacking. Therefore, many of the parameters are obtained through indirect measurement or correlation with model predictions. To determine the parameters of the outlined model for PMR-15 neat resin, predictions from the model are compared and correlated to the experimental observation of the oxidation layer growth obtained at 288°C. These comparisons provide quantitative values for various parameters of the model, especially the temperature-dependent saturation reaction rate $R_O(T)$, the behavior of the proportionality α between reaction rate and the weight loss, the polymer availability state variable ϕ , and the apparent diffusivity of the oxidized region D_{ij}^{ox} .

The diffusion–reaction system of equations is solved using numerical solutions to differential algebraic equations in the one-dimensional domain. These methods are computationally effective when performing parametric sensitivity analysis. This section describes the solution algorithms used to solve the diffusion–reaction system with the reaction rate described as follows

$$R(C, T) = \begin{cases} R_O(T)2\xi(1 - \xi/2), & \phi > \phi_{ox}, \\ 0, & \phi = \phi_{ox}, \end{cases} \quad (9.19)$$

where

$$\xi = \frac{\beta C}{1 + \beta C}, \quad (9.20)$$

as given by (9.11). The diffusion–reaction system is solved in MATLAB™ using a modified implementation of *ode15s* and *Pdepe* solvers. The *ode15s* is a variable order multistep solver based on the numerical differentiation formulas (NDFs) and uses the backward differentiation formulas (BDFs, also known as Gear’s method). *Pdepe* solves initial–boundary value problems for systems of parabolic and elliptic partial differential equations (PDEs) in the one space variable x and time variable t . The ordinary differential equations (ODEs) resulting from discretization in space are integrated to obtain approximate solutions at times specified in t span. The *Pdepe* function returns values of the solution on a mesh provided in *xmesh*. *Pdepe* solves PDEs of the form

$$c(x, t, u, \partial u / \partial x) \frac{\partial u}{\partial t} = x^m \frac{\partial}{\partial x} (x^m f(x, t, u, \partial u / \partial x)) + s(x, t, u, \partial u / \partial x). \tag{9.21}$$

The PDE in (9.21) is solved for a time interval of $t_i \leq t \leq t_f$ and over a spatial domain of $a \leq x \leq b$. The initial time is represented by t_i , the final time of the simulation as t_f , and the boundary points of the computational domain are $x = a$ and $x = b$. The interval $[a, b]$ must be finite, while m can be 0, 1, or 2, corresponding to slab, cylindrical, or spherical symmetry, respectively. If $m > 0$, then a must be ≥ 0 . In the above equation, $f(x, t, u, \partial u / \partial x)$ is a flux term and $s(x, t, u, \partial u / \partial x)$ is a source term. The coupling of the partial derivatives with respect to time is restricted to multiplication by a diagonal matrix $c(x, t, u, \partial u / \partial x)$. The diagonal elements of this matrix are either identically zero or positive. The diffusion–reaction system given in (9.1) can be put into the form shown in (9.21) for the one-dimensional case by using $m = 0$ and the following functions:

$$\begin{aligned} u &= C, \\ c(x, t, u, \partial u / \partial x) &= 1, \\ f(x, t, u, \partial u / \partial x) &= D^* du / dx, \\ s(x, t, u, \partial u / \partial x) &= -R^*(u). \end{aligned} \tag{9.22}$$

For $(t - t_0)$ and all x , the solution components satisfy the initial conditions of the form

$$C(x, t_0) = C'(x), \tag{9.23}$$

where $C'(x)$ is the known initial state of oxygen concentration. For all t and either $x = a$ or $x = b$, the solution components satisfy a boundary condition of the form

$$p(x, t, u) + q(x, t) f(x, t, u, \partial u / \partial x) = 0. \tag{9.24}$$

The boundary conditions for the present problem can be written as follows:

$$\begin{aligned} @ x = a (= 0) & \left\{ \begin{aligned} p(0, t, u) &= u - C^S, \\ q(0, t) &= 0, \end{aligned} \right. \\ @ x = b (= L) & \left\{ \begin{aligned} p(L, t, u) &= 0, \\ q(L, t) &= 1. \end{aligned} \right. \end{aligned} \tag{9.25}$$

The oxidation-dependent diffusivity D_{ij} is determined at each computational point using (9.8). The oxidation state variable ϕ is determined at every time step during the computation using the weight loss relationship shown in (9.6)

$$\phi = \min \left\{ \phi_{\text{ox}}, \left(1 - \int_0^t \alpha(\zeta) R(\zeta) d\zeta \right) \right\}. \tag{9.26}$$

For initial results, the proportionality constant α relating the weight loss and reaction rate is assumed constant with aging time. In later simulations, we consider the variation of α with time, as discussed below.

Influence of saturation reaction rate, R_o

Figure 9.41 shows the experimental observations and the predictions of oxidation layer (Zones I + II) growth at 288°C. The simulations shown are with a constant diffusivity ($D_{ij}^{\text{ox}} = D_{ij}^{\text{un}} = 53.6 \times 10^{-6} \text{ mm}^2 \text{ min}^{-1}$) and a constant value of the proportionality constant ($\alpha = 0.01$). Several values of reaction rates (5.5, 3.5, and 0.5 mol (m³ min)⁻¹) are considered. The oxidation layer growth predictions show little dependence on the reaction rate $R_o(T)$. Moreover, the simulations overpredict the oxidation layer growth at longer aging times. As mentioned earlier, the choice of saturation reaction rate mainly influences the size of the active reaction zone (II). A larger reaction rate results in a decrease in the size of the active zone (II), whereas a smaller value results in an increase in the size of the active reaction zone (II). The experimental measurements of Ripberger et al. [78] support greater reaction rates during the initial aging period which then decrease at longer aging times.

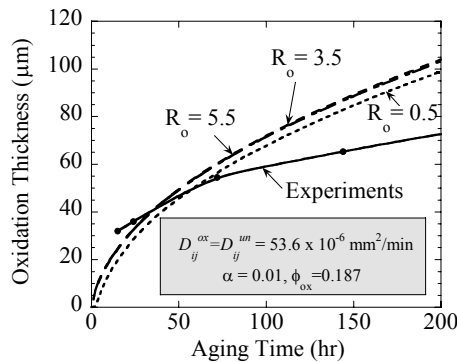


Fig. 9.41. Influence of R_o on oxidation layer growth predictions

Influence of polymer availability state, ϕ_{ox}

Figure 9.42 shows the influence of ϕ_{ox} on oxidation layer growth predictions using constant values of $D_{ij}^{ox} = D_{ij}^{un} = 53.6 \times 10^{-6} \text{ mm}^2 \text{ min}^{-1}$, $R_o(T) = 3.5 \text{ mol (m}^3 \text{ min)}^{-1}$, and $\alpha = 0.01$. An average ϕ_{ox} value of 0.187 is determined using the weight loss data during the initial 100 h of aging. For this figure, two other constant ϕ_{ox} values, 0.1 and 0.3, were considered. Clearly, the oxidation layer thickness predictions are seen to increase with increasing values of ϕ_{ox} . A larger value of ϕ_{ox} implies earlier exhaustion of polymer availability for reaction leading to a more rapid advancement of the reaction zone (II) and ultimately a larger oxidation layer thickness.

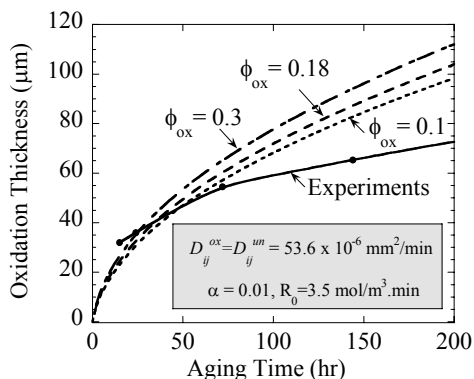


Fig. 9.42. Influence of ϕ_{ox} on oxidation layer growth predictions

Influence of proportionality factor, α

The proportionality constant α relates the molar reaction rates with observed weight loss with respect to aging time. Although we do not present a direct correlation with known physical or chemical mechanisms, the experimental results by Ripberger et al. [78] indicate that the initial weight loss rate is much more rapid than rates at longer aging times and approaches a constant rate for longer aging times. It is, therefore, reasonable to assume that the proportionality constant α is larger at the beginning of aging and decreases with aging time. For these simulations, a linear relation for α is assumed for the first 40 h of aging which leads to numerical predictions of oxidation layer growth that correlates well with experimental measurements.

Figure 9.43 shows the influence of α on oxidation layer growth predictions using a constant diffusivity ($D_{ij}^{\text{ox}} = D_{ij}^{\text{un}} = 53.6 \times 10^{-6} \text{ mm}^2 \text{ min}^{-1}$) and a constant value of the saturation reaction rate ($R_0 = 3.5 \text{ mol (m}^3 \text{ min)}^{-1}$). Initially, it is assumed that the proportionality factor α is constant with aging time. As seen in Fig. 9.43, the larger value of $\alpha = 0.01$ predicts the data well for early aging times but clearly overpredicts it at longer aging times. On the other hand, the smaller value of $\alpha = 0.0033$ vastly underpredicts at smaller aging times but provides a better correlation to the trends of the experimental data for longer aging time periods. This, therefore, indicates that the weight loss proportionality factor α is not a constant but is a function of the oxidative aging time.

For the third simulation shown in Fig. 9.43, α is assumed to vary linearly from a value of 0.01 to 0.0033 within the first 40 h and then remain constant after 40 h. With this assumed variation (which is in agreement with larger weight loss rates observed for early aging times), the numerical simulations of oxidation layer growth are still underpredicted but, qualitatively the predicted curve matches the experimental data. For this parametric study, simple functional relationships are used to represent α . However, more complex functional relationships can be used to qualitatively match the experimental trends for extended aging times.

The proportionality between the oxygen consumption rate and weight loss rate is established by Abdeljaoued [1] using simplifying assumptions of which some of them, e.g., existence of a relationship between termination rate constants, are rejected by Gillen et al. [45]. Thus, a value of α which does not remain constant with time, as seen from our simulations, bodes well with the findings of Gillen et al. [45].

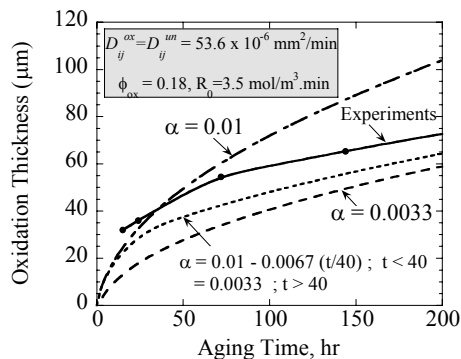


Fig. 9.43. Influence of α on oxidation layer growth predictions

Influence of diffusivities, D_{ij}^{ox} and D_{ij}^{un}

Thermooxidative aging of the polymeric material will change the chemical composition of the polymer and, hence, the physical properties of the material. In general, the diffusivities for each of three zones of the material (Regions I–III) will be different. Parametric analyses show that the diffusivity of the oxidized phase region (I) D_{ij}^{ox} controls the growth of the oxidation layer. Since a direct measurement of D_{ij}^{ox} is difficult to obtain and the value is not available in the literature, estimation is obtained from simulations.

Figure 9.44 shows the experimental oxidation layer growth data at 288°C compared with several simulations based on assuming different diffusivities. It is initially assumed that the diffusivity of the oxidized material D_{ij}^{ox} is the same as the diffusivity of the unoxidized material $D_{ij}^{\text{un}} = 53.6 \times 10^{-6} \text{ mm}^2 \text{ min}^{-1}$. For the next simulation, the diffusivity for both the oxidized and unoxidized regions is both increased to $78 \times 10^{-6} \text{ mm}^2 \text{ min}^{-1}$, i.e., setting $D_{ij}^{\text{ox}} = D_{ij}^{\text{un}} = 78 \times 10^{-6} \text{ mm}^2 \text{ min}^{-1}$, for which the predictions overestimate the oxidation layer even further at longer aging times. The predictions deviate even further from the experimental results using $D_{ij}^{\text{ox}} = D_{ij}^{\text{un}} = 100 \times 10^{-6} \text{ mm}^2 \text{ min}^{-1}$. Increasing the diffusivity value in the oxidized region from 53.6×10^{-6} to $78 \times 10^{-6} \text{ mm}^2 \text{ min}^{-1}$ and keeping $D_{ij}^{\text{un}} = 53.6 \times 10^{-6} \text{ mm}^2 \text{ min}^{-1}$ shows very little change from the earlier simulation with $D_{ij}^{\text{ox}} = D_{ij}^{\text{un}} = 78 \times 10^{-6} \text{ mm}^2 \text{ min}^{-1}$. This illustrates that the oxidation region growth is predominantly controlled by the diffusivity of the oxidized region and is far less sensitive to the diffusivity of the unoxidized material. In the case of low conversion ratios, it is generally assumed that the diffusivity does not change during oxidation. This assumption has been checked experimentally for some linear polymers (PP, PE) and thermosets (epoxy), but the issue remains unresolved in the case of high oxidation conversion ratios. However, it can be reasonably considered, in a first approximation, that the diffusivity increases when the chemical structure significantly changes (presence of many oxygenated species) and the original chemical network is destroyed during oxidation (presence of many dangling chains). As a result, it can be assumed that diffusivity increases in the superficial layers where high conversion ratios are reached.

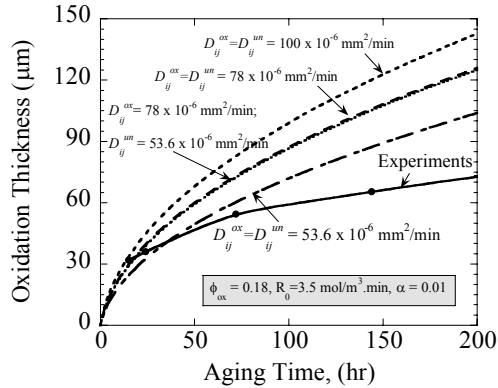


Fig. 9.44. Influence of diffusivity on oxidation layer growth predictions

Combined influence of controlling parameters

Figure 9.45a shows that, if the diffusivity of the resin is left unchanged with $D_{ij}^{un} = D_{ij}^{ox} = 53.6 \times 10^{-6} \text{ mm}^2 \text{ min}^{-1}$ but α is assumed to vary linearly from a value of 0.01 to 0.0033 within the first 40 h and kept constant beyond that time, the numerical simulations of oxidation layer growth are underpredicted but the shape of the predicted curve is approximately parallel to the experimental measurements. Next, if the diffusivity value in the oxidized region is increased from 53.6×10^{-6} to $78 \times 10^{-6} \text{ mm}^2 \text{ min}^{-1}$ and kept $D_{ij}^{un} = 53.6 \times 10^{-6} \text{ mm}^2 \text{ min}^{-1}$ in conjunction with a linear variation of α for the first 40 h, a very good agreement between the predictions and the measurements of the oxidation layer (see Fig. 9.45b) can be obtained. This good agreement, therefore, gives credence to the assumptions that the diffusivity values within the oxidized region are larger compared to the values in the unoxidized region and that the value of α changes with aging with a larger value obtained initially, which is also in agreement with larger weight loss rates observed during the beginning of the experiments. With a diffusivity value of $78 \times 10^{-6} \text{ mm}^2 \text{ min}^{-1}$ for the oxidized region at 288°C and assuming that the activation energy E^a remains unchanged in the oxidized region, the constant $D^0 = 8.9 \times 10^{-11} \text{ m}^2 \text{ s}^{-1}$ can be evaluated for the oxidized region, as listed in Table 9.1.

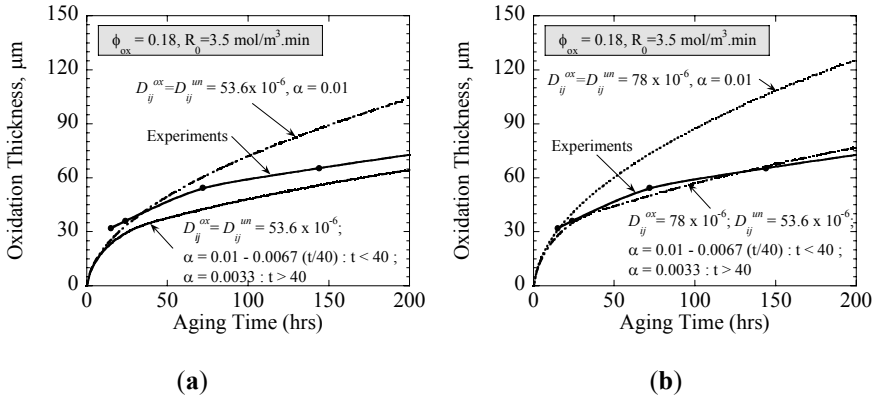


Fig. 9.45. Combined influence of controlling parameters on oxidation layer growth predictions

Extrapolations to longer aging times

To project the oxidation layer growth to thousands of hours of aging, extrapolations from the simulation of the first 200 h of the oxidation layer growth are used. The oxidation layer size is fitted using a power law dependence with time, and the long-term predictions are obtained by extrapolation. The oxidation layer size, extrapolated to 1,500 h of aging, is compared with experimental measurements in Fig. 9.46. The values of the parameters used in the simulations are also listed in the figure. The results

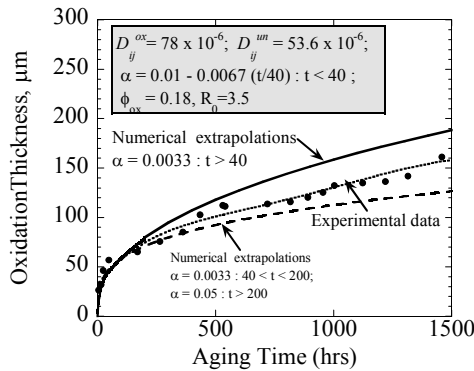


Fig. 9.46. Comparison of extrapolated oxidation layer growth predictions with measurements

indicate that the comparisons, using a constant $\alpha = 0.0033$ beyond 40 h of aging, are reasonable for 500 h of aging but are overestimated at longer time periods. However, when the layer growth by reducing is simulated the value of α from 0.0033 to 0.000165 for aging from 200 to 400 h, the predictions underestimate the oxidized layer thickness at longer aging times. These extrapolations and comparisons for longer aging times illustrate, therefore, that the proportionality factor (α) is not a constant but depends upon the aging time. Further work is needed to help establish this correspondence from the weight loss data.

Simulation of Arrhenius temperature dependence

The temperature dependence of the diffusivity D_{ij} (9.7) and the reaction rate $R(C, T)$ through the saturation reaction rate $R_0(T)$ are expressed by Arrhenius-type relationships. Along with experimental oxidation layer thickness measurements for neat resin PMR-15 specimens aged at 288°C (550°F), oxidation thickness measurements were also obtained for specimens aged at 316°C (600°F) and 343°C (650°F). Figure 9.47 shows predictions of the oxidation layer thicknesses for 288°C (550°F), 316°C (600°F), and 343°C (650°F) neat resin PMR-15 specimens based on 288°C (550°F) properties. The figure shows that the model accurately predicts the 316°C (600°F) and 343°C (650°F) oxidation layer thicknesses, and the temperature dependence of the reaction rate and diffusivity are accurately represented.

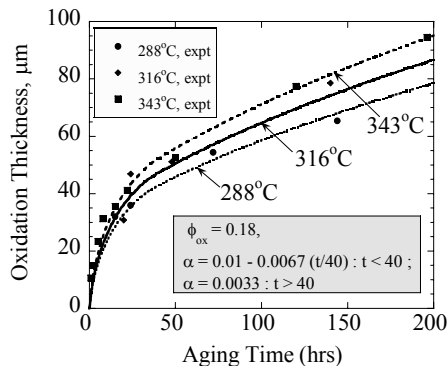


Fig. 9.47. Prediction of oxidation thickness at 316 and 343°C based on 288°C model parameters

Influence of pressure on oxidation growth

Thermal aging in a pressurized environment has been shown, in Figs. 9.27 and 9.28, to accelerate the oxidation layer growth rate and increase the weight loss. Since the partial pressure of a gas is directly proportional to the total pressure and, in general, the solubility of gases increases with increasing pressure, the sorption, as expressed by (9.2), is expected to increase with increasing pressure. Figure 9.48 shows the results of a parametric evaluation of how changes in the sorption affect the predicted oxidation layer thickness. Oxidation layer thickness for neat resin PMR-15 specimens aged at ambient and elevated pressures at 288°C is also shown in the figure. The predicted oxidation layer thickness increases with increasing oxygen concentration on the boundary and for the sorption value $C^S = 1.25$, there is a good correlation with the pressurized aging data for aging times up to 200 h. Figure 9.49 shows the predicted oxidation layer thickness for predictions of up to 800 h of aging time. The results show good agreement with the experimental data.

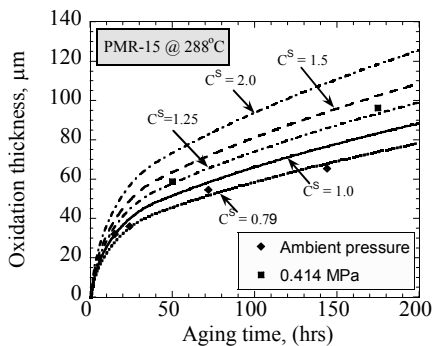


Fig. 9.48. Influence of sorption on the oxidation layer thickness

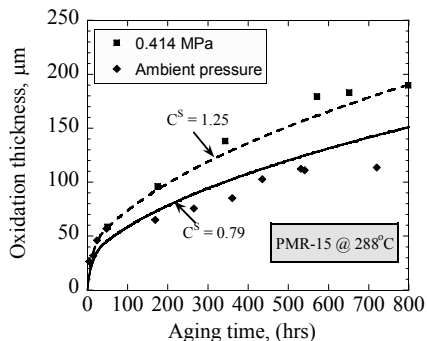


Fig. 9.49. Prediction of oxidation thickness for pressurized aging of PMR-15

9.4.2 Unit Cell Modeling

Both two- [101] and three-dimensional unit cell models capable of discrete crack analysis coupled with thermooxidative aged analysis can be used to model and identify the origins of degradation and mechanisms of failure initiation representative of that in unidirectional composites. Traditionally, the fibers are assumed to be chemically static for short-aging times (this assumption may not be valid for extended aging times), and residual stresses must be taken into account due to the strong coupling between stress, diffusion, and aging. Of primary importance is the characterization of the interface/interphase behavior that may have different reaction/diffusion kinetics than the polymer matrix phase of the composite. The fiber–matrix interphase region developed during the composite cure cycle is likely dependent on the fiber surface (unsized or sized) and the composition of the fiber sizing, if it is present [34]

Fiber-reinforced composites degrade several times more rapidly than their matrix and fiber constituents, as illustrated by Skontorp [95] in Fig. 9.50. The figure shows the weight loss (normalized with respect to the surface area) of a sample of IM6 fibers and an Avimid-N neat resin specimen for up to 200 h of aging at 343°C. A rule of mixtures is used to predict weight loss of a unidirectional Avimid-N/IM6 with 50% fiber volume based on the weight loss of the fiber and resin constituents and surface area fractions. The measured weight loss from the unidirectional specimen's axial surfaces S_3 is five times greater than the predicted rule-of-mixtures weight loss. The difference between the measured and predicted weight loss is attributed by Skontorp [95] to the fiber–matrix interface that is significantly more susceptible to oxidation than the fiber and resin constituents. As shown in Fig. 9.51, the intraply cracking typically occurs

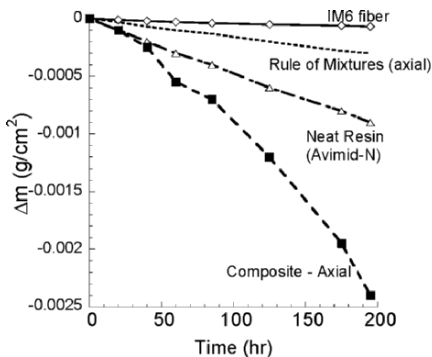


Fig. 9.50. Normalized weight loss for Avimid-N/IM6 at 650°F/343°C [95]

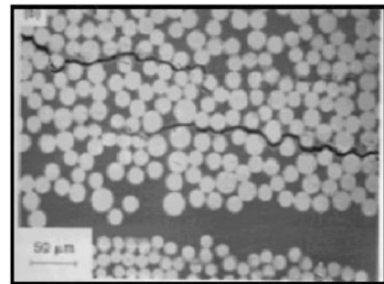


Fig. 9.51. Intraply cracks along fiber–matrix interface

along fiber–matrix interfaces providing pathways for oxidizing agents to penetrate deeper into the material, accelerating the degradation process. Incorporation of accurate polymer constitutive models into a unit cell micro-mechanics analysis, along with proper characterization and representation of the fiber–matrix interface/interphase region (including debonding), can provide a link between the degradation kinetics and chemical state of the polymer matrix and the performance of individual lamina or unidirectional composites.

The diffusion–reaction oxidation model is implemented into a three-dimensional Galerkin finite element analysis (GFEA). The GFEA method is more appropriate for studying structural scale problems than the one- and two-dimensional implementation, however the computational requirement of the three-dimensional analysis precludes its use in parametric analyses required for correlation with experimental results and parameter determination. The GFEA requires mesh sizes in the 1- μm scale and time increments in 1-s steps. A 200-h oxidation simulation with 100- μm oxidation zone size typically requires problem sizes in the order of 100,000 degrees of freedom (DOF) and 720,000 time steps. The domain Ω is discretized by a union of finite elements as $\Omega = \bigcup_{e=1}^{N_e} \Omega^{(e)}$, where $\Omega^i \cap \Omega^j = 0$, if $i \neq j$, and N_e is the total number of elements in Ω . The approximate element solution for the concentration $C(x, y, z, t)$ in the diffusion model is defined as

$$C(x, y, z, t) = [\Phi(x, y, z)]^T [C(t)], \quad (9.27)$$

where $\Phi(x, y, z)$ is the spatial interpolation function and $C(t)$ is the time varying nodal concentration values. Using the Galerkin method, i.e., using a weight function the same as the interpolation Φ ,

$$w = \Phi(x, y, z). \quad (9.28)$$

The residual for the diffusion–reaction equation (9.1) must vanish as given in (9.29)

$$\begin{aligned} & \oint \left(\Phi \Phi^T \frac{\partial C(t)}{\partial t} \right) dV + \oint (\Phi R^*(C)) dV \\ & + \oint \left(D_{11}^* \left(\frac{\partial \Phi}{\partial x} \frac{\partial \Phi^T}{\partial x} C(t) \right) + D_{22}^* \left(\frac{\partial \Phi}{\partial y} \frac{\partial \Phi^T}{\partial y} C(t) \right) + D_{33}^* \left(\frac{\partial \Phi}{\partial z} \frac{\partial \Phi^T}{\partial z} C(t) \right) \right) dV = 0. \end{aligned} \quad (9.29)$$

As before, the superscript * indicates the additional dependence of the diffusivity and reaction rate on the temperature T and oxidation state variable ϕ . After some mathematical manipulations, (9.29) can be written in matrix form as

$$[\mathbf{C}] \frac{\partial C(t)}{\partial t} + [\mathbf{B}]C(t) + \{\mathbf{R}\} = 0, \tag{9.30}$$

where, assuming orthotropic diffusivity, the matrices, $[\mathbf{B}]$ and $[\mathbf{C}]$, and vector $\{\mathbf{R}\}$ are given by

$$[\mathbf{B}] = \oint_v \left(D_{11}^* \frac{\partial \Phi}{\partial x} \frac{\partial \Phi^T}{\partial x} + D_{22}^* \frac{\partial \Phi}{\partial y} \frac{\partial \Phi^T}{\partial y} + D_{33}^* \frac{\partial \Phi}{\partial z} \frac{\partial \Phi^T}{\partial z} \right) dV, \tag{9.31}$$

$$[\mathbf{C}] = \sum_e \int_{\Omega(e)} \Phi \Phi^T d\Omega, \tag{9.32}$$

$$\{\mathbf{R}\} = \sum_e \int_{\Omega(e)} \Phi R^*(C) d\Omega. \tag{9.33}$$

Equation (9.30) is discretized by the backward Euler method in time domain, where $\Delta t = t^{n+1} - t^n$. Therefore, (9.30) can be denoted as a system of linear algebraic equations

$$[\mathbf{C}] \left\{ \frac{C^{n+1} - C^n}{\Delta t} \right\} + [\mathbf{B}] \{C^{n+1}\} + \{\mathbf{R}\} = 0. \tag{9.34}$$

In summary, the diffusion–reaction equations in their discretized form can be written as

$$[\mathbf{D}] \{C^{n+1}\} = [\mathbf{E}], \tag{9.35}$$

where

$$[\mathbf{D}] = [\mathbf{C}] + \Delta t [\mathbf{B}], \tag{9.36}$$

$$[\mathbf{E}] = [\mathbf{C}] \{C^n\} - \{\mathbf{R}\} \Delta t. \tag{9.37}$$

Equation (9.35) is solved using a direct solution with the Frontal technique and using an iterative solution with Jacobi conjugate gradient (JCG) iterative method [106] for problems with a large number of DOF.

Effective orthotropic diffusivity estimations for the lamina

The representative volume element (RVE) is used to determine the effective diffusivity of the lamina using homogenization. At the lamina scale, the homogenized diffusivity tensor is transversely isotropic or orthotropic depending upon the constituent diffusivities. Using a three-dimensional RVE, a cube of periodicity $(0, \varepsilon) \times (0, \varepsilon) \times (0, \varepsilon)$ is scaled into the unit cube $Q = (0, 1) \times (0, 1) \times (0, 1)$, as shown in Fig. 9.52a, under the change of variables $\xi_1 = x_1 / \varepsilon$, $\xi_2 = x_2 / \varepsilon$, $\xi_3 = x_3 / \varepsilon$, to find the effective coefficients \hat{D}_{ij} . Let \mathbf{F} be the domain in the unit cell which corresponds to the fiber cross section and \mathbf{M} is the domain occupied by the matrix. Set:

$$\hat{D}_{ij}(\xi_1, \xi_2, \xi_3) = \begin{cases} D_{ijf}, & \text{for } (\xi_1, \xi_2, \xi_3) \in \mathbf{F}, \\ D_{ijm}, & \text{for } (\xi_1, \xi_2, \xi_3) \in \mathbf{M}. \end{cases} \quad (9.38)$$

Let $C(\xi_1, \xi_2, \xi_3)$ be the concentration field variable that satisfies the Laplace equation in the fiber and matrix domains, and the field is computed explicitly using numerical methods under applied concentration gradients (9.39), periodic boundary conditions (9.40), and continuity conditions (9.41) imposed at the fiber–matrix interface

$$C|_{\xi_q=0} = 0, \quad C|_{\xi_q=1/2} = 1/2, \quad (9.39)$$

$$\left. \frac{\partial C}{\partial \xi_q} \right|_{\xi_q=0} = \left. \frac{\partial C}{\partial \xi_q} \right|_{\xi_q=1/2} = 0, \quad (9.40)$$

$$\sum_{i,j=1}^3 \frac{\partial}{\partial \xi_i} \left(D_{ijf,m}(\xi_1, \xi_2, \xi_3) \frac{\partial C}{\partial \xi_j} \right) = 0. \quad (9.41)$$

The three diagonal components of the orthotropic effective diffusivity tensor D_i are estimated from the concentration fields using the averaging method as given in (9.42)

$$D_i = 8 \int_0^{1/2} \int_0^{1/2} \int_0^{1/2} \sum_{q=1}^3 \hat{D}_{iq}(\xi_1, \xi_2, \xi_3) \frac{\partial C}{\partial \xi_q} d\xi_1 d\xi_2 d\xi_3, \quad (9.42)$$

where the factor “8” derives from the fact that symmetry on each orthogonal axis plane allows for the modeling of 1/8 of the fiber–matrix unit cell.

At the lamina scale, axial and transverse diffusivities are determined by applying unit concentration gradients across the unit cell in two separate simulations along the axial and transverse directions, respectively. Isotropic diffusivities denoted by D_f and D_m are assumed for the fibers and matrix, respectively, unless otherwise noted. The simulations are performed with $D_f = D_m/1,000$. Table 9.2 shows the effective diffusivity in the axial and the transverse directions for a unidirectional lamina with two volume fractions. While the effective diffusivity in the axial direction is approximately proportional to the volume fraction, the transverse diffusivity is inherently lower due to the microstructure geometry effects. The ratio D_2/D_1 of transverse to axial diffusivity is a measure of the effective anisotropic composite response.

Table 9.2. Fiber volume-dependent effective diffusivity for unidirectional lamina

	D_1/D_m	$D_2/D_m = D_3/D_m$	D_2/D_1
Unidirectional $V_f = 50.0\%$	0.50	0.32	0.64
Unidirectional $V_f = 59.4\%$	0.40	0.23	0.58

Interface/interphase issues

The fiber–matrix interface/interphase region of HTPMCs has long been suspected of being a major factor in the thermooxidative stability of the material. The fiber–matrix interphase region may have a different chemical structure and morphology due to the presence of fiber sizing or fiber coupling agent, the development of localized residual stresses, the coefficient of thermal expansion mismatch between the fiber and matrix, and other chemical interactions between the fiber and matrix during the cure processing cycle. Furthermore, the interphase region may have different reaction/diffusion kinetics than the polymer matrix phase of the composite. Typically, sizings on carbon fibers are on the order of a few molecules thick, which presumably results in an interphase region that is very thin compared to the fiber diameter. It follows that the interphase region represents a very small-volume percentage of the composite. The ability to directly characterize this region through testing is extremely limited due to its small size. Therefore, investigators typically rely on observations of the composite behavior to postulate what role the fiber–matrix interphase region has on the observed behavior. In most cases (including the simulations here), this is done without full knowledge of the role of the fiber and matrix phases of the composite. Although studies on neat bulk resins are numerous, characterization of the oxidative properties of the in situ resin and the role of the fibers in the diffusion process are not well understood.

To investigate the role of the interphase, parametric variation of the ratio of the interphase diffusivity to matrix diffusivity D_i / D_m is considered from a value of 1 to 100, using the RVE model shown in Fig. 9.52b. In addition, the interphase thickness is varied from $R_f/50$ (one-fiftieth of the radius of the fiber) to $R_f/10$. Figure 9.53 shows the effective transverse diffusivity (S_1 and S_2 surfaces) of the composite as a function of the interphase diffusivity and the thickness of the interphase. For these simulations, the diffusivity of the fiber is assumed to be zero. The figure shows that having a nondiffusive interphase results in a composite that has

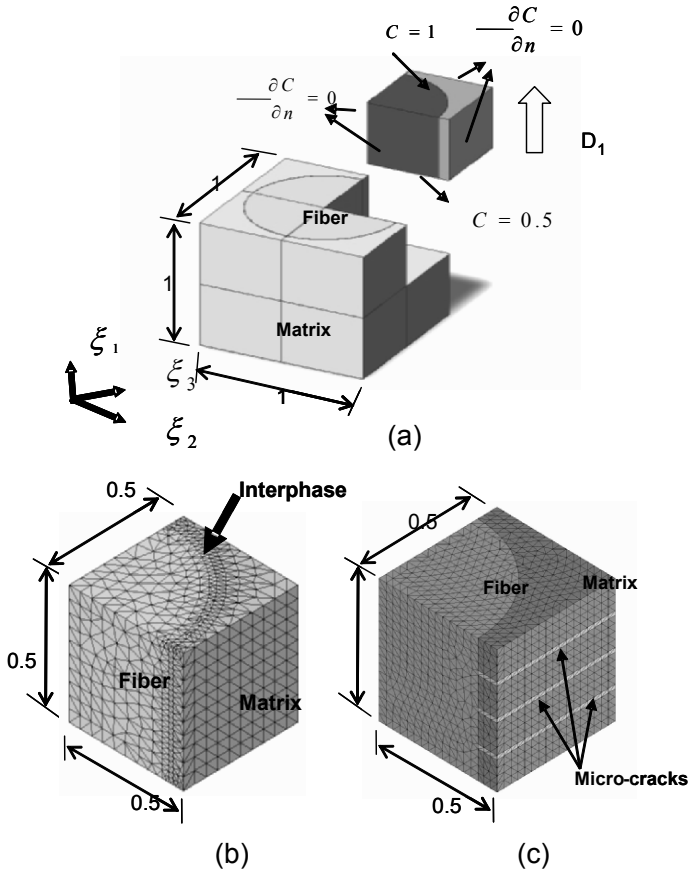


Fig. 9.52. RVE models (a) without interphase region, (b) with interphase region, and (c) with matrix microcracks

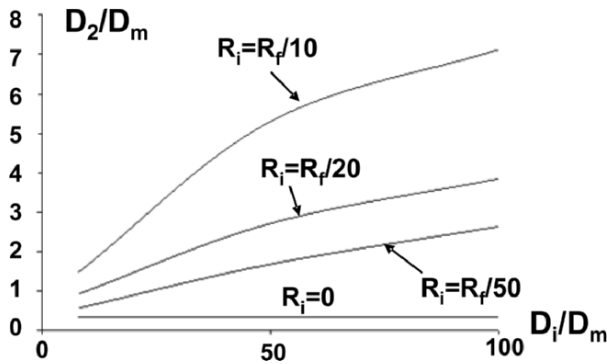


Fig. 9.53. Effect of interphase diffusivity on composite material diffusivity

an effective transverse diffusivity D_2 less than that of the diffusivity of the matrix D_m . As seen in Fig. 9.53, a highly diffusive interface can substantially increase the effective diffusivity of the composite. An interphase thickness of 5% that of the fiber radius and 100 times more diffusive than the matrix results in a composite (with 50% fiber volume fraction) with an effective transverse diffusivity of three times that of the matrix.

Effective diffusivity with discrete cracks in the RVE

A homogenization method is used to obtain the effective diffusivity of unit cells with discrete microcracks. Figure 9.52c shows the unit cell models of lamina with transverse cracks. The microcracks are modeled both as additional surfaces (with boundary sorption conditions) and highly permeable pseudomaterials with an artificial thickness assigned to them. The homogenization method described earlier is used to obtain the effective diffusivity of the unit cell in the presence of microcracking.

The fiber, matrix, and crack domains are individually modeled for a nominal fiber volume fraction of 50%, while the number of cracks modeled is varied. The matrix diffusivity $D_m = 3.45 \mu\text{m}^2 \text{s}^{-1}$, the fiber diffusivity $D_f = 0.00345 \mu\text{m}^2 \text{s}^{-1}$ ($D_f = D_m/1,000$), and the diffusivity across the crack faces is taken to be $D_c = 345 \mu\text{m}^2 \text{s}^{-1}$ ($D_c = 1,000D_m$). The effective axial D_1 and transverse D_2 diffusivities with transverse matrix cracking are shown in Table 9.3. The transverse diffusivity is substantially affected by the presence of the microcracks, while the axial diffusivity is affected to a much lesser extent [35].

Table 9.3. Effective axial and transverse diffusivity with matrix cracking

	D_1/D_m (axial)	D_2/D_m (transverse)
No crack	0.498	0.323
Two cracks	0.553	3.509
Four cracks	0.621	6.709
Six cracks	0.709	9.902

Modeling oxidation propagation in the unit cell

Three-dimensional oxidation modeling is performed using GFEA on RVEs of the composite. Inputs to the model include material properties, simulation parameters, and the unit cell geometry. Unit cells, as shown in Fig. 9.54, describe the geometry of the constituents, volume fraction, and orientation of the constituents in the composite, while the model allows multifiber and

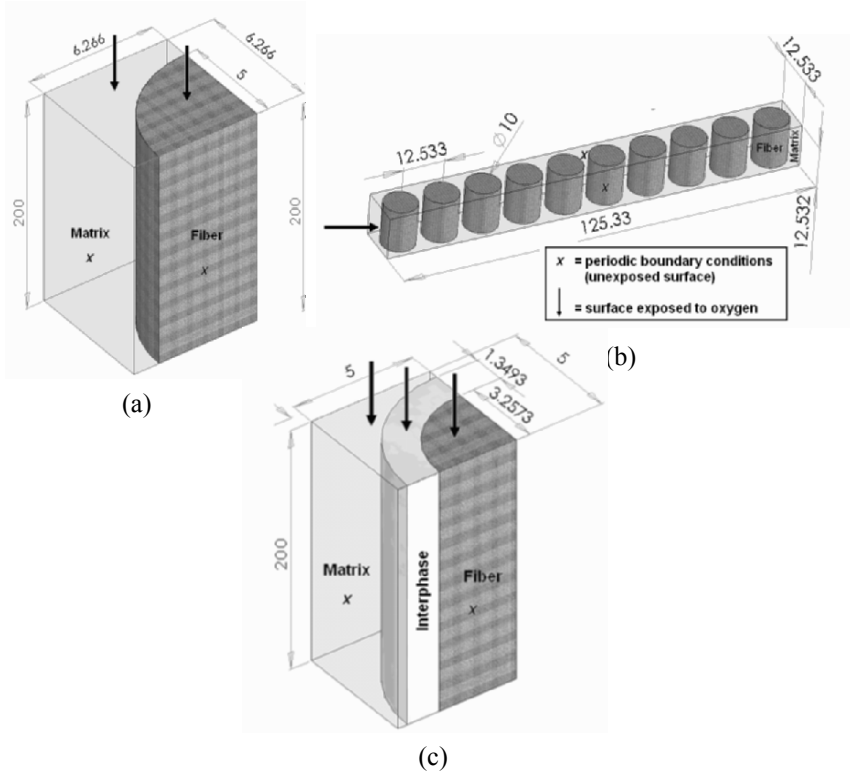


Fig. 9.54. Unit cells for modeling (a) axial oxidation, (b) transverse oxidation, and (c) the influence of interphase on oxidation growth in a unidirectional composite

multicell simulations to be performed. The unit cell geometry and element meshes are generated using commercially available computer-aided design (CAD) and FEM programs. For pure oxygen, the boundary concentration C^S is taken to be 3.74 mol m^{-3} . For air (as used for all simulations in this work), it is 0.79 mol m^{-3} . The model is meshed such that all constituents are perfectly bonded with continuity of the oxygen concentration imposed at the interface. The mesh size is varied between simulations. Two output files describing the concentration profiles (C) and the oxidation state (ϕ) in the model are produced at every time step.

For the majority of the PMC simulations presented, a 50% fiber volume fraction is assumed with no explicit representation of the inter-phase region, unless otherwise noted. It is assumed that the fibers are in a square packing arrangement, with each having a diameter of $10 \mu\text{m}$ and a spacing of $12.532 \mu\text{m}$ (center to center) between adjacent fibers. To reduce simulation time, the RVE model consists of only one quarter of a unit cell single fiber and the surrounding matrix as shown in Fig. 9.54a. The mesh has an element size of $1.28 \mu\text{m}$, with a total of 13,226 nodes and 6,845 elements. The length of this model is $200 \mu\text{m}$. Resin properties corresponding to PMR-15, as given in Table 9.1, are used.

The results of the oxidation simulation of the RVE with the surface exposed to the air being parallel to the fiber cross section are shown in Fig. 9.55. The figure shows the region where the ϕ values are within 5% of

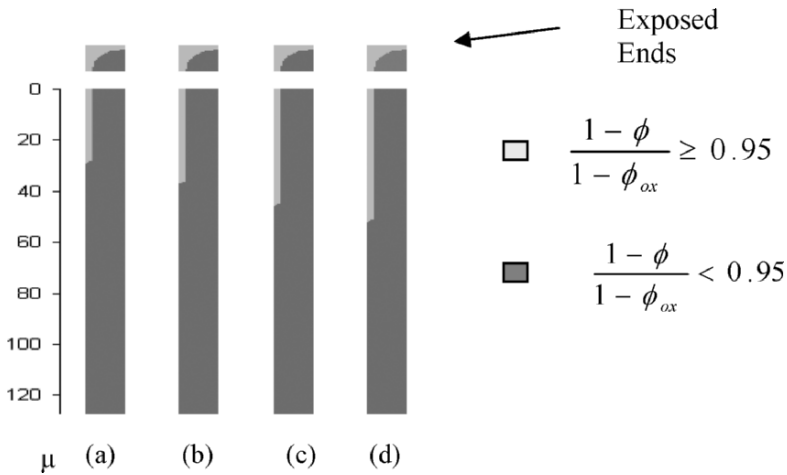


Fig. 9.55. Simulations of oxidation growth in axial direction at (a) 50 h, (b) 100 h, (c) 150 h, and (d) 200 h of exposure

completely oxidized (light gray, $\phi = \phi_{ox}$) and unoxidized (dark, $\phi = 1$) at 50, 100, 150, and 200 h of exposure. The fiber diffusivity (D_f) is taken to be 1/1,000 that of the unoxidized diffusivity of the matrix ($D_f = D_m^{un} / 1,000$). The prediction of oxidation propagation along the fiber direction is less than the experimentally observed extent of oxidation, indicating that the diffusion of oxygen in the fiber direction is not fully accounted for in this model. Next, several simulations are performed to determine the impact of the fiber diffusivity on the oxidation of the matrix. The fiber diffusivity is varied such that $D_f = (1/1,000, 1/100, 1/10, 1, 10) \times D_m^{un}$. The results are shown in Fig. 9.56. The differences between the effective unit cell diffusivity – assuming that the fiber diffusivity D_f is 1/10, 1, and 10 – and matrix diffusivity D_m^{un} are significant, indicating that fiber diffusivity has a considerable effect on composite oxidation behavior. For fiber diffusivities below $1/10 \times D_m^{un}$, oxygen diffusion through the fiber becomes insignificant. There is little change in overall oxidation, and oxidation is driven by matrix diffusivity alone.

Simulations corresponding to the exposure of transverse surfaces of the lamina were also performed. Since the repeated unit is not a single fiber, a model consisting of ten fibers in a single row was created, as shown in Fig. 9.54b. As before, the fibers have a diameter of $10 \mu\text{m}$ and a spacing of $12.532 \mu\text{m}$ (center to center). The mesh has an element size of $1.86 \mu\text{m}$, with a total of 34,300 nodes and 22,493 elements. As before, the fiber

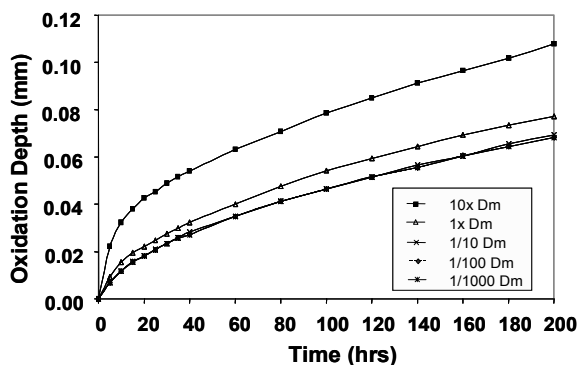


Fig. 9.56. Effect of fiber diffusivity on matrix oxidation

diffusivity is taken to be 1/1,000 that of the unoxidized diffusivity of the matrix ($D_r = D_m^{un} / 1,000$). The resin parameters corresponding to that of PMR-15 in Table 9.1 are used. Figure 9.57 illustrates the simulation of oxidation growth transverse to the fibers, while Fig. 9.58 shows a detailed view of the active reaction zone as oxidation occurs around the fiber. The observed active reaction front (Zone II) is approximately one fiber diameter in size (10 μm), which is smaller than that observed in the neat resin. The smaller active reaction zone (II) is a result of lower effective diffusivity in the transverse direction due to the presence of the fiber.

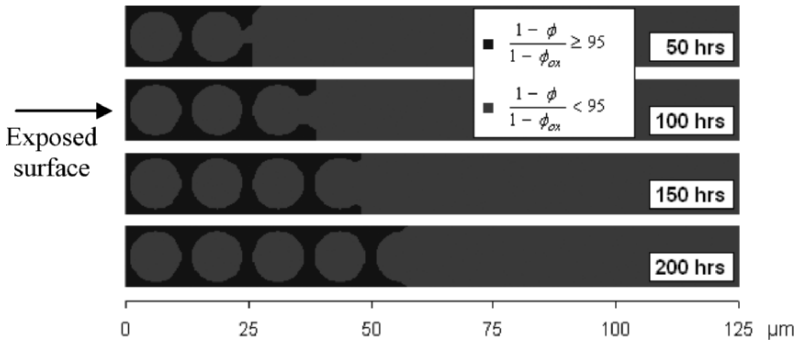


Fig. 9.57. Transverse oxidation growth in a composite lamina

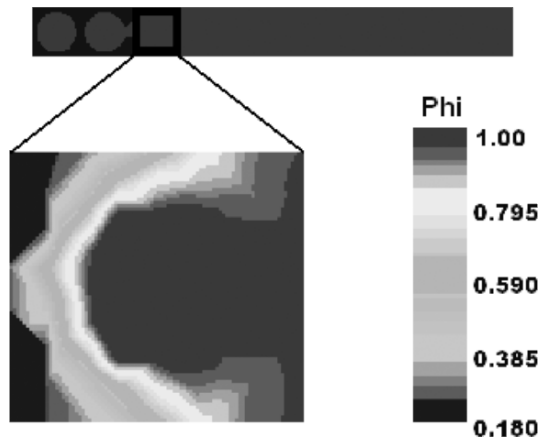


Fig. 9.58. Detail of active reaction zone from transverse simulation

A comparison of the anisotropic nature of the oxidation growth in the transverse and axial directions for 200 h of aging is shown in Fig. 9.59. The differences in the transverse and axial oxidation growth are observed to be small for the simulations performed. This is to be expected because the diffusion process for these simulations is dominated by the diffusivity of the matrix alone, since the fiber diffusivity is assumed to be negligible ($D_f = D_m^m / 1,000$). Moreover, the RVE unit cells shown in Fig. 9.54a,b do not include the fiber–matrix interphase region that can greatly contribute to the diffusion along the fiber axis direction. Neither have we accounted for the increase in effective diffusivity due to presence of damage such as fiber–matrix debonds and/or matrix microcracking.

To investigate the role of the interphase region, particularly if the interphase thickness and its diffusivity are large, a parametric study is conducted to understand the influence of the interphase parameters on the oxygen diffusivity and transport in the composite. This is accomplished by adding a concentric region around the fiber that has distinct material properties to represent the interphase region. A high interphase volume fraction (33%) and a low fiber volume fraction (33%) are chosen to exaggerate the effects of the presence of the interphase. For geometric and meshing convenience, the model assumes that the fiber diameter is $6.51 \mu\text{m}$, the interphase thickness is $1.35 \mu\text{m}$, and the fiber spacing is $10 \mu\text{m}$ (center to center), as shown in Fig. 9.54c. This produces a quarter model unit cell measuring $5 \times 5 \times 200 \mu\text{m}$ in size. PMR-15 properties (Table 9.1) are used for the matrix in the unit cell model. In addition, the

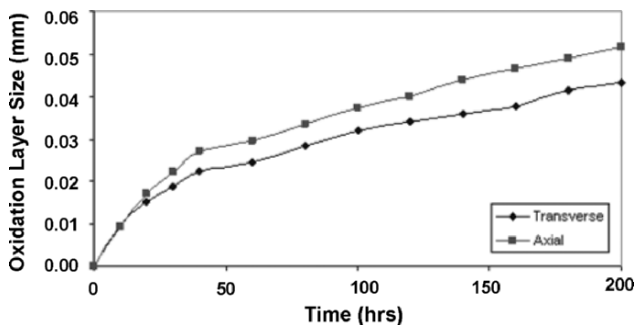


Fig. 9.59. Transverse vs. axial oxidation depth in a unidirectional composite

fiber is assigned an anisotropic diffusivity. For the initial simulations, the axial diffusivity is assumed to be equal to that of the resin (D_m^{un}) and the transverse diffusivity is taken to be $D_m^{\text{un}}/10$. The interphase layer is assigned diffusivity values of $100\times$, $1\times$, and $1/100\times$ that of the unoxidized resin (D_m^{un}). Both the fiber and the interphase region are assumed to be nonoxidized, and only the matrix phase reacts with oxygen.

Figure 9.60 shows the parametric analysis of axial oxidation region growth for the three interphase diffusivity values. The simulation with the high interphase diffusivity value shows considerable oxidation layer thicknesses and accelerated growth even during the early hours of aging. The diffusion-controlled behavior is clearly evident as the oxidation process is accelerated due to the presence of additional diffusion paths through the interphase.

Where the path of the oxygen to the matrix/interphase region is due to the fiber–matrix debonds, the effective diffusivity and, hence, the oxidation process can be effectively modeled without a discrete representation of the debonds. This can be accomplished by assigning an artificially high diffusivity value to the fiber. In such a case, it is assumed that the path the oxygen takes to penetrate to the interior is inconsequential and that it is the consequence of having the oxygen available for the oxidation process in the interior of the composite that is important. Using this approach may eliminate the need to do costly modeling of the discrete fiber–matrix debonds in the analysis. Further analysis is in progress to parametrically estimate the increase in the oxidation layer depth in the matrix due to the presence of a diffusive fiber and interphase region.

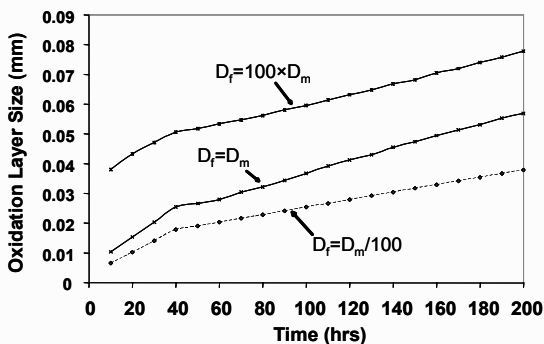


Fig. 9.60. Oxidation layer size variation with interface diffusivity

9.4.3 Lamina/Laminate Oxidation

Utilization of multiscale modeling to accurately predict the oxidative behavior of polymer composite and multidirectional laminates requires knowledge of the individual aging mechanisms, their synergistic effects, and the spatial variability of the thermooxidative degradation [78, 79, 90]. Integration of the unit cell models as input to the lamina and laminate scale models is a formidable task based on the fact that the effective tensorial properties at each material point evolve with aging time. Since the diffusion-limited oxidation process creates a large spatial variability of the oxidation state, particularly near the free surfaces, a given unit cell RVE is applicable only over material regions with common oxidation states, as well as common mechanical and thermal stresses. To use the unit cell model to predict the spatial variability of the ply properties, a finite element analysis method needs the capability to represent unique material properties for each integration point. In addition, it is well documented that multidirectional composite laminates degrade faster than unidirectional laminates [56], presumably due to the presence of ply-level residual stresses. To properly account for free-edge residual stresses and stresses due to thermomechanical loading, as well as to meet the requirements of identifying unique material properties for each integration point, a three-dimensional model in which each ply is represented discretely is warranted.

In addition, the development of damage in HTPMCs exacerbates the chemical and physical aging by introduction of stress concentrations that accelerate physical aging effects and exacerbates the chemical aging by introducing pathways for oxidants and other agents to advance deeper into the material. Damage typically takes the form of matrix cracks and fiber–matrix interface debonds with the micromechanical cracks and transverse ply cracks coalescing to form larger ply-level cracks. The mechanistic approach of modeling discrete damage, such as transverse ply cracks [58, 89], provides accurate assessments of the effective response for a given damage state but has limitations on the number of discrete cracks or amount of discrete damage that can be represented. Therefore, mechanistic damage modeling is often reserved for analyzing local details and small components or it can be used as a local model in a global analysis. Ultimately, for modeling large structures, phenomenological approaches of continuum damage mechanics [4, 100] can be used to represent the evolution of effective local damaged properties through the constitutive relationships, whereby widespread dispersed damage can be more easily represented.

Viscoelastic modeling of physical aging and thermomechanical loading

Although current aerospace applications for HTPMCs are typically limited to secondary or lightly loaded structures, the insertion of these materials into critical load-bearing structural applications will require the ability to model their creep/relaxation and long-term fatigue performance. Linear viscoelastic models are applicable in the cases where the stress levels are low such that the creep strain is proportional to the stress level. However, if the applied stress levels or the temperatures are high, nonlinear viscoelastic–plastic models may be required to adequately represent the long-term behavior [84]. To maintain acceptable factors of safety, particularly for human-rated vehicles, the use of HTPMCs in the nonlinear constitutive range for flight-critical structures will likely be limited. Nevertheless, to predict the behavior of HTPMCs for such cases as accelerated aging at higher than use temperatures and determination of the material response for load and temperature excursions, a nonlinear viscoelastic–plastic model may be needed.

Studies of the creep behavior of neat resin high-temperature polymers provide the basis for micromechanical unit cell modeling for HTPMCs. Marais and Villoutreix [57] show the effect of physical aging on the relaxation constants and relaxation times of thermostable PMR-15 resin. In that work [57], the viscoelastic behavior is described by the Kohlrausch function, and, combined with the Maxwell relation, enables the creep compliance to be modeled for short-loading times. However, it is not possible to establish an equivalence between time and temperature using Williams, Landel, and Ferry (WLF)-type shift factors [124]. The master curve, constructed graphically on the basis of linear viscoelastic strains, short times, and a reference temperature of 250°C, deviates significantly from the experimental curves at longer times. Thus, the long-loading time response could not be determined from the short-loading time viscoelastic response as the material undergoes a slow plastic deformation. Although such approaches may be appropriate and adequate for treating homogeneous materials, their applicability to the material designer is limited. The shift functions and master curves are needed for each composite system and can only be determined after extensive and expensive testing. Methodologies that construct the material behavior from the constituent's age-influenced response are scant and nascent.

The nonlinear viscoelastic theory by Schapery [84] has been substantially exploited for evaluating PMCs in high-temperature applications. Nicholson et al. [69] investigated the effect of molecular weight and temperature on the elastic and viscoelastic properties of thermoplastic

polyimides. They found that the lower molecular weight materials have higher creep compliance and creep compliance rate and are more sensitive to temperature than the higher molecular weight materials.

As discussed previously, for a micromechanical unit cell analysis, the fiber, matrix, and interphase region can all be modeled explicitly. The polymer matrix is typically assumed to be viscoelastic while the fiber is assumed to be elastic [21, 72, 127]. Modeling of the time and temperature variation of the reinforced composite material's compliance typically utilizes effective properties derived from the unit cell analysis, or treats the problem at the lamina scale in the context of classical lamination theory. A general method for incorporating the influence of physical aging on the material stiffness has been to study the relaxation behavior of the composite material. Most of the approaches are empirical and treat composite as a homogeneous continuum. They characterize the relaxation moduli and relaxation times based on dynamic mechanical analyzer (DMA) testing, and add an additional physical, age-based shift to the time-temperature-shifted reduced time. Hashin [46] observed that, for unidirectional composites, the viscoelastic effects can be significant for axial shear, transverse shear, and transverse normal stresses (matrix-dominated properties), with the effects becoming more pronounced with increase in temperature and loading.

It is beyond the scope of this chapter to review all of the relevant research on this important subject. Reviews such as that by Scott et al. [93] can be referred to for a more comprehensive treatment of the topic. In lieu of a comprehensive review of the topic, a review primarily focused on the viscoelastic models as they have been applied to HTPMCs will be given. Such a limited review would not be complete without inclusion of the significant body of work performed in the NASA HSR program [21, 42, 49, 68, 115, 116]. Much of this work focuses on the use of linear viscoelasticity theory using the time-temperature-based superposition principles to model long-term physical aging behavior based on short-term observations. A large volume of work on describing the short- and long-term physical aging of amorphous (glassy) polymers and PMCs is based on the free-volume concept by Struik [98]. Struik showed that Boltzmann's superposition principle could be used to describe physical aging in many polymers. This concept is widely accepted in the linear viscoelastic or small deformation range [21, 23, 36, 99]. In time aging, time superposition [98], based on the premise that the shape of the creep curves for a given material does not change with aging time, aging primarily affects the creep properties by way of changes in the relaxation times. Modeling one aspect of the HTPMC's aging response, namely physical aging, Brinson and Gates [21] described the momentary creep compliance of the material by a three-parameter fit model as

$$S(t) = S_0 \exp(t / \tau(t_e))^\beta \tag{9.43}$$

with

$$\tau(t_e) = \tau(t_{\text{eref}}) / a_{t_e}, \tag{9.44}$$

where t_{eref} is the reference aging time, and the aging time shift factor a_{t_e} can be written as

$$a_{t_e} = (t_{\text{eref}} / t_e)^\mu \tag{9.45}$$

with the reference aging time shift factor set equal to unity. Numerous expressions for the shift factor have been presented in the literature including the temperature-dependent WLF empirically derived relationship that has been found to work well above the material's T_g [124]. Therefore, the parameters needed to describe the momentary creep compliance at any aging time are the initial compliance S_0 , the shape parameter β , the shift rate μ , and the relaxation time τ [21]. Struik characterized aging by the double-logarithmic shift rate μ , defined as

$$\mu = - \frac{d(\log a_{t_e})}{d(\log t_e)}, \tag{9.46}$$

where μ is constant over a wide range of aging times and is approximately unity when the material is far removed from thermodynamic equilibrium. Through horizontal shifting on the log scale, the momentary creep curves can superpose through changing the relaxation time. In the case where the testing time t is greater than the initial aging time t_e^0 , such that the total aging time is given by $t + t_e^0$, the long-term response is expected to deviate from the momentary response. If the reference aging time is taken to be the initial aging time $t_{\text{eref}} = t_e^0$, the shift factor $a_{t_e^0}$ for any time t is given as

$$a_{t_e^0}(t) = (t_e^0 / (t_e^0 + t))^\mu. \tag{9.47}$$

Furthermore, the effective time is defined as the accumulation of the shift factors given by

$$\lambda = \int_0^t a_{t_e^0}(\xi) d\xi. \tag{9.48}$$

Using the effective time in place of the testing time in (9.43) given by

$$S(t) = S_0 \exp(\lambda / \tau(t_e^0))^\beta \tag{9.49}$$

allows for the prediction of long-term response based on short-term observations [21]. Based on experimental observations [99] that the S_{22} and S_{66} terms of the compliance tensor are dominated by matrix properties,

the viscoelastic response of a unidirectional laminate is typically modeled by representing S_{22} and S_{66} as viscoelastic and the other compliance terms as elastic. Brinson and Gates [21] determined that, for tension tests, the aging shift rate is the most critical parameter in predicting long-term performance. Later work focused on utilization of this approach for compression-loaded composites [115, 116].

During the thermal aging process, in which both physical and chemical aging are occurring, chemical oxidative aging results in changes to the thermomechanical properties of the material and damage evolution. To account for the aging time-dependent chemical/oxidative aging, characterization of the oxidation-dependent viscoelastic constitutive parameters may be required. That is, the viscoelastic constitutive properties/parameters as a function of the polymer availability state variable $\phi(t, T)$ for all times t and temperatures T of interest will be required. Additionally, ϕ will be path dependent if the range of temperatures of interest entails changes in the oxidation mechanisms. Such an experimental characterization program would be overwhelming. In lieu of such an experimental program, a capability to predict mechanical properties based on the oxidative state of the neat resin is needed. However, this capability does not currently exist. Various simplifying assumptions can be used to overcome these deficiencies. One alternative is to represent the oxidative degradation as smeared or discrete damage in the viscoelastic framework. Both linear [3, 85] and nonlinear [127] viscoelastic models with damage evolution have been used to account for both physical aging and the damage associated with oxidative aging.

These viscoelastic material representations at the micromechanical level and the lamina level can predict the effective response of the material subjected to physical aging. Generalizations of these models to include damage and in the case of Skontorp and Wang [96] to represent chemical aging have been presented. However, for PMCs subjected to environmental conditions in which the predominant aging effect is chemical oxidative aging, a satisfactory model to predict long-term performance has yet to be completed. It is likely that the viscoelastic models discussed here will be an integral part of a global-local model where the ply-level homogenized continuum representation of the effective anisotropic behavior and spatial property variability of degraded plies is determined through micromechanical models. However as mentioned earlier, for lack of simulation-based tools, composite material designers routinely perform weight loss studies for specimens aged in simulated operating and accelerated aging conditions to assess the thermooxidative stability of materials.

The relative oxidative stability of the composite is determined by comparing the percent weight lost during the exposure for various materials. While this is an effective way of comparing materials, the test yields little information that can be used to determine the quantitative response of the materials for in-service operating conditions. In general, the relationship between weight loss and property changes can be highly nonlinear and does not provide a measure of the spatial variability of degradation within the specimen. The reliability of predicting performance using methods based entirely on weight loss, in which small changes in weight can result in significant declines in mechanical properties, is questionable. However, in the absence of methods to predict end-of-life properties, weight loss has been an accepted method to compare the thermooxidative stability of different materials [94] and is discussed in subsequent sections.

9.4.4 Lamina Weight Loss Models for Oxidative Aging

One of the most widely used methods of characterizing the level of thermo-oxidative degradation is presented by Nam and Seferis [66] where specimen weight loss is correlated to mechanical performance. In this method, specimens are aged under isothermal conditions and weight loss measurements are recorded as a function of aging time. It is assumed that weight loss is primarily due to oxidation (neglecting moisture weight loss) and that oxidation is the dominant cause of changes in the properties of the polymer composite. The method provides valuable screening information on the thermooxidative stability of material systems and can be used to compare the stability of different material systems. Although the method has been used by numerous researchers [24, 30, 55, 97, 108], it only provides an effective measure of the degradation of the specimen as a whole and does not provide any measure of the spatial variability of degradation within the specimen. In addition, the correlation of weight loss to mechanical and dielectric properties combines all of the effects of aging (physical and chemical) into a single scalar quantity.

Weight loss observations

Since the weight loss as a function of isothermal aging time has traditionally been used to compare the thermooxidative stability of HTPMCs, it is necessary to understand the specimen parameters affecting the weight loss. As mentioned earlier, the anisotropy of oxidation (and in turn, weight loss behavior) of PMCs was first documented by Nelson [67] when he observed that the oxidation process is sensitive to the surface area for the

different test specimens that he aged. He found that the materials degraded preferentially at the specimen surface perpendicular to the fiber (0° edges) and that the rate of oxidation is hastened by microcracks opening on the 0° edges. The enhanced weight loss from surfaces cut perpendicular to the fiber direction has also been noted and reported by numerous investigators, e.g., Bowles and Novak [12], Bowles [7], Bowles et al. [16], Skontorp et al. [97], Chung et al. [24], Bellenger et al. [6], and Kung [54]. Further, interlaminar residual curing stresses play a significant role in the thermooxidation process at the free-edge of composites, resulting in much greater weight loss in crossply laminates compared to that of unidirectional laminates [15].

In a recent work [91], four different unidirectional G30-500/PMR-15 composite specimen geometries representing different surface area ratios were selected, as reported in Table 9.4. The total surface areas for the R1, R2, and R4 specimens are all approximately equal ($\sim 800 \text{ mm}^2$), while the total surface area of the R3 specimens is nearly double that of the other specimens ($\sim 1,500 \text{ mm}^2$). In Table 9.5, the surface areas and the surface area ratios of the four specimen geometries are given. Figures 9.61–9.64 show the weight loss history for the four specimen geometries isothermally aged at 288°C in both air and argon gaseous environments. Comparing the four specimen types aged in an inert argon environment shows that the specimen geometry does not significantly influence the weight loss when normalized to the total surface area of the specimens. Volume changes and weight loss resulting from nonoxidative degradation are likely a result of degassing of low molecular weight components created by chain cleavage in the polymer [24]. Nonoxidative aging is expected to be independent of surface area and surface type and is a volumetric response. Therefore, the percentage weight change for the argon-aged specimens is expected to be independent of the specimen geometry. For all four geometries, the argon weight loss appears to approach an asymptote between 2,000 and 2,500 h. However, the weight loss data for the air-aged specimens for each of the specimen geometry show that there is a strong dependence of the weight loss on the surface area ratio $(S_1 + S_2)/S_3$, indicating that the weight loss is dependent on surface type. The lower the magnitude of the surface area ratio $(S_1 + S_2)/S_3$, the greater the normalized weight loss, as seen in Fig. 9.65. In addition, the weight loss in air appears to be nonlinear in time with an increase in oxidation rate for increasing aging times. This is consistent with weight loss increases due to surface cracking that increases the actual total surface area through which oxygen can diffuse.

Figure 9.66 shows plots of the nonoxidative weight loss as a percentage of the total weight loss in air for the four specimen geometries as a function of the aging time. Although such results are dependent on specimen volume-to-surface area ratios, some general trends can be inferred. For early aging times, the nonoxidative weight loss is a substantial percentage of the total weight loss of the composites. For the specimen geometries that were tested, the nonoxidative weight loss is in the range of 25–50% up to the first 500 h of aging. Since the nonoxidative weight loss tended toward an asymptote between 2,000 and 2,500 h and the overall weight loss tends to accelerate for long-aging times, the contribution of the nonoxidative aging decreases for long-aging times. It is also noted that the ratio of the weight loss increases with an increasing $(S_1 + S_2)/S_3$ ratio.

Table 9.4. Dimensions of four specimen geometries

Specimens (three each)	Width (mm) axial	Length (mm) transverse	Thickness (mm)
R1	37.77	7.57	2.47
R2	17.52	17.58	2.44
R3	25.09	25.08	2.39
R4	7.58	37.76	2.70

Table 9.5. Surface areas and area ratios for four specimen geometries

Specimens	S_1 (mm ²)	S_2 (mm ²)	S_3 (mm ²)	$S_1 + S_2 + S_3$ (mm ²)	$(S_1 + S_2)/S_3$
R1	571.0	37.3	186.3	794.6	3.27
R2	616.0	85.8	85.5	787.3	8.21
R3	1,258.2	119.7	119.7	1,497.6	11.51
R4	572.5	203.9	40.9	817.3	18.98

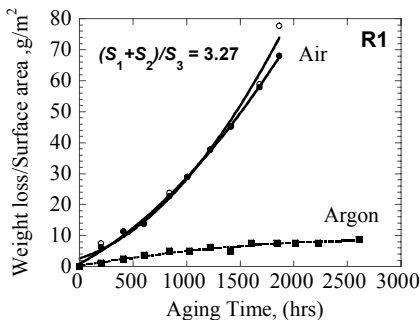


Fig. 9.61. Normalized weight loss for R1 specimens aged in air and argon

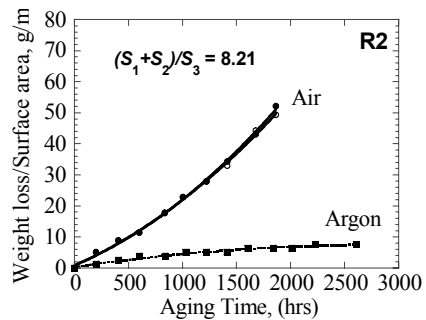


Fig. 9.62. Normalized weight loss for R2 specimens aged in air and argon

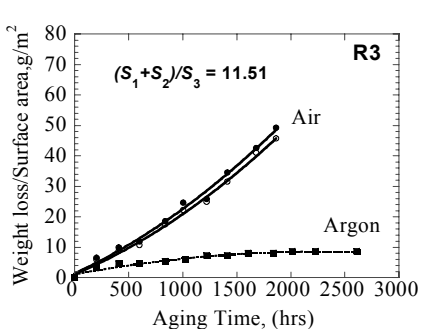


Fig. 9.63. Normalized weight loss for R3 specimens aged in air and argon

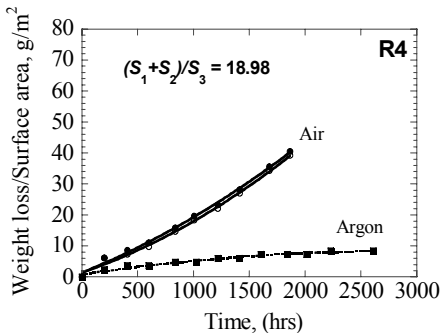


Fig. 9.64. Normalized weight loss for R4 specimens aged in air and argon

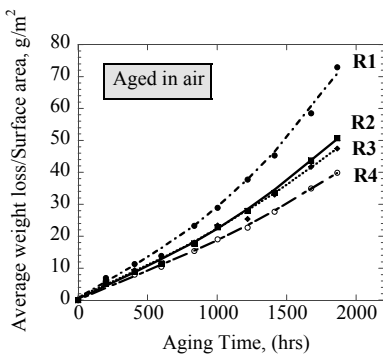


Fig. 9.65. Comparison of normalized weight loss in air for four specimen geometries

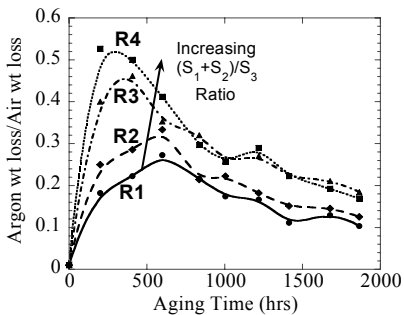


Fig. 9.66. Percentage of total weight loss attributed to nonoxidation weight loss

Empirically derived weight loss models

Led by the work of Bowles and Meyers [11], several weight loss models for predicting the long-term aging of HTPMCs based on weight loss surface fluxes have been developed [12, 24, 94, 95]. Most weight loss models found in the literature assume that weight loss is due to surface-controlled oxidation mechanisms and, to a lesser extent, to thermally induced reactions in the bulk of the material. However, it is shown in Fig. 9.66 that the surface-independent weight loss in the inert argon environment can account for a substantial part of the overall weight loss, particularly for short-aging times. Although the existing empirical weight loss models do not separately account for nonoxidative weight loss, its effect on the overall weight loss is inherently accounted for when determining the empirical weight loss parameters.

Bowles and Nowak [12] considered three different rates of weight loss from three different types of unidirectional composite surfaces shown in Fig. 9.15. The weight losses were expressed as weight loss fluxes or weight loss per unit surface area per unit of time. The composite weight loss is expressed as

$$Q(t) = At^B + C, \quad (9.50)$$

where A , B , and C are determined from an empirical curve fit. Further A is given as $A = S_1k_1 + S_2k_2 + S_3k_3$ and t is the aging time. The material parameters k_1 , k_2 , and k_3 are the respective weight loss fluxes or weight loss per unit surface area per unit of time. Knowing A from empirical curve fitting to the total weight loss for a given specimen k_1 , k_2 , and k_3 can be determined from three different specimen geometries. Bowles and Nowak [12] found that k_1 and k_2 were nearly equal, indicating that the weight loss rates from the transverse machined surface S_2 and the transverse tool surface S_1 are approximately the same. Further, the nonlinear time dependence of the flux rates is accounted for in the B exponent which is found to be time and temperature dependent. Based on testing composite specimens with different thickness, Bowles et al. [18] commented that only specimens of like dimensions can be directly compared on the basis of mass loss. That is, the model parameters, in particular the weight loss fluxes k_1 , k_2 , and k_3 , and the parameter B , are dependent on the geometry of the specimen and B is not necessarily constant for a given aging temperature. Therefore, caution must be used when utilizing (9.50) to predict weight loss for specimen geometries and aging times that have not been tested.

As an alternative to using the surface weight loss fluxes (k_i , $i = 1, 2, 3$), Skontorp [95] and Wong et al. [126] approximated the total isothermal aging weight loss $Q(t)$ of a unidirectional composite by using weight loss per unit area (q_i , $i = 1, 2, 3$) as

$$Q(t) = (S_1 + S_2)q_1 + S_3q_3, \quad (9.51)$$

where the weight loss per unit area, q_1 and q_2 , was assumed to be equivalent based on experimental data. Knowing S_1 , S_2 , and S_3 , the weight loss per unit area parameters q_1 and q_3 can be determined empirically by aging two specimens with different ratios of $(S_1 + S_2)/S_3$ in identical environments and solving the resulting set of linear equations. For discrete times throughout the oxidative aging, these weight loss factors can be calculated to provide a history of the weight loss rates for each of the three surface types. Additionally, the parameters can be determined for a range of isothermal aging temperatures to obtain both their time and temperature dependence for a given material system.

Using a similar expression, Chung et al. [24] also expressed the total weight loss in terms of the weight loss rates as

$$Q(t) = S_1q_1 + S_2q_2 + S_3q_3, \quad (9.52)$$

where q_i is the weight loss per unit area defined using the shrinking core weight loss model [66], namely $q_i = D_{Ei}t^{n_i}$, where n_i are time exponent factors and D_{Ei} are effective diffusion coefficients that may be described by Arrhenius expressions. The weight loss expression is similar to that of Bowles and Nowak [12], differing by the use of independent time exponential factors for each of the surface-specific weight loss parameters. Chung et al. [24] found it necessary to include an additional extrinsic term q'_3 giving the final weight loss relationship as $Q(t) = S_1q_1 + S_2q_2 + S_3(q_3 + \kappa q'_3)$, where κ is a modeling parameter representing a dimensionless characteristic diffusion length and $q'_3 = D'_{E3}t / (D'_{E3}t + 1)$ with an effective diffusion coefficient D'_{E3} . This additional term accounted for the nonoxidation thermal degradation such as that highlighted in Fig. 9.66. The weight loss model (9.52) requires six independent parameters, including two extrinsic parameters.

The use of weight loss expressions given in (9.50)–(9.52) is based on weight loss rates from the three types of specimen surface areas. The surface areas S_1 , S_2 , and S_3 are the preaging surface areas of the specimens. Due to shrinking, material loss from exposed surfaces, and surface

microcracking, the surface areas of the specimens change throughout the aging process. Therefore, surface areas S_1 , S_2 , and S_3 should more accurately be described as the initial areas based on the original specimen dimensions. Since the surface areas S_1 , S_2 , and S_3 are used for the duration of the prediction, the change in the surface areas due to aging damage is effectively accounted for in the weight loss rate parameters q_1 , q_2 , and q_3 . The weight loss rate parameters q_3 and θ_3 (defined in a later section) are also strongly influenced by the fiber–matrix interface or interphase properties [95]. Theoretically, it is possible to measure the effect of different fiber sizings using weight loss rate parameters, however the practicality of this depends on the magnitude of the influence of the sizing on weight loss.

Weight loss predictions in unidirectional composites

In [91], the weight loss model used for the predictions is based on that of Skontorp [95]. The parameters q_1 , q_2 , and q_3 were calculated for aging times up to 1,864 h using the 288°C (550°F) air-aged weight loss data (Figs. 9.61–9.64) for the four specimen geometries. To determine the range of the parameters as a function of which three of the four specimen geometries were used for the calculations, four unique combinations of three of the four specimens were used. That is, four different sets of q_1 , q_2 , and q_3 parameters were calculated for the data set over the time range shown. Figure 9.67 shows the data for q_1 , q_2 , and q_3 based on the weight loss data for the four specimen geometries. This is referred to as the three-parameter model. It is shown that there is little variation of the parameters

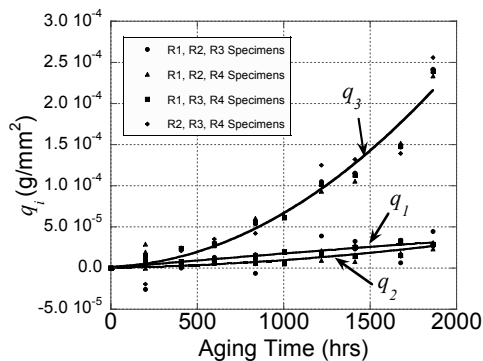


Fig. 9.67. Parameter determination using data from all four specimen geometries

as a function of which three of the four data sets were used for the calculations. Quadratic curves were fitted through the combined four data sets for each of the q_1 , q_2 , and q_3 parameters. It can be seen that the weight loss per unit surface area for the S_1 and S_2 surfaces is nearly identical for aging times up to 1,864 h. In addition, it can be seen that q_3 is increasing nonlinearly for increasing aging times (indicative of surface cracking), while q_2 and q_3 are increasing nearly linearly.

Next, q_1 and q_2 are assumed to be equal in (9.52) which results in the weight loss relationship expressed by (9.51). Equation (9.51) is then used to independently evaluate the q_1 and q_3 parameters. An advantage of using (9.51) rather than (9.52) is that it requires two rather than three specimen geometries to obtain the needed weight loss parameters. The data based on (9.51) are referred to as the two-parameter model. While there is some variation of the weight loss factors depending on the particular selection of two specimens used in their determination, the agreement for all specimen combinations is considered acceptable [91]. Further, the curve fits for the two-parameter model were found to be consistent with the curve fits for the three-parameter model. Finally, using the evaluated two-parameter curve fit functions, (9.51) is used to calculate the weight loss of the four specimen types. The experimental data (discrete points) and the weight loss determined by (9.51) (solid lines) are shown in Fig. 9.68. The figure demonstrates that specimens with different geometry and different overall surface areas can be characterized with single time-dependent weight loss per unit area expressions for q_1 and q_3 .

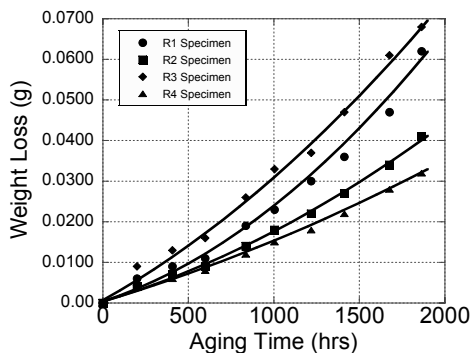


Fig. 9.68. Weight loss predictions for four specimens with four surface area ratios compared to experimental weight loss data

Weight loss predictions in woven composites

To demonstrate the predictive capability of (9.51) for multidirectional laminates, literature data of T650-35/PMR-15, 8-harness, satin-weave composites from Bowles et al. [20] are used. In that work [20], four specimen geometries with different $\Sigma_1 / (\Sigma_2 + \Sigma_3)$ surface area ratios aged at five different temperatures ranging from 204 to 343°C were examined. The specimen designation used by Bowles et al. [20], along with the area fraction ratios and total surface areas ($\Sigma_{\text{total}} = \Sigma_1 + \Sigma_2 + \Sigma_3$) of the specimens, is given in Table 9.6.

Table 9.6. Specimen geometries from Bowles et al. [20]

Specimen	$\Sigma_1 / (\Sigma_2 + \Sigma_3)$	Σ_{total} (mm ²)
T-3	68.66	19,898.5
T-5	34.16	20,385.5
T-12	13.68	21,962.8
T-50	6.01	3,233.6

The equivalent form of the weight loss relationship of (9.51) for the woven composites is given by $Q(t) = \Sigma_1 \theta_1 + (\Sigma_2 + \Sigma_3) \theta_3$, where, in a manner similar to unidirectional composites, the weight loss per unit surface area for the warp and fill surface areas Σ_2 and Σ_3 is assumed to be equal. For each of the five test temperatures, two of the four specimen types were used to calculate θ_1 and θ_3 . Figures 9.69 and 9.70 show the variation of the

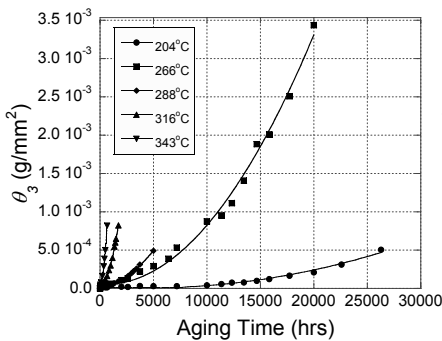


Fig. 9.69. Weight loss rate function θ_3 as a function of aging temperature (based on experimental data from Bowles et al. [20])

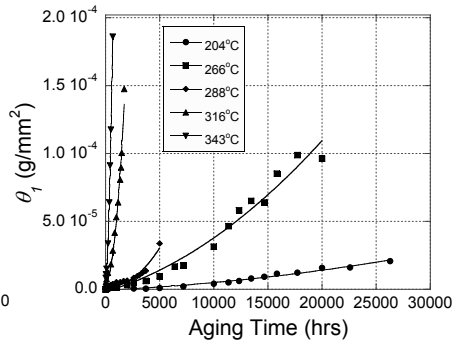


Fig. 9.70. Weight loss rate function θ_1 as a function of aging temperature (based on experimental data from Bowles et al. [20])

weight loss factors θ_1 and θ_3 as a function of aging temperature and aging time. As with the unidirectional PMR-15 composites, the weight loss rate on the edge surfaces of the specimen θ_3 is an order of magnitude greater than the weight loss rate on the top and bottom surfaces θ_1 for all aging temperatures. In addition, Fig. 9.69 illustrates the increase in the rate of θ_3 with an increase in aging time. This “apparent” rate increase is likely due to increases in the actual surface area due to aging cracks. Since the oxidation process is typically diffusion rate limited rather than reaction rate limited, the crack development provides pathways for oxygen to diffuse deeper into the composite increasing the overall oxidation rate. Figures 9.69 and 9.70 show the extraordinary temperature dependence of the weight loss rates. The maximum sustained use temperature of PMR-15 composites is typically considered to be 288°C and at this temperature, the weight loss rates θ_1 and θ_3 are relatively small compared to the rates at 316 and 343°C. In part, this can be explained by the early initiation of cracks in specimens aged at these higher temperatures.

Figure 9.71 shows the prediction of T-5 weight loss history at 204°C over 25,000 h of aging time. The T-5 specimen predictions are based on the functions θ_1 and θ_3 determined from the T-3 and T-12 specimen data for 204°C aging. There is an excellent correlation of the predicted weight loss of the T-5 specimens and the measured weight loss over the entire 25,000-h history. Thus, using an equivalent form of the weight loss relationship for woven composites, the empirically based model is also successfully used to predict the weight loss of 8-harness satin composites using data from the literature. Thus, the long-term isothermal weight loss response of both unidirectional and woven composites is successfully predicted.

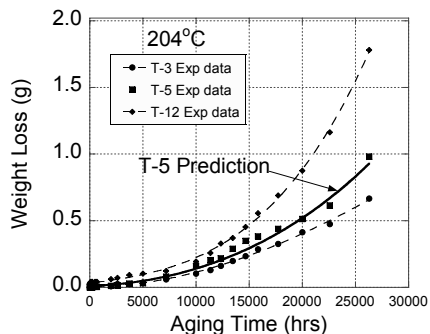


Fig. 9.71. Weight loss rate functions θ_3 and θ_1 (based on T-3 and T-12 specimen data) used to predict T-5 weight loss history at 204°C for aging times over 25,000 h (based on experimental data from Bowles et al. [20])

Design recommendation

The practice of using weight loss measurements on small specimens ($4\text{--}5\text{ cm}^2$) used by the aerospace industry to screen candidate PMCs for high-temperature applications could provide significantly more information than is currently being obtained. Modifying this practice by including one additional specimen with a different $(S_1 + S_2)/S_3$ surface area ratio would provide weight loss rates per unit area for the transverse q_1 and axial q_3 surfaces rather than an average weight loss per unit area for the entire specimen. This would allow designers to predict the performance of the components made from the candidate material for in-service environments. Whereas the weight loss from the axial surface may have a dominate contribution to the overall weight loss for small specimens, it may have a negligible contribution to the weight loss of aircraft components. This is due to the fact that only a very small percentage (or more likely none) of the exposed surface of components is the axial surface. Therefore, the weight loss rate per unit area for the transverse surface q_1 is what controls the thermooxidative weight loss of aircraft components and its value cannot be determined using a single specimen.

Accelerated aging behavior

The concept of equivalent property time (EPT) was established by Seferis [94] to understand degradation of polymers and composites, both for isothermal and dynamic elevated temperature exposures. According to Seferis [94], conversion may be defined as the ratio of actual weight loss to total weight loss corresponding to a given stage of the degradation process, i.e.,

$$\alpha = \frac{(M_0 - M)}{(M_0 - M_f)}, \quad (9.53)$$

where M , M_0 , and M_f are the current, initial, and final weights of the specimen, respectively. When activation energy (E) and time (t_{ref}) to a certain conversion at reference temperature T_{ref} under isothermal conditions are known, the time to the same conversion at other temperatures can be obtained from

$$t = \text{EPT} = t_{\text{ref}} \exp \left[\frac{E}{R} \left(\frac{1}{T} - \frac{1}{T_{\text{ref}}} \right) \right], \quad (9.54)$$

where R is the universal gas constant, and the activation energy is assumed to be independent of temperature. In cases where the activation energy is

not a constant over the entire temperature range of interest (implying that the weight loss mechanisms vary or differ over the temperature range), multiple subtemperature ranges have to be considered and constant activation energy E values evaluated over the temperature subdivisions for describing the weight loss behavior. The EPT concept is used to describe thermal gravimetric analysis (TGA) weight loss of bismaleimide and epoxy composites [94] and was demonstrated as a useful tool in designing aging experiments and assessing the lifetime of composite systems. An extension of this concept was developed to include equivalent cycle time (ECT), where ECT is defined as the characteristic time that equated properties of an isothermally aged material to that subjected to temperature cycles. Collectively, the EPT and ECT methodologies were shown to have the potential for correlating the data relating to the time and temperature equivalence of properties that continuously change.

9.5 Conclusions

Thermooxidative degradation of PMCs is clearly a subject of major importance as designers push the high-temperature endurance limits of polymer composites to improve the performance of aerospace systems. In recognition of recent developments of more thermally stable and durable high-temperature polyimides for replacing the legacy high-temperature polyimides such as PMR-15, the importance of a service life prediction capability for HTPMCs cannot be overstated.

The extraordinary cost of qualifying and developing empirically based material design allowables for new materials is prohibitive for today's low-rate production aircraft, particularly when affordability is a major concern. Robust analysis and design tools to predict service performance and service life enable the insertion of new materials that offer superior performance. This is accomplished by replacing the empirically based allowables generation methodology with one that relies primarily on predictive tools and strategic testing. Of course the challenge of implementing this methodology is to develop predictive tools with a level of robustness such that the analytical derived design allowables can be used with the same level of confidence and fidelity as the empirically based design allowables. Added to all of the tremendous challenges of modeling the performance and strength of composites in benign thermal environments are the difficult challenges of modeling the age-dependent properties of composites at high temperature. These added challenges are manifested even at the molecular scale at which an understanding of the basic chemical degradation

mechanisms of the polymer of interest is lacking. Until robust predictive capabilities are developed, designers will continue to rely on expensive long-term testing to establish design allowables for thermooxidative stability of PMCs.

Recognition that the molecular level oxidative and hydrolytic degradation reactions of the matrix polymer of composites can ultimately influence the structural response prescribes that multiple scales need to be considered for analyzing their behavior. However, difficulties in relating the chemical state of a material to its physical and mechanical properties are a pervasive problem in the materials science community. This is particularly true when the initial state of the material may not be adequately known, and the material's chemical state continuously evolves by reacting with its environment. Although large-scale molecular dynamics simulations offer future potential to resolve these difficulties, application of molecular dynamics to highly crosslinked polyimides is beyond current modeling capabilities. Empirically derived relationships that relate the chemical state of polymers to physical and mechanical properties are a known alternative to the mechanistic modeling of molecular dynamics. However, experimental evaluation of the time-dependent evolution of the chemical state of polymers is particularly challenging for long-term aging.

The strong interaction of the physical, chemical, and mechanical aging behavior of HTPMCs is due to the significant contrast in the properties of the fiber and matrix constituents of the composite. These interactions are particularly apparent in the critical fiber–matrix interface/interphase where the interface/interphase has been shown to play a dominant role in the thermooxidation process. Difficulties associated with modeling the interface/interphase region include characterization of its properties (interface fracture toughness and strength [40, 102] and interphase thermal–physical–mechanical properties), determination of the size of the interphase region, and proper treatment of the coupling between the mechanical (damage) and chemical processes. Since direct measurements of the properties of the interphase are deficient, interphase properties and model parameters may be *estimated* based on indirect observations of the composite behavior. HTPMCs have high glass transition temperatures (high by polymer standards), and the temperatures at which they are cured may be on the order of 200°C greater than the cure temperature for epoxy composites. High curing temperatures exacerbate the detrimental fiber–matrix residual cure stresses (as well as the interlaminar residual cure stresses). The contribution and role of these micromechanical residual curing stresses at the interface/interphase to the thermooxidative stability require additional consideration.

As with the interface/interphase, experimental characterization of anisotropic physical and mechanical properties of carbon fibers is elusive. Although the degradation of the in situ fiber in the composite has long been considered to be negligible, the role of the fiber and its contribution to the oxidation process has not been fully explored. Specifically, little is known about the diffusivity of oxygen in the fiber and its contribution to the transport of oxygen to the interior of the composite. Alternative pathways for transport of oxygen into the interior of the composite are fiber–matrix debonds that propagate with the oxidation front. This possible mechanism for accelerated oxidation along the composite fiber direction is an excellent example of the intrinsic coupling of chemical oxidative aging and damage. Whereas cracks can accelerate oxidation by providing pathways for oxidants, oxidation can lead to cracking in the resin matrix and at fiber–matrix interfaces. The critical nature of the fiber–matrix interphase on degradation and failure processes in composites signifies the importance of proper representation of its behavior in predictive models. Since failure initiation is typically associated with the fiber–matrix interface/interphase region, the importance of modeling the coupling effects of damage and oxidation cannot be overemphasized.

Integration of constitutive models for the composite constituents into a unit cell micromechanical representation provides a foundation for understanding the mechanisms of degradation for long-term environmental exposure and loading. Although the accuracy of the unit cell analysis is certainly dependent on the accuracy of the constitutive models for the constituents, even rudimentary constitutive models can provide constructive insight into the primitive mechanisms of degradation. This is particularly true for short-aging times when the coupling effects of the physical and chemical aging and the damage may be less prominent. Indeed, in the absence of a robust predictive model for composite oxidation, researchers routinely apply models that represent only limited facets of the mechanistic behavior. Such is the case for the application of linear viscoelastic analyses in the NASA HSR program to model the long-term (60,000 h at 177°C) behavior of composites. Clearly, the linear viscoelastic models are expected to perform most favorable for cases in which oxidation is a secondary effect, e.g., lower temperatures and shorter aging times but inherent in determination of the viscoelastic model parameters are phenomenological contributions from the oxidative degradation if it is present. Although these models were used with success in the HSR program, these limited representations of long-term thermal aging can lead to large prediction errors particularly for extended aging times if used without discretion.

Of greatest importance to the use of predictive tools for development of material design allowables is the capability to accurately predict long-term performance based on short-term observations for the same loading environment. An associated issue is the capability to predict the long-term performance based on accelerated aging observations. Moreover, the latter capability would be particularly beneficial if the predictive tool could properly account for changes in the degradation mechanism for accelerated test methods. This would provide opportunities to expand the testing environment envelope allowing, for example, shorter duration accelerated aging test that would ultimately reduce the cost of generating material design allowables.

An overview of the experimentally observed thermooxidative behavior of PMR-15 neat polymer and carbon fiber/PMR-15 composites has been presented along with a theoretical treatment of oxidation development. Numerous shortcomings of existing analytical/numerical models and the challenges of experimentally characterizing or measuring the parameters required by the models have been pointed out. The listing of modeling and characterization challenges for HTPMCs provided herein is only a small subset of the issues that must be addressed to reach the goal of developing a robust modeling tool. Some of the other overarching areas for which only a cursory treatment is given include hygrothermal degradation, thermo-mechanical cyclic loading at high temperatures, and coupling of the mechanical response (including damage) with the chemical evolution of properties, to name just a few. To identify problem areas needing further study, one only needs to start with a review of the section titles of the topics covered here.

Acknowledgments

This work is supported by the Air Force Office of Scientific Research under the Materials Engineering for Affordable New Systems (MEANS) program sponsored by Dr. Charles Lee. Particular thanks are due to Mr. Erik Ripberger (AFRL/MLSA) and Mr. Josh Briggs (UDRI) for their help with aging experiments, Mr. Ken Goecke (UDRI) for mechanical testing, Dr. Sirina Putthanarat (UDRI) for nanoindentation measurements, and Stevens Institute of Technology students (Eva Yu, Harold Cook, and Tan Huan) for numerical analyses.

References

1. Abdeljaoued K (1999) Thermal oxidation of PMR-15 polymer used as a matrix in composite materials reinforced with carbon fibers. MS Thesis, Ecole Nationale Supérieure des Arts et Métiers, Paris
2. Accelerated Test Methods for Durability of Composites, High Speed Research Materials Durability (Task 23), High Speed Research Program, March 1998
3. Ahoi E, Talreja R (2006) Characterization of viscoelasticity and damage in high temperature polymer matrix composites. *Composites Science and Technology* 66:2506–2519
4. Allen DH, Harris CE, Groves SE, Norvell RG (1988) Characterization of stiffness loss in cross-ply laminates with curved matrix cracks. *Journal of Composite Materials* 22:71–80
5. Audouin L, Langlois V, Verdu J, De Bruijn JCM (1994) Review: role of oxygen diffusion in polymer aging: kinetic and mechanical aspects. *Journal of Materials Science* 29:569–583
6. Bellenger V, Decelle J, Huet N (2005) Aging of a carbon epoxy composite for aeronautic applications. *Composites Part B: Engineering* 36:189–194
7. Bowles K (1991) Effect of fiber reinforcements on thermo-oxidative stability and mechanical properties of polymer matrix composites. NASA TM 103648
8. Bowles KJ (1992) Effect of fiber reinforcements on thermo-oxidative stability and mechanical properties of polymer matrix composites. *SAMPE Quarterly*, April 2–12
9. Bowles KJ (1998) Thermal and mechanical durability of graphite-fiber-reinforced PMR-15 composites. NASA TM 113116/REV1
10. Bowles KJ (1999) Durability of graphite-fiber reinforced PMR-15 composites aged at elevated temperatures. *Journal of Composites Technology & Research* 21:127–132
11. Bowles KJ, Meyers A (1986) Specimen geometry effects on graphite/PMR-15 composites during thermo-oxidative aging. In: *Proceedings 31st International SAMPE Symposium*
12. Bowles KJ, Nowak G (1988) Thermo-oxidative stability studies of Celion 6000/PMR-15 unidirectional composites, PMR-15, and Celion 6000 fiber. *Journal of Composite Materials* 22:966–985
13. Bowles KJ, Jayne D, Leonhardt TA (1992) Isothermal aging effects on PMR-15 resin. NASA TM 105648
14. Bowles KJ, Jayne D, Leonhardt TA (1993) Isothermal aging effects on PMR-15 resin. *SAMPE Quarterly* 24:2–9
15. Bowles KJ, Jayne D, Leonhardt TA, Bors D (1993) Thermal stability relationships between PMR-15 resin and its composites. NASA Technical Memorandum 106285
16. Bowles KJ, Jayne D, Leonhardt TA, Bors D (1993) Thermal stability relationships between PMR-15 resin and its composites. NASA TM 106285

17. Bowles KJ, Madhukar M, Papadopolous DS, Inghram L, McCorkle L (1995) The effects of fiber surface modification and thermal aging on composite toughness and its measurement. NASA TM-106765
18. Bowles KJ, McCorkle L, Ingraham L (1998) Comparison of graphite fabric reinforced PMR-15 and Avimid N composites after long term isothermal aging at various temperatures. NASA/TM-1998-107529
19. Bowles KJ, Papadopoulos DS, Inghram, LL, McCorkle LS, Klan OV (2001) Longtime durability of PMR-15 matrix polymer at 204, 260, 288 and 316°C. NASA/TM-2001-210602
20. Bowles KJ, Tsuji L, Kamvouris J, Roberts GD (2003) Long-term isothermal aging effects on weight loss, compression properties, and dimensions of T650-35 fabric-reinforced PMR-15 composites – data. NASA TM-2003-211870
21. Brinson LC, Gates TS (1995) Effects of physical aging on long term creep of polymers and polymer matrix composites. *International Journal of Solids and Structures* 32:827
22. Celina M, Wise J, Ottesen DK, Gillen KT, Clough RL (2000) Correlation of chemical and mechanical property changes during oxidative degradation of neoprene. *Polymer Degradation and Stability* 68:171–184
23. Chung K, Seferis JC (2001) Evaluation of thermal degradation on carbon fiber/cyanate ester composites. *Polymer Degradation and Stability* 71:425
24. Chung K, Seferis JC, Nam J-D (2000) Investigation of thermal degradation behavior of polymeric composites: prediction of thermal cycling effect from isothermal data. *Composites Part A: Applied Science and Manufacturing* 31:945–957
25. Ciutacu S, Budrugaec P, Niculae I (1991) Accelerated thermal aging of glass-reinforced epoxy resin under oxygen pressure. *Polymer Degradation and Stability* 31:365–372
26. Colin X (2000) Kinetic modeling of thermal oxidation of high performance polymer and composite materials. MS Thesis, Ecole Nationale Supérieure des Arts et Métiers, Paris
27. Colin X, Verdu J (2003) Thermal aging and lifetime prediction for organic matrix composites. *Plastics Rubber and Composites* 32:349–356
28. Colin X, Verdu J (2005) Strategy for studying thermal oxidation of organic matrix composites. *Composites Science and Technology* 65:411–419
29. Colin X, Marais C, Favre JP (1999) Damage/weight loss relationship of polymer matrix composites under thermal aging. In: *Proceedings of ICCM-12, ICCM Europe Publications, Massard T, Vautrin A, Eds*
30. Colin X, Marais C, Cochon JL, Verdu J (1999) Damage/weight loss relationship for bismaleimide matrix under isothermal oxidation aging. In: *Proceedings of the International Conference on Recent Developments in Durability Analysis of Composite Systems, Brussels University, Belgium*
31. Colin X, Marais C, Verdu J (2001) Thermal oxidation kinetics for a poly(bismaleimide). *Journal of Applied Polymer Science* 82:3418–3430

32. Colin X, Marais C, Verdu J (2001) A new method for predicting the thermal oxidation of thermoset matrices: application to an amine cross-linked epoxy. *Polymer Testing* 20:795–803
33. Colin X, Marais C, Verdu J (2002) Kinetic modeling and simulation of gravimetric curves: application to the oxidation of bismaleimide and epoxy resins. *Polymer Degradation and Stability* 78:545–553
34. Colin X, Marais C, Verdu J (2005) Kinetic modeling of the stabilizing effects of carbon fibers on thermal aging of thermoset matrix composites. *Composites Science and Technology* 65:117–127
35. Colin X, Mavel A, Marais C, Verdu J (2005) Interaction between cracking and oxidation in organic matrix composites. *Journal of Composite Materials* 39:1371–1389
36. Crasto AS, Kim RY (1995) Creep behavior of high-temperature composites. In: *Proceedings of ICCM-10, Whistler, BC, Canada IV*:423
37. Cunningham RA (1996) High temperature degradation mechanisms in polymer matrix composites. MS Thesis, Massachusetts Institute of Technology, Cambridge, MA
38. Decelle J, Huet N, Bellenger V (2003) Oxidation induced shrinkage for thermally aged epoxy networks. *Polymer Degradation and Stability* 81:239–248
39. Eckstein BH (1981) The oxidation of carbon fibers in air between 230°C and 375°C. *Fiber Science and Technology* 14:139–156
40. Foster DC, Tandon GP, Zoghi M (2006) Evaluation of failure behavior of transversely loaded unidirectional model composites. *Experimental Mechanics* 46:217–243
41. Gates TS (2003) On the use of accelerated test methods for characterization of advanced composite materials. NASA/TP-2003-212407
42. Gates TS, Feldman M (1994) The effects of physical aging at elevated temperatures on the viscoelastic creep of IM7/K3B. NASA-TM-109114
43. Gibbs HH, Wendt RC, Wilson FC (1979) Carbon fiber structure and stability studies. *Polymer Engineering Science* 19:342–349
44. Gibson T, Price W, Arnold F, Uttermohlen D, Storage T, Jacques A (2006) Physical and mechanical properties of AFR-PE-4 and BIM-15 with S-2 and Astroquartz-III composites. Presented at 26th High Temp Workshop, Austin, TX
45. Gillen KT, Wise J, Clough RL (1995) General solution for the basic autoxidation scheme. *Polymer Degradation and Stability* 47:149–161
46. Hashin Z (1966) Viscoelastic fiber reinforced materials. *AIAA Journal* 4:1141–1147
47. Hergenrother PM, Smith GJ (1997) Chemistry and properties of imide oligomers end-capped with phenylethynylphthalic anhydrides. *Polymer* 35:4857–4864
48. Iarve EV (1996) Spline variational three-dimensional stress analysis of laminated composite plates with open holes. *International Journal of Solids and Structures* 44:2095–2118

49. Johnson TF, Gates TS (2001) High temperature polyimide materials in extreme temperature environments. In: AIAA Paper 2001-1214 42nd AIAA/ASME/ASCE/AHS/ASC Structures, Structural Dynamics and Materials Conference and Exhibition, Seattle, WA
50. Johnson LL, Eby RK, Meador MAB (2003) Investigation of oxidation profile in PMR-15 polyimide using atomic force microscope (AFM). *Polymer* 44:187–197
51. Klett JW, Ervin VJ, Edie DD (1999) Finite element modeling of heat transfer in carbon/carbon. *Composites Science and Technology* 59:593–607
52. Kulkarni R, Ochoa O (2006) Transverse and longitudinal CTE measurements of carbon fibers and their impact on interfacial residual stresses in composites. *Journal of Composite Materials* 40:733–754
53. Kung HK (1996) High-temperature oxidation, aging and creep in carbon-fiber reinforced polyimide composites during thermal fatigue. Ph.D. Thesis, University of Houston, TX
54. Kung HK (2006) Effects of surface roughness on high-temperature oxidation of carbon-fiber-reinforced polyimide composites. *Journal of Composite Materials* 39:1677–1687
55. Leung CL, Ghaffarian R, Leung, KC (1997) Thermo-oxidative stability of polyimides. I. Effect of prepolymer molecular weight. *Polymer Degradation and Stability* 58:1–14
56. Lincoln JE (2001) Structure–property–processing relationships and the effects of physical structure on the hygrothermal durability and mechanical response of polyimides. Ph.D. Thesis, Michigan State University
57. Marais C, Villoutreix G (1998) Analysis and modeling of the creep behavior of the thermostable PMR-15 polyimide. *Journal of Applied Polymer Science* 69:1983–1991
58. McCartney LN (1995) A recursive method of calculating stress transfer in multiple-ply cross-ply laminates subjected to biaxial loading. NPL Report DMMA(A)150
59. McKenna GB (1992) Aging of polymeric resins: implications for composite performance. In: *Proceedings of the Conference of the American Chemical Society*
60. McMahan PE (1978) Oxidative resistance of carbon fibers and their composites. In: *Advanced Composite Materials – Environmental Effects*, ASTM STP 658, Vinson JR, Ed., American Society for Testing and Materials, pp 254–266
61. McManus HL, Cunningham RA (1995) Coupled materials and mechanics analyses of durability tests for high temperature polymer matrix composites. NASA/CR-95-112619
62. McManus HL, Foch BJ, Cunningham RA (2000) Mechanism-based modeling of long-term degradation. *Journal of Composites Technology & Research* 22:146–152
63. Meador MA, Lowell CE, Cavano PJ, Herrera-Fierro P (1996) On the oxidative degradation of nadic endcapped polyimides. I. Effect of thermocycling on weight loss and crack formation. *High Performance Polymers* 8:363–379

64. Meador MA, Johnston JC, Cavano PJ, Frimer AA (1997) On the oxidative degradation of nadic endcapped polyimides. 2. Evidence for reactions occurring at high temperature. *Macromolecules* 30:3215–3223
65. Meador MA, Johnston JC, Frimer AA, Gilinsky-Sharon P (1999) On the oxidative degradation of nadic endcapped polyimides. 3. Synthesis and characterization of model compounds for end-cap degradation products. *Macromolecules* 32:5532–5538
66. Nam JD, Seferis JC (1992) Anisotropic thermo-oxidative stability of carbon fiber reinforced polymeric composites. *SAMPE Quarterly* 24:10–18
67. Nelson JB (1983) Thermal aging of graphite polyimide composites. In: *Long-Term Behavior of Composites*, ASTM STP 813, O'Brien TK, Ed., American Society for Testing and Materials, Philadelphia, pp 206–221
68. Nicholson LM, Whitley KS, Gates TS (2000) The combined influence of molecular weight and temperature on the aging and viscoelastic response of a glassy thermoplastic polyimide. NASA-2000-TM210312
69. Nicholson LM, Whitley KS, Gates TS (2002) The role of molecular weight and temperature on the elastic and viscoelastic properties of glassy thermoplastic polyimide. *International Journal of Fatigue* 24:185–195
70. Paipetis A, Galiotis C (1996) Effect of fiber sizing on stress transfer efficiency in carbon/epoxy model composites. *Composites Part A: Applied Science and Manufacturing* 27A:755–767
71. Paris O, Loidl D, Peterlik H, Müller M, Lichtenegger H, Fratzl P (2000) The internal structure of single carbon fibers determined by simultaneous small and wide-angle x-ray scattering. *Journal of Applied Crystallography* 33:695–699
72. Pasricha A, Tuttle ME, Emery AF (1996) Time-dependent response of IM7/5260 composites subjected to cyclic thermo-mechanical loading. *Composites Science and Technology* 56:55–62
73. Pochiraju KV, Tandon GP (2004) Time dependent composite material behavior under thermo-oxidative environmental conditions. In: *Proceedings of IMECE, Anaheim, CA*
74. Pochiraju KV, Tandon GP (2006) Modeling thermo-oxidation layer growth in high temperature resins. *Journal of Engineering Materials and Technology* 128:107–116
75. Popov AA, Krysyuk BE, Zaikov GY (1980) Translation of vysokomol soyed. *Polymer Science, USSR*, 22
76. Reifsnider KL, Lesko J (1998) Mechanics of long-term behavior of high temperature polymer composites. Report AFRL-SR-BL-TR-98-0835
77. Reynolds WN (1973) Structure and physical properties of carbon fiber. *Chemistry and Physics of Carbon* 11:1–67
78. Ripberger E, Tandon GP, Schoeppner GA (2004) Characterizing oxidative degradation of PMR-15 resin. In: *Proceedings of the Spring SAMPE 2004 Symposium/Exhibition, Long Beach, CA*
79. Ripberger E, Tandon GP, Schoeppner GA (2004) Characterizing oxidative layer development in AFR-PE-4 resin. In: *Proceedings of the Fall SAMPE 2004 Symposium/Exhibition, Long Beach, CA*

80. Ripberger ER, Tandon GP, Schoeppner GA (2005) Experimental techniques for characterizing thermo-oxidative behavior in high temperature polyimide composites. In: Proceedings of the 2005 SEM Annual Conference & Exposition, Portland, OR
81. Roy S, Vengadassalam K, Wang Y, Park S, Liechti KM (2006) Characterization and modeling of strain assisted diffusion in an epoxy adhesive layer. *International Journal of Solids and Structures* 43:27–52
82. Saff C, Hahn G, Griffith J, Ingle R, Nelson K (2005) Accelerated Insertion of Materials – Composites AIAA-2005-2165 46th AIAA/ASME/ASCE/AHS/ASC Structures, Structural Dynamics and Materials Conference, Austin, TX
83. Salin IM, Seferis JC (1993) Anisotropic effects in thermogravimetry of polymeric composites. *Journal of Polymer Science* 31:1019–1027
84. Schapery RA (1966) A theory of non-linear thermoviscoelasticity based on irreversible thermodynamics. In: Proceedings of the 5th US National Congress of Applied Mechanics, ASME, pp 511–530
85. Schapery RA (2002) Homogenized constitutive equations for linear viscoelastic unidirectional composites with growing transverse cracks. *Mechanics of Time-Dependent Materials* 6:101–131
86. Schapery RA, Sicking DL (1995) On nonlinear constitutive equations for elastic and viscoelastic composites with growing damage. *Mechanical Behavior of Materials* 47:45–76
87. Schieffer A, Maire J-F, Lévêque D (2002) A coupled analysis of mechanical behavior and aging for polymer-matrix composites. *Composites Science and Technology* 62:543–549
88. Schoeppner GA, Curliss DB (2002) Model-based design for composite materials life management. In: Proceedings of the 9th AIAA/ISSMO Symposium on Multidisciplinary Analysis and Optimization Conference, 4–6 September, Atlanta, GA, AIAA-2002-5516
89. Schoeppner GA, Pagano NJ (1999) 3D thermoelastic moduli and saturation crack density for cross-ply laminates with transverse cracks. *International Journal of Damage Mechanics* 8:273–309
90. Schoeppner GA, Tandon GP (2003) Aging and durability of PMR-15 high temperature polyimide. In: Proceedings of 35th International SAMPE Technical Conference, Dayton, OH
91. Schoeppner GA, Tandon GP, Ripberger ER (2007) Anisotropic oxidation and weight loss in PMR-15 composites. *Composites Part A: Applied Science and Manufacturing* 38:890–904
92. Scola DA, Vontell JH (1988) High temperature polyimides, chemistry and properties. *Polymer Composites* 9:443–452
93. Scott DW, Lai JS, Zureick A-H (1995) Creep behavior of fiber reinforced polymeric composite: a review of the technical literature. *Journal of Reinforced Plastics and Composites* 14:588–617
94. Seferis JC (1999) Aging analyses of polymer composites through time-temperature equivalence. *Journal of Composites Technology & Research* 21:173–179

95. Skontorp A (1995) Isothermal high-temperature oxidation, aging and creep of carbon-fiber/polyimide composites. Ph.D. Thesis, University of Houston, TX
96. Skontorp A, Wang SS (1995) High temperature creep with physical and chemical aging, and associated viscoelastic constitutive equations of polyimide-matrix composites. In: *Recent Advances in Composite Materials*, White SR, Hahn HT, Jones WF, Eds., ASME MD, Vol. 56, American Society of Mechanical Engineers, New York, NY, pp 57–70
97. Skontorp A, Wong M-S, Wang S-S (1995) High-temperature anisotropic thermal oxidation of carbon-fiber reinforced polyimide composites. Theory and experiment. In: *Proceedings of ICCM-10*, Whistler, BC, Canada, IV:375
98. Struik LCE (1978) *Physical Aging in Amorphous Polymers and Other Materials*. Elsevier, Amsterdam
99. Sullivan JL (1990) Creep and physical aging of composites. *Composites Science and Technology* 39:207
100. Talreja R (1985) Transverse cracking and stiffness reduction in composite laminates. *Journal of Composite Materials* 19:355–375
101. Tandon GP (1995) Use of composite cylinder model as representative volume element for unidirectional fiber composites. *Journal of Composite Materials* 29:388–409
102. Tandon GP, Kim RY, Bechel VT (2000) Evaluation of interfacial normal strength in SCS-0/epoxy composite using cruciform specimen. *Composites Science and Technology* 60:2281–2295
103. Tandon GP, Ripberger ER, Schoeppner GA (2005) Accelerated aging of PMR-15 resin at elevated pressure and/or temperature. In: *Proceedings of the SAMPE 2005 Symposium and Exhibition*, Seattle, WA
104. Tandon GP, Pochiraju KV, Schoeppner GA (2006) Modeling of oxidative development in PMR-15 resin. *Polymer Degradation and Stability* 91:1861–1869
105. Tandon GP, Briggs J, Schoeppner GA (2006) Thermo-oxidative degradation of carbon fibers for high-temperature polymer matrix composites. In: *Proceedings of American Society for Composites, 21st Technical Conference*, University of Michigan-Dearborn, Dearborn, MI
106. Tang LQ, Pochiraju K, Chassapis C, Manoochehri S (1998) A computer-aided optimization approach for the design of injection mold cooling systems. *Journal of Mechanical Design: Transactions of the ASME* 120:165–174
107. Thorp KE (2000) Hydrolytic degradation of norbornene-terminated addition polyimides: a mechanistic and kinetic study. Ph.D. Thesis, University of Dayton
108. Tsotsis TK (1995) Thermo-oxidative aging of composite materials. *Journal of Composite Materials* 29:410–422
109. Tsotsis TK (1998) Long-term thermo-oxidative aging in composite materials: experimental methods. *Journal of Composite Materials* 32:1115–1135

110. Tsotsis TK, Lee SM (1998) Long-term thermo-oxidative aging in composite materials: failure mechanisms. *Composites Science and Technology* 58:355–368
111. Tsotsis TK, Keller S, Bardis J, Bish J (1999) Preliminary evaluation of the use of elevated pressure to accelerate thermo-oxidative aging in composites. *Polymer Degradation and Stability* 64:207–212
112. Tsotsis TK, Keller S, Lee K, Bardis J, Bish J (2001) Aging of polymeric composite specimens for 5000 hours at elevated pressure and temperature. *Composites Science and Technology* 61:75–86
113. Tsuji LC, McManus HL, Bowles KJ (1998) Mechanical properties of degraded PMR-15 resin. NASA Technical Report, 1998-208487, pp 1–18
114. Upadhyaya D, Tsakiroopoulos P (1995) Evaluation of the effect of sizing levels on transverse flexural and shear strengths of carbon/epoxy composites. *Journal of Materials Processing Technology* 54:17–20
115. Veazie DR, Gates TS (1995) Physical aging effects of the compressive linear viscoelastic creep of IM7/K3B composite. NASA-95-TM110224
116. Veazie DR, Gates TS (1998) Effects of aging-time reference on the long term behavior of the IM7/K3B composite. In: *Proceedings of 39th AIAA/ASME/ASCE/AHS/ASC Structures, Structural Dynamics, and Materials Conference Paper AIAA 98-1962*
117. Verdu S, Verdu J (1997) A new kinetic model for polypropylene thermal oxidation at moderate temperatures. *Macromolecules* 30:2262–2267
118. Waldron WK Jr. and McKenna GB (1995) The nonlinear viscoelastic response and apparent rejuvenation of an epoxy glass. *Journal of Rheology* 39:471–497
119. Wang SS, Chen X (2006) Computational micromechanics for high-temperature constitutive equations of polymer-matrix composites with oxidation reaction, damage, and degradation. *Journal of Engineering Materials and Technology* 128:81–89
120. Wang SS, Chen X, Skontorp A (2003) High temperature mechanics modeling and experiments of thermal oxidation, degradation and damage evolution in carbon fiber/polyimide composites. In: *Proceedings of American Society for Composites 18th Technical Conference, University of Florida, Gainesville, FL*
121. Wang SS, Chen X, Skontorp A (2003) High-temperature mechanics modeling and experiments of thermal oxidation, degradation and damage evolution in carbon/fiber/polyimide composites. Technical Report CEAC-TR-03-0106, University of Houston
122. Weitsman Y (1987) Stress assisted diffusion in elastic and viscoelastic materials. *Journal of the Mechanics and Physics of Solids* 35:73–97
123. Whitley KS, Collins TJ (2006) Mechanical properties of T650/AFR-PE-4 at elevated temperatures for lightweight aeroshell designs. In: *AIAA-2006-2202 47th AIAA/ASME/ASCE/AHS/ASC Structures, Structural Dynamics, and Materials Conference, Newport, Rhode Island, AIAA-2006-2202*

124. Williams ML, Landel RF, Ferry JD (1955) The temperature dependence of relaxation mechanisms in amorphous polymers and other glass-forming liquids. *Journal of the American Chemical Society* 77:3701–3707
125. Wise J, Gillen KT, and Clough RL (1997) Quantitative model for the time development of diffusion-limited oxidation profiles. *Polymer* 38:1929–1944
126. Wong MS, Skontorp A, Wang SS (1994) Thermal oxidation of carbon fibers and carbon-fiber reinforced high-temperature polyimide composite at elevated temperature. In: *Proceedings of the American Society for Composites 9th Technical Conference*, Technomic Publishing Co., Lancaster, PA, pp 458–467
127. Zhang Y, Xia Z, Ellyin F (2005) Nonlinear viscoelastic micromechanical analysis of fibre-reinforced polymer laminates with damage evolution. *International Journal of Solids and Structures* 42:591–604